



CHALMERS
UNIVERSITY OF TECHNOLOGY

Aging models and Adaptive SOC Estimation for Lithium ion Batteries

A Master of Science thesis in which life cycle models for Lithium ion cells are built under different loading conditions and also the SOC and parameters of the battery are estimated using recursive regulators.

Master's thesis in Electric Power Engineering

Yuwei Zhou
Shivadeep Maheshwar

MASTER'S THESIS 2018

Aging models and Adaptive SOC Estimation for Lithium ion Batteries

Thesis for the Degree of Master of Science in Engineering

Yuwei Zhou
Shivadeep Maheshwar



CHALMERS
UNIVERSITY OF TECHNOLOGY

Department of Electrical Engineering
Division of Electric Power Engineering
CHALMERS UNIVERSITY OF TECHNOLOGY
Gothenburg, Sweden 2018

Aging models and Adaptive SOC Estimation for Lithium ion Batteries
Yuwei Zhou
Shivadeep Maheshwar

© Yuwei Zhou, Shivadeep Maheshwar, 2018.

Supervisor: Evelina Wikner, Department of Electrical Engineering
Michael Palander, CEVT
Examiner: Prof. Torbjörn Thiringer, Department of Electrical Engineering

Master's Thesis 2018
Department of Electrical Engineering
Division of Electric Power Engineering
Chalmers University of Technology
SE-412 96 Gothenburg
Telephone +46 31 772 1000

Typeset in L^AT_EX
Gothenburg, Sweden 2018

Abstract

The thesis mainly consists of two significant parts namely, State of Charge estimation and the State of Health estimation. Firstly, the SOC estimation makes use of two critical methods which are Recursive Least Square method (RLS) and Extended Kalman Filter (EKF) to estimate the battery parameters and to update the battery state equations respectively. The model is tested for synthetic test cases and driving cycles like NEDC. The results obtained from real drive cycle cases are compared with the reference data provided by the supervisors. The primary advantage of this estimation algorithm is that it allows for better accuracy than existing methods like Coulomb counting and Open Circuit Voltage (OCV) estimation methods.

The second part of this thesis majorly focuses on deriving life cycle models for Lithium-ion cells. The cells under consideration are Lithium iron (LFE) and NMC cells for which three models are built namely, Model A, Model B and Model C. The Models A & B focus on the Lithium iron cells while Model C on NMC cells. The main parameters under discussion are temperature, C-rate, SOC window (DOD) and capacity throughput. All these factors are deemed as stresses acting on the cell which affects the life of the battery. To start with a single stress model is built and further, based on the reflections from Model A, a multi-stress models B and C are developed.

Keywords: Battery, Kalman filter, recursive least square, stress, temperature, C-rate, SOC window

Acknowledgements

We would like to first and foremost thank Prof. Törbjorn Thiringer for extending the scope of the thesis initially, help with the technical and writing details.

We would especially thank our supervisor Evelina Wikner for clearing our doubts and have weekly meetings which were inspiring and encouraging us to do well. Secondly, we would also like to convey our gratitude to Björn Fridholm for helping us with the SOC estimation part of the thesis.

We would also like to thank Michael Palander and Sandeep David for giving us this opportunity to work in CEVT and having meaningful discussions and technical assistance throughout the Thesis.

Finally, we are grateful to our parents for supporting us throughout our master program amidst hardships.

Yuwei and Shiva, Gothenburg, May 2018

Contents

Nomenclature	xi
List of Figures	1
List of Tables	1
1 Introduction	1
1.1 Background	1
1.2 Aim	2
1.3 Scope	2
1.4 Sustainability and Ethical aspect	3
2 Theory	5
2.1 General structure of State-of-charge estimator	5
2.2 Zero order hold method	6
2.3 Linear regression form	6
2.4 Battery parameters observer	7
2.4.1 Recursive least squares	7
2.4.2 Kalman filter	7
2.5 Battery state-of-charge observer	8
2.5.1 Extended Kalman filter	8
2.6 Ageing in Lithium Ion batteries	9
2.7 Ageing in NMC/LMO cells	9
2.8 Empirical models	11
2.8.1 Power Law	11
2.8.2 Relation between the Tafel's equation and Arrhenius equation	12
2.8.3 Parameterised Aging model	13
3 Test cases for SOC estimation	15
3.1 Synthetic data test	15
3.1.1 Input signals	16
3.1.1.1 Sine-wave	16
3.1.1.2 NEDC test cycle	17
3.1.1.3 Noise signals	17
3.1.2 Validation test for ohmic resistance R_0 estimation	17
3.1.3 Validation test for time constant τ estimation	18
3.1.4 Validation test for SOC estimation	19

3.1.5	Combined test with complete algorithm	19
4	Available data and cell specifications	21
4.1	Available test data	21
4.2	Cell Specifications	23
5	Method for SoC estimation	25
5.1	Battery parameters estimation	25
5.1.1	Ohmic resistance estimation	25
5.1.2	RC parameter estimation	25
5.2	Factors influencing the accuracy	26
5.2.1	Model errors	26
5.2.2	Dead zone in RLS method	27
5.2.3	Time variant forgetting factor in RLS method	28
5.2.4	Adaptive Kalman filter	29
5.2.5	Data scaling	29
5.3	State-of-charge estimation	30
5.3.1	State space equation building	30
5.3.2	Curve-fitting for OCV	30
6	Calculations for Aging models for LFP cells	33
6.1	Model A	33
6.1.1	Temperature and C-rate dependent loss factor	33
6.1.2	SOC window loss function	34
6.1.3	Loss function dependent on capacity throughput of segment on the Anode	35
6.2	The loss function K_{SoH}	36
6.2.1	Summary of the loss functions	36
6.3	Model B	37
6.3.1	Calculation of Activation Energy	37
6.3.2	Parameterising rate constant and activation energy with C-rate	38
6.3.3	Combined C-rate and Temperature function	40
6.3.4	Parameterising severity factor with SOC window	40
6.3.5	Combining all the loss functions	42
7	Developing model for NMC/LMO cells	45
7.1	Structure of the algorithm	45
7.2	Deciding the shaping factor b	46
7.3	Extracting the activation energy at 2 C-rate	47
7.4	Loss functions for SOC effects on ageing	49
7.4.1	Guessing the loss function at different C-rates and temperature	52
8	Results and discussion: SOC	55
8.1	R_0 estimation result	55
8.1.1	High sampling rate result	55
8.1.2	Low sampling rate result	56
8.1.3	Noise effects	57

8.1.4	Dead zone implementation	59
8.2	Time constant τ estimation	61
8.2.1	Scaling factor test	61
8.2.2	Relationship with SOC estimation	62
8.2.3	Noise effects	63
8.3	SOC estimation	65
8.3.1	Test with different initial guess	65
8.3.1.1	Relationship with time constant estimation	66
8.3.2	Noise effects	67
8.4	Combined test	68
8.4.1	Test results with optimal setting	68
8.4.2	Noise effects	71
9	Results and Discussions: SOH	73
9.1	Model Performances	73
9.1.1	Performance of model at Low Current rates	73
9.1.2	Model performances at High current rates	75
9.1.3	SOC related aging	80
9.2	Results: NMC/LMO cells	82
9.2.1	Effect of SOC and temperature	82
9.2.2	Mid SOC range and temperature effects	83
9.2.3	High SOC range and temperature effects	85
9.2.4	Different C-rates at 60-70% SOC range	86
9.2.5	COMSOL validation	87
9.2.6	Error Ageing value at different condition	88
10	Conclusion	91
10.1	Conclusion	91
10.2	Future work	92
	Bibliography	93

Nomenclature

Physical value

η	Coulomb efficiency
τ	RC circuit time constant
C_1	RC circuit capacity
i_{cell}	Cell current
k_n, k_{ns}, k_{nNs}	are the coefficients for the loss functions for Model A, B & C
$K_{SOC,A/L}$	SOC dependent loss function for Model A (LFP)
$k_{SOC,LFP}$	SOC dependent loss function for Model A (LFP)
$k_{ST,A/L}$	SOC and temperature dependent loss function for Model A (LFP)
$k_{TC,LFP}$	Current and temperature dependent loss function for Model B (LFP)
$k_{TC,NMC}$	Current and temperature dependent loss function for Model C (NMC)
$K_{TI,A/L}$	Current and temperature dependent loss function for Model A (LFP)
Q_{nom}	Battery nominal capacity
R_0	Ohmic resistance
R_1	RC circuit resistance
u_{cell}	Cell voltage
u_{RC1}	RC circuit voltage

Abbreviations

<i>EKF</i>	Extended Kalman filter
<i>EOL</i>	End of Life
<i>FEC</i>	Full Equivalent Cycles
<i>ICA</i>	Incremental Capacity Analysis
<i>LFP</i>	Lithium Iron Phosphaste
<i>LMO</i>	Lithium Manganese Oxide
<i>NEDC</i>	New european driving cycle
<i>NMC</i>	Nickel Manganese Cobalt oxide
<i>OCV</i>	Open circuit voltage
<i>RLS</i>	Recursive least squares
<i>SEI</i>	Solid Electrolyte Interphase
<i>SNR</i>	Signal-to-noise ratio
<i>SOC</i>	State of charge
<i>SOH</i>	State of health

1

Introduction

1.1 Background

In the past few years, the market for electric cars (BEV's, HEV's, PHEV's) has been growing faster than before due to the wish of gaining higher energy autonomy, moving towards a limited oil usage from the transport division and reducing the greenhouse gas emission [1]. In order reduce the global warming, many rebates and programs have been initiated by the governments which demand the increase of electric cars. In Sweden, a government rebate called "super green car" has been undertaken in 2012, which encourages the customers to buy electric vehicles as it provides a discount for cars emitting less than 50g of carbon dioxide per kilometre. This has resulted in an increase of electric vehicles share from 0.3% to 3.2% from 2012 to 2017 in Sweden.

For HEV and EV, the ability to calculate the electric range is vital to the power-train control system. Accurate information is needed to deliver the correct control strategy. The calculation is mainly based on the state of charge (SOC) and power demands. As a result, better accuracy of SOC estimation can be a benefit to the hybrid car control strategy. The battery is a complex chemical plant where no existing method is available to directly simulate the chemical behaviours in a state space model, which makes the estimation of SOC difficult [7]. The most common method for SOC estimation is the Coulomb counting method. It is direct and straightforward measuring the current flow, integrating it and normalising it with the capacity. However, it has the drawback that the estimation error continuously increases at every cycle[8]. As a result, some enhancements have to be implemented into the Coulomb counting method to overcome the drawback.

Lithium-ion batteries are complex systems, the capacity and power fade occur due to multiple processes and interactions within them. The physical-chemical mechanisms occurring are intensified by factors such as high C-rates, operating temperature, state of charge, overcharge and discharge conditions [16]. These factors are termed as stress factors, and semi-empirical models can be developed using these, which represent the physical-chemical phenomena that occur. The parameters in the model can be associated with a particular phenomenon caused due to a particular operating condition. The semi-empirical models highlight the danger, moderate and safe operating conditions for a given battery. The inference thus obtained can be used for instance in an electric vehicle to tune ECUs (Electronic Control Unit)

and help in increasing the durability by bypassing danger zones of operation. Also, an empirical model can be used for battery SOH estimation and as a part of SOC estimation in a Battery Management System (BMS).

1.2 Aim

The aim of this thesis is to develop an adaptive SOC estimation algorithm which is capable of estimating SOC under different conditions with admissible errors. The thesis also aims at building semi-empirical relations for lithium-ion cells based on extensive experimental data which covers a wide range of temperatures, C-rates and SOC ranges.

1.3 Scope

The SOC estimation will make use of an Extended Kalman Filter (EKF) technique to combine two different SOC calculation methods namely coulomb counting and OCV measurement. To measure the OCV, an adaptive parameter estimation algorithm will be implemented which estimates the parameters of a 1 RC model. This approach avoids the usage of look up tables which often are a result from extensive experiments at different conditions. Thus two Kalman filters interact with each other forming a closed loop system delivering the State of Charge. The aim for the accuracy is less than 5% drift error.

The scope of the State of health in this thesis is divided into two major parts of which the first one is to understand and implement the ageing model built by [19] for power-optimised LiFePo₄ cells and the second part focuses on modelling empirical relations for NMC/LMO cells. The model will cover a wide range of temperature varying from 20 to 50 degree Celsius, SOC in the range of 0-90% and also at different DOD 10% for LiFePo₄ and 20% for NMC /LMO cells and C-rates from 1C to 4C. Since the empirical ageing models do not entirely follow the physical-chemical phenomena, the exactness depends on the level of complexity required and the size of the experiment matrix.

The SOC estimations and Aging models are independent of each other and are not integrated. The primary reason is that the SOH model is not sensitive to the unsymmetric cycles. Secondly, there is lack of validation data for drive cycles (e.g. NEDC, HYZEM) which makes the results look uncertain and using SOC estimation for symmetric cycles produces results which are similar to the results from coulomb counting. The SOC estimation models are validated using the generated synthetic data and the test log data provided by CEVT. On the other hand, ageing models are validated using the experimental data that are not used for developing the semi-empirical equations.

1.4 Sustainability and Ethical aspect

The automotive industry's hunt to limit its impact on the environment and mutate automotive mobility into a sustainable mode of transport has continued and is quite intense at the present as all the companies have at least one variant with batteries as a part of the propulsion system. However, batteries could be a part of the green revolution if they take care of the following

1. **Re-use of the batteries:** Typically automotive batteries lose about 80 percent of their life in ten years based on the use and the chemistry. The battery is said to have reached EOL at this stage. The range, and power capabilities are reduced at this time. The batteries after this stage can be used for storage purposes in household, balancing power plants and power off-the-grid communities in rural areas [25].
2. **Standards for recycling:** Since the batteries are used extensively there will apparently be a huge requirement to recycle them in the future. There are different chemistries of cells that are available in the market, and the recycling process is different for different chemistries. Which has posed a challenge for recycling process as the present process of recycling like smelting is not a very sustainable method as the gains from recycling are decidedly less compared to the cost of recycling. Therefore standards for recycling batteries must be generalised and more research is required in this area.
3. **Carbon emission:** Batteries provide green energy as they have less emission in comparison to a conventional ICE vehicle. However, the production and charging the batteries are not comparatively sustainable. It takes a lot of energy to extract the raw materials and electricity to manufacture them during which the emissions might be higher and eventually exceed the emissions when compared to ICE cars. To reduce this, renewable energy sources like Solar, Wind and biogas must be used in manufacturing and charging the batteries instead of coal power.
4. **Socio-Economic conditions:** Cobalt mining is so vast in the Democratic Republic of Congo such that 65% of the world's cobalt is from them. However the situation of the workers in the mining is pitiful, the following are the most frequent problem faced:
 - (a) **Child labour:** According to the survey it is said that 40000 children are involved in mining activities. It is pathetic that the childhood and health of the innocent are taken away in the name of sustainability. Giants of telecom and automotive industries must take this condition seriously and make sure that children are not involved in mining activities and help to improve their conditions[25].
 - (b) **The health of the workers:** The workers in the mining companies lack proper gears for mining and most of them mine with bare hands. It has frequently been reported that the workers suffer from skin problems and lung diseases like "hard metal lungs" caused due to the polluted air[26].

When it comes to the ethical aspects, IEEE code of ethics are followed. The points that suit our thesis are selected and used as follows:

1. **To be honest and realistic in stating claims or estimates based on**

available data: The significant part of this thesis is built based on the experimental data provided. The ageing models are fit according to the data claiming certain assumptions. All these assumptions and drawbacks of the models are stated in different instances in the report.

2. **Understanding the battery technology:** there was a substantial requirement to comprehend about batteries and its ageing. For instance variation of the resistance of a cell at different SOC's and temperatures, understanding the basics of SEI layer growth and ageing of cells under different conditions etc.

2

Theory

2.1 General structure of State-of-charge estimator

The main idea of the SOC estimation is to simulate the plant model using a single RC model and implement a Kalman filter on to it to estimate the SOC. A recursive least square parameter estimation method is implemented to estimate the parameters of the RC model. If the initial guess of the parameters is not quite far from the actual estimate, in most cases, the RLS algorithm will converge to the correct solution. A Kalman filter will be built on the estimated model and it will produce the estimated SOC.

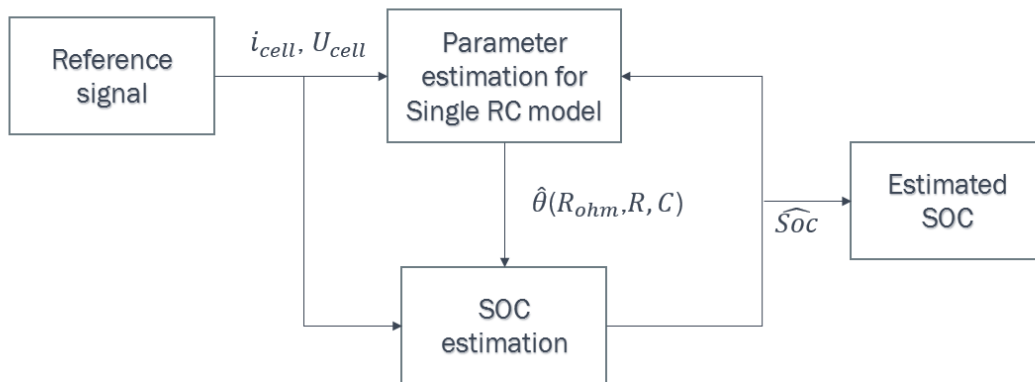


Figure 2.1: State-of-charge estimator structure

The figure 2.1 shows the structure of the whole system. A dual RC model is used as the reference signal generator. Hence, the single RC model is tuned such that it has the same behaviour as the reference model. With all parameters available, the Kalman filter estimates the states that are listed from the input and output of the single RC model.

2.2 Zero order hold method

The simplest and a common method to discretize the continuous system into a discrete system with sampling time is to hold the output constant until the next sample is retrieved.[11] This approach is called Zero-Order-Hold, and the reconstructed signal $f(t)$ is given as,

$$f(t) = f(kh), \quad kh < t < kh + h \quad (2.1)$$

where k is the current step, and h is the step size.

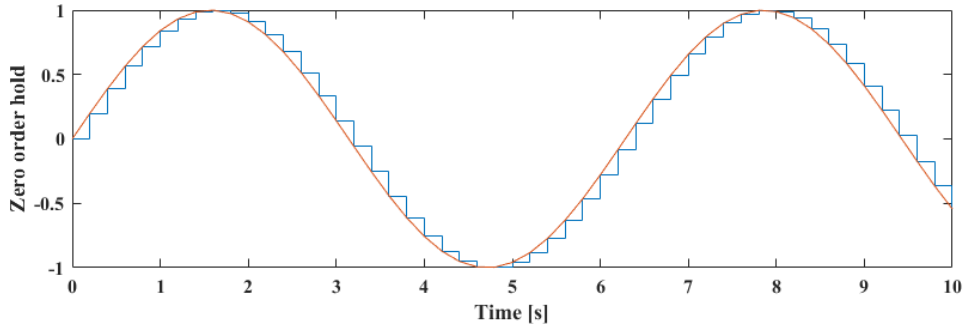


Figure 2.2: Sampling a sinusoid by Zero-Order-Hold

2.3 Linear regression form

Starting from state-space equations,

$$\begin{aligned} \dot{x}(k) &= Ax(k) + Bu(k) \\ y(k) &= Cx(k) + Du(k) \end{aligned}$$

Laplace transform is usually used to solve differential equations. The transformation equation from state space equation is

$$G(s) = C(sI - A)^{-1}B + D \quad (2.2)$$

where s is a complex number frequency parameter, I is an identity matrix and $G(s)$ is the transfer function built on the original state space equations. The transfer function is represented as

$$G(s) = \frac{b_m s^m + \dots + b_0}{a_n s^n + a_{n-1} s^{n-1} + \dots + 1} \quad (2.3)$$

The relation between input, output and transfer function is given as

$$y(k) = G(s)u(k) \quad (2.4)$$

then rewriting the dynamic system equation into

$$y(k) + a_1 s y(k) + \dots + a_n s^n y(k) = b_0 u(k) + \dots b_m s^m u(k) \quad (2.5)$$

since the project is focused on discrete systems, (2.5) is transferred into,

$$y(k) + a_1y(k-1) + \dots + a_ny(k-n) = b_0u(k) + \dots + b_mu(k-m) \quad (2.6)$$

which is commonly referred to as an ARX-model (Auto-Regressive with eXogenous in-put). With the parameter vector,

$$\theta(k) = \begin{bmatrix} a_1 \dots a_n & b_0 \dots b_m \end{bmatrix}^T$$

and the regression vector,

$$\varphi(k) = \begin{bmatrix} -y(k-1) \dots -y(k-n) & u(k) \dots u(k-m) \end{bmatrix}^T$$

2.4 Battery parameters observer

In the following sections, the recursive least squares (RLS) method and the Kalman filter will be presented which are related to the linear regression model,

$$y(k) = \varphi^T(k)\theta(k) \quad (2.7)$$

where y is the measured system output, φ is the regressive states vector which contains the information of inputs and outputs, θ is the parameter vector to be estimated.

2.4.1 Recursive least squares

The core iteration equations of the RLS method are

$$\hat{\theta}(k) = \hat{\theta}(k-1) + K(k)\varepsilon(k) \quad (2.8)$$

$$\varepsilon(k) = y(k) - \varphi^T(k)\hat{\theta}(k) \quad (2.9)$$

$$K(k) = P(k-1)\varphi(k)(\lambda + \varphi^T(k)P(k-1)\varphi(k))^{-1} \quad (2.10)$$

$$P(k) = (I - K(k)\varphi^T(k))P(k-1)/\lambda \quad (2.11)$$

where λ is a forgetting factor introduced to weigh the recent data more than the old, $K(k)$ is the estimator gain, $P(k)$ is the covariance estimate and $\varepsilon(k)$ is the difference between the measured and estimated output [9].

2.4.2 Kalman filter

The Kalman filter is a special case of RLS algorithm; the difference is that the parameter variations are modelled as random walks,

$$\theta(k+1) = \theta(k) + \omega(k) \quad (2.12)$$

where $\omega(t)$ is a Gaussian white noise and $\theta(t)$ represents the states which are to be estimated. The measurement $y(k)$ is distorted by a Gaussian noise $\nu(k)$ as well

$$y(k+1) = \varphi^T(k)\theta(k) + \nu(k) \quad (2.13)$$

The iteration steps are similar to the normal RLS case,

$$\hat{\theta}(k) = \hat{\theta}(k-1) + K(k)\varepsilon(k) \quad (2.14)$$

$$K(k) = P(k-1)\varphi(k)(R_\nu + \varphi^T(k)P(k-1)\varphi(k))^{-1} \quad (2.15)$$

$$P(k) = P(k-1) - K(k)\varphi^T(k)P(k-1) + R_\omega \quad (2.16)$$

R_ω and R_ν are the covariances of white noises that are used to replace the noise statistics, and they are considered as tuning parameters. More detailed information can be found in [4]. Since the Kalman filter can not be used directly for nonlinear systems, an extended Kalman filter is required.

2.5 Battery state-of-charge observer

As the description in the introduction section, a Kalman filter is needed in the battery SOC observer and the system is nonlinear according to the open circuit voltage. So, extended Kalman filter is used here.

2.5.1 Extended Kalman filter

Since the Extended Kalman filter will be used for state estimation and not for parameter estimation, the iteration steps for the system are written in the state space form instead of recursive form. The state space equations written as nonlinear equations are

$$\begin{aligned} x_{k+1} &= f(x_k, u_k, \omega_k) \\ y_k &= h(x_k, u_k, \nu_k) \end{aligned} \quad (2.17)$$

A linearization applied to (2.17) at the current working point to get the Jacobian matrices gives

$$\begin{aligned} \hat{A}_k &= \left. \frac{\partial f(x_k, u_k, \omega_k)}{\partial x_k} \right|_{x_k = \hat{x}_k^+} \\ \hat{C}_k &= \left. \frac{\partial h(x_k, u_k, \nu_k)}{\partial x_k} \right|_{x_k = \hat{x}_k^-} \end{aligned}$$

since the input u_k is usually controlled, matrix B and D are related to the control input and are already linear. The iteration steps are,

$$P_k^- = \hat{A}_{k-1}P_{k-1}^+ \hat{A}_{k-1}^T + R_\omega \quad (2.18)$$

$$K_k = P_k^- \hat{C}_{k-1}^T (R_\nu + \hat{C}_k P_k^- \hat{C}_{k-1}^T)^{-1} \quad (2.19)$$

$$\hat{x}_k^+ = \hat{x}_k^- + K_k(y_k - \hat{y}_k) \quad (2.20)$$

$$P_k^+ = (I - K_k \hat{C}_k) P_k^- \quad (2.21)$$

where R_ν and R_ω are the same covariance matrices for the model and measurements as in the Kalman filter, \hat{x}^- and P_k^- are the first calculated states and error covariance matrix according to the state space equations. The Kalman gain K will be calculated based on the predicted and measured system output. The estimated values will be corrected by the Kalman gain K and gives the new states \hat{x}^+ and error covariance matrix P_k^+ .

2.6 Ageing in Lithium Ion batteries

In this segment ageing phenomena occurring in lithium-ion cells are briefly discussed. Also, the combination of different loading conditions which cause different ageing events is presented.

2.7 Ageing in NMC/LMO cells

Lithium-ion batteries are intricate in nature and to study their ageing is even more complicated. The reason for either capacity or power fade cannot be pointed out to a particular reason; they most often result from several processes and interactions that occur inside a battery[24]. Figure 2.3 shows the overall ageing at the interface of the anode-electrolyte interface which is as represented in J. Vetter et al.[22]. Usually, the electrolytes used in the cells are hydrocarbons like LiFP6 along with co-solvents like ethylene carbonates (EC), dimethyl carbonates (DC) and methyl ethyl carbonate (EMC) which are highly reactive. During the formation phase, the electrolytes react with the anode material giving rise to a passivated layer called solid electrolyte interphase (SEI). The layer formed during this phase is favourable as it forms a protective layer covering the anode electrode's surface from further reactions and corrosion of charged electrode figure 2.3. However, at a higher potential, the co-solvents react with the Lithium ions and the reaction products precipitate and grow on the anode surface as shown in figure 2.3 which mainly affects the intercalation and de-intercalation kinetics. The adverse outcome of the SEI layer formation is the loss of cyclable lithium ions as the Lithium ions have to tunnel through these the passive layer to reach the anode and eventually the number reduces[23]. Further, Table 2.1 describes the combination of different loading conditions and its outcome on ageing.

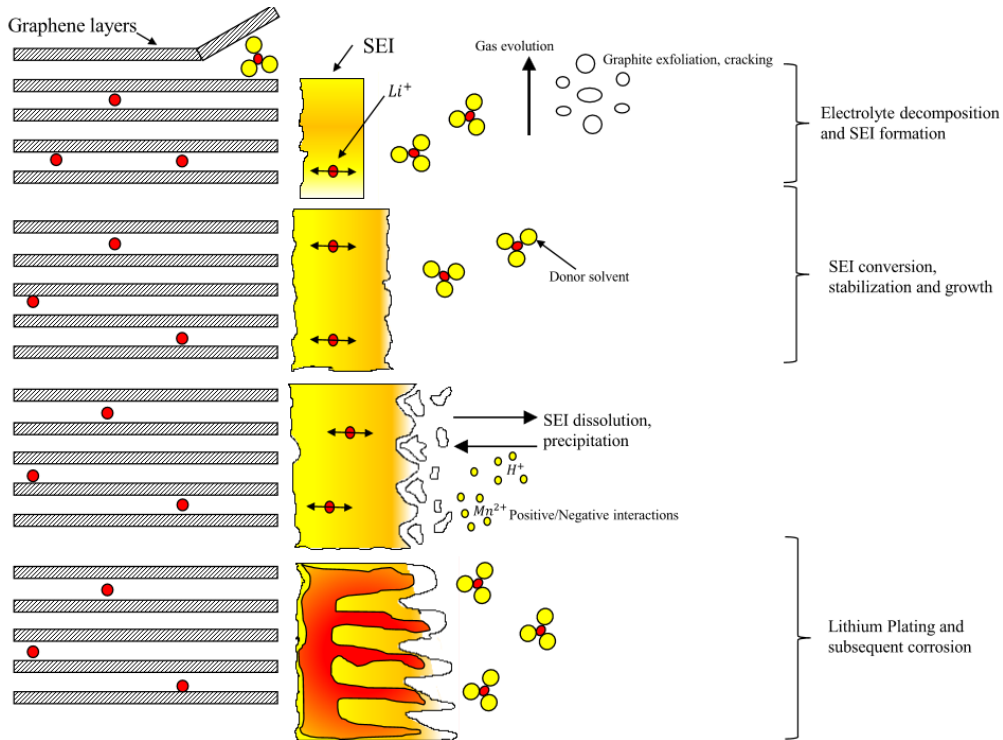


Figure 2.3: Ageing of a NMC cell at the anode electrolyte interface as in J.Vetter et al.

Table 2.1: Loading conditions and the corresponding ageing phenomena

Case	Combination of operating condition	Process at the Anode/Electrode interface	Result	Type of Fade
1	High temperature & high SOC	SEI growth	Loss of Lithium and impedance rise	Capacity and power fade
2	High cycling rate & high DOD	Contact loss of active material	Loss of active material	Capacity fade
3	High cycling rate & high SOC	SEI formation and growth	Impedance rise and Overpotentials	Power fade
4	High cycling rate & low temperature	Metallic lithium plating	Loss of lithium	Capacity fade
5	Overcharge	Gas evolution and cracking	Loss of Lithium and active material	Capacity fade
6	Overdischarge & low SOC	Current collector corrosion	Overpotentials and Impedance rise	Power fade

2.8 Empirical models

Empirical relations like power laws can be used to represent the capacity retention curves for different types of cells. However, there is a need to parameterise empirical relations with the electrochemical models to improve the accuracy as well as understand the behaviour of the ageing in the cells under various conditions. In this section, a brief discussion is presented on how power law and Arrhenius equation can represent ageing data. Also, the integration of single stress models to form a multistress model is explained further in this section.

2.8.1 Power Law

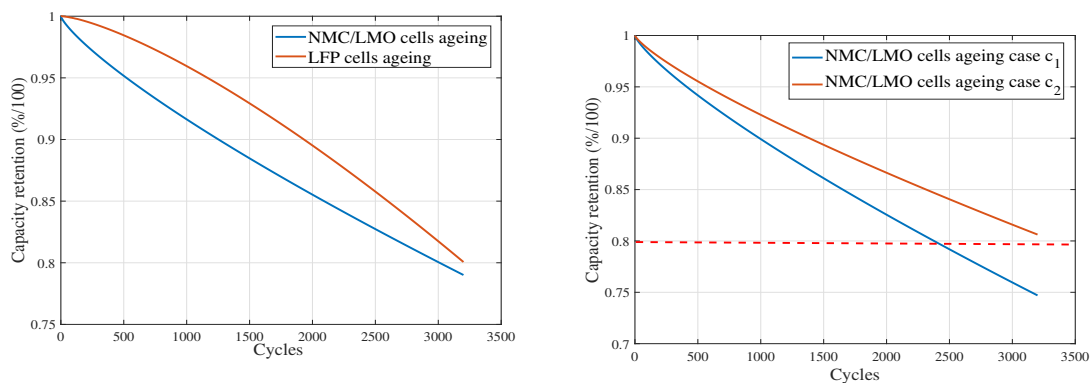
As the time progresses the battery starts to lose its capacity, the relative loss in the capacity is given as

$$\varepsilon = S_0 - S(t) \quad (2.22)$$

where S is the capacity at the beginning of life and $S(t)$ is the capacity at the instant of time. The relative loss in capacity is referred to as the damage measure according to [16], the value of the damage factor is zero at BOL and one at the EOL. The rate at which the damage progresses (capacity reduces) depends on the external operating conditions like temperature, SOC and the current rate. Further, the damage measure points from the experiments can be fitted according to the power law equation

$$\varepsilon(n) = a(p) \times n^b \quad (2.23)$$

where $a(p)$ and b are the curve fitting coefficients. The coefficient a depends on the parameter p which are the operating conditions mentioned above, higher the value of a , more is the stress on the cells. The coefficient b is fixed for a particular type of chemistry and it decides the shape of the aging curve as shown in the figure 2.4a.



(a) Capacity retention curve for LFP and NMC cells at 2C and 25°C. Solid blue is NMC/LMO cells and solid orange is LFP cells
 (b) Ageing of NMC/LMO cells for two cases. Solid blue at 2C rate and 30 °C, solid orange at 2C rate and 40 °C

Figure 2.4: Shaping factor b and severity factor a

The above figure illustrates the shaping factor b and variation of severity factor b . As mentioned before the capacity retention shape differs from one chemistry to another as in the figure 2.4a, LFP cells have a shaping factor which is above 1 and for NMC cells it is less than 1. The process of calculating this is illustrated in chapter 7. In this thesis, a purely statistical approach is followed which might affect the accuracy of the model since the shape of the ageing curve is also dependent on the type of the ageing mechanism (which is dependent on the loading condition). Another vital term is the severity factor a which is dependent on the loading conditions like temperature, SOC and C-rate. Figure 2.4b depicts two conditions, namely case c_1 and case c_2 at 2C rate, 90% SOC and 30 and 40°C respectively. It is apparent from the figure that the second case reaches the EOL faster, meaning that the rate of change of capacity is higher for c_1 . In the ageing model/ power law, the severity factor a guides the rate of capacity retention. The method of parameterising a is described in chapter 6 and 7. The stress factors obtained from the experimental data is purely empirical involving polynomial equations in which temperature, SOC and C-rate as variables. Y Cui et al.[14] used the Arrhenius expression to fit the irreversible loss of capacity due to parasitic reactions to represent the severity factor a as

$$a = A \times \exp\left(\frac{-E_a}{RT}\right) \quad (2.24)$$

where A is the pre exponential factor, E_a is the activation energy and R is the universal gas constant. The relation between the empirical equation (2.24) and Tafel's equation is described in the next section.

2.8.2 Relation between the Tafel's equation and Arrhenius equation

According to [14], the Tafel equation can be used to represent the parasitic reaction. These are the reactions that cause irreversible loss of lithium ions which is very much in line with the assumption that the loss of lithium ions is the primary reason for the capacity loss. The Tafel equation is given as

$$i = i_o \exp\left(-\frac{\alpha F n_o}{RT} \eta_s\right) \quad (2.25)$$

where, F is Faraday's constant, i_o is exchange current density, α is charge transfer coefficient, n_o is the number of transferred electrons, η_s is the overpotential and i is the parasitic reaction current. Integrating (2.25) over time gives the capacity loss. Y.cui et al.[7] compared the Tafel equation with the Arrhenius equations and gave an equation for capacity loss as

$$Q_{loss}(T, Ah) = A \exp\left(-\frac{E_a}{RT}\right) (Ah)^b \quad (2.26)$$

where E_a is the activation energy and corresponds to the numerator of the exponential term in (2.25), R is the ideal gas constant, A is the rate constant(or called as the pre-exponential factor), and T is the temperature in Kelvin. The complete loss of capacity is based on (2.26) where parametrised severity factor plays an important role. Nevertheless, ampere hour throughput(or charge) plays an important

part in the capacity fade. The rate constant and activation energy vary based on the loading conditions like the current-rate, temperature and the SOC value as shown in [16]. Hence, there is a need for parameterizing A and E_a as a function of these loading conditions.

2.8.3 Parameterised Aging model

A Multi-stress model is built based on the expression (2.26) by parameterising the pre-exponential A as a function of SOC and C-rate apart from solely being a function of temperature and capacity throughput. The pre-exponential factor $A(p)$ is made of single stress model $A(\text{SOC})$, $A(\text{C-rate})$. The combined multi stress is given as

$$Q(\text{SOC}, T, C - \text{rate}, Ah) = A(\text{SOC}) \cdot A(\text{C-rate}) \cdot \exp\left(\frac{-E_a}{RT}\right) \cdot (Ah)^b \cdot A_e \quad (2.27)$$

the term A_e is a fitting term which is used to tune the model to the experimental data. If the value of this term is greater or less than one, it signifies that the model deviates from the assumption that loss of active anode is the main reason for the loss of capacity. Figure 2.5 shows the process of building an empirical aging model.

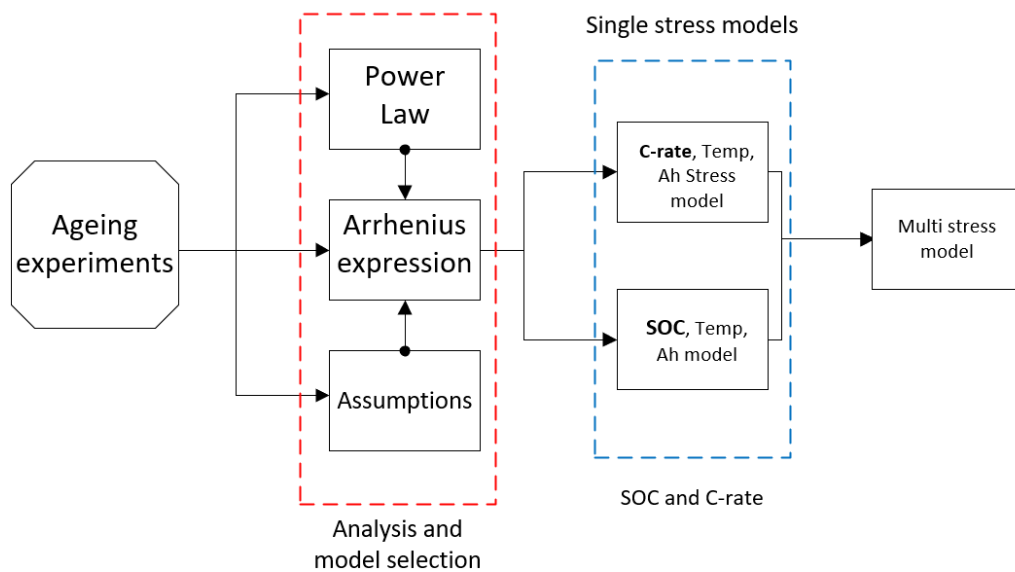


Figure 2.5: The structure of the proposed empirical aging model

3

Test cases for SOC estimation

3.1 Synthetic data test

To validate the algorithm accuracy, each parameter value is needed to be known, and the system behaviour should be fixed in the expected region. Therefore, a single-RC simulation model is used to create the voltage signals for all the test cases. Since the system is online, the equations which represent the voltage drop across the cell (u_{cell}), the RC network (u_{RC_1}) and the SOC (z_{soc}) are discretized with sampling time Δt and the zero order hold method. The discrete state space equations are,

$$u_{RC_1}(k+1) = e^{-\frac{\Delta t}{R_1 C_1}} u_{RC_1}(k) + R_1(1 - e^{-\frac{\Delta t}{R_1 C_1}}) i_{cell}(k) \quad (3.1)$$

$$z_{soc}(k+1) = z_{soc}(k) + \frac{\eta \Delta t}{Q_{nom}} i_{cell}(k) \quad (3.2)$$

$$u_{cell}(k) = u_{ocv}(z_{soc}(k)) + u_{RC_1}(k) + R_0 i_{cell}(k) \quad (3.3)$$

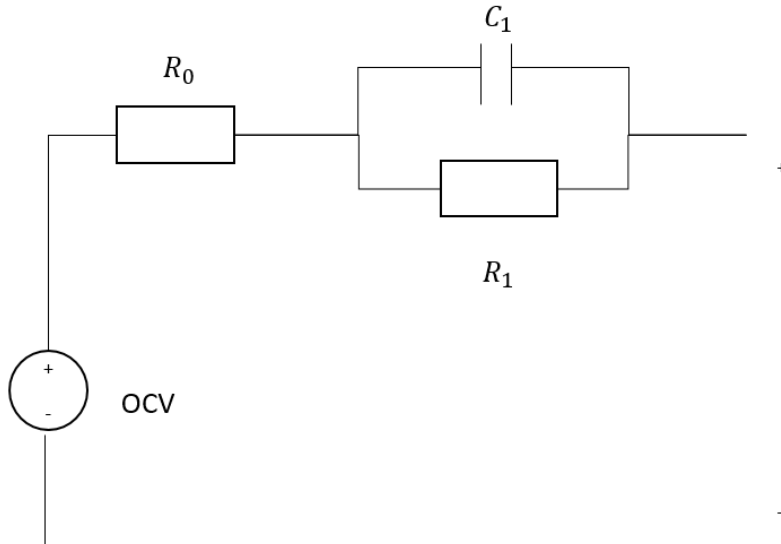


Figure 3.1: Structure for the simulation model

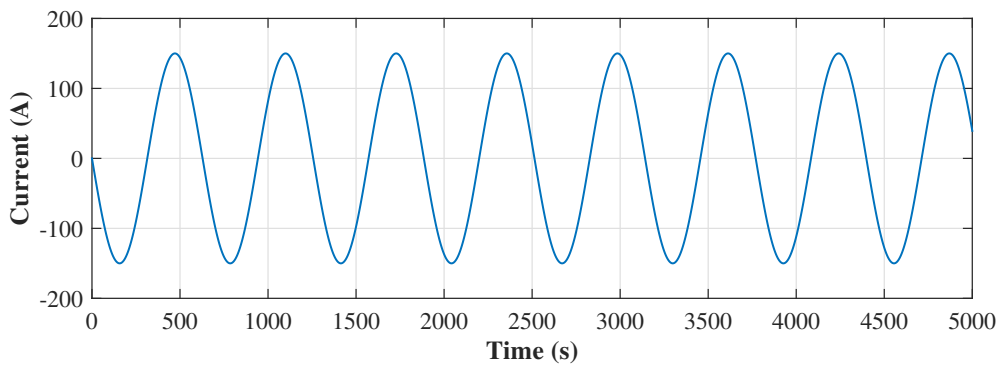
where, u_{RC_1} is the voltage across the RC_1 network, τ is the time constant which depends on the value of R_1 and C_1 elements, R_0 is the ohmic resistance, z_{soc} is the state of charge calculated using coulomb counting.

3.1.1 Input signals

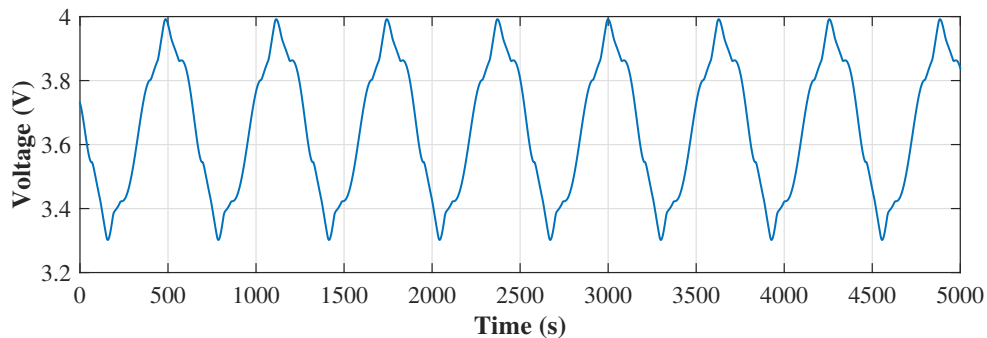
Two different kinds of input signals have been used in this report. One is the sine wave and the other is the NEDC test cycle which is provided by CEVT.

3.1.1.1 Sine-wave

A sine wave shaped signal is used in order to have a basic stability test for the estimation algorithms. The sine wave has a fixed frequency which is helpful in finding the bandwidth of the system. Also, the sine wave has a nonlinear differential value with time progress, and this can cover more situations (or conditions) than a first order step input signal.



(a) The sin-wave input current signal



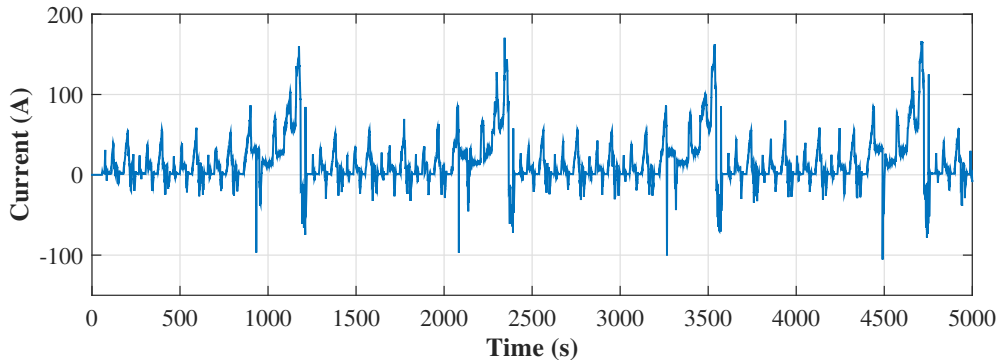
(b) The output voltage signal based on the simulation model

Figure 3.2: Sin-wave test inputs

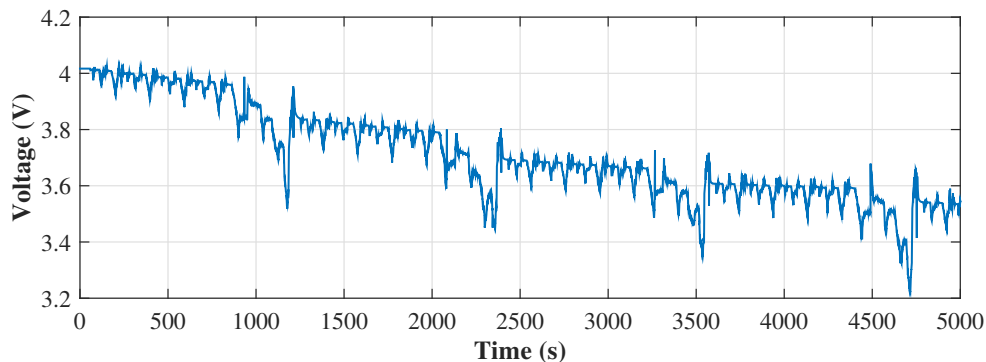
As shown in figure 3.2a, the sine wave current has an amplitude of 150A and a frequency of 0.01(rad/s). The corresponding voltage is as shown in the figure 3.2b.

3.1.1.2 NEDC test cycle

A driving cycle as shown in figure 3.3a is used as a test case, it represents five consecutive NEDC cycles. Figure 3.3a and figure 3.3b show the current and voltage drop (U_{cell}) respectively. Since the whole algorithm is a closed loop estimation meaning which the estimation error generated in one block will affect the estimation of the other block. Hence, the complete algorithm must be capable of working under practical conditions and it is one of the main motive.



(a) The NEDC test cycle input current signal



(b) The output voltage signal based on the simulation model

Figure 3.3: NEDC test inputs

3.1.1.3 Noise signals

The stability of the system is a point of concern under noisy conditions. In this thesis white noise is used to evaluate the algorithm performance under extreme conditions. Noise signals are added to the sine wave, and to the NEDC test signals after which the parameters of the system will be tuned accordingly.

3.1.2 Validation test for ohmic resistance R_0 estimation

Estimation of R_0 is a part of the algorithm, to test its estimation all the parameters are fixed. The inputs and outputs illustrated in figure 3.2a and 3.3a will be used during the trial, and a 1-D look table with reference R_0 as a function of SOC will be

3. Test cases for SOC estimation

employed. The purpose of the validation test is only to check whether estimation function can catch up the reference R_0 or not.

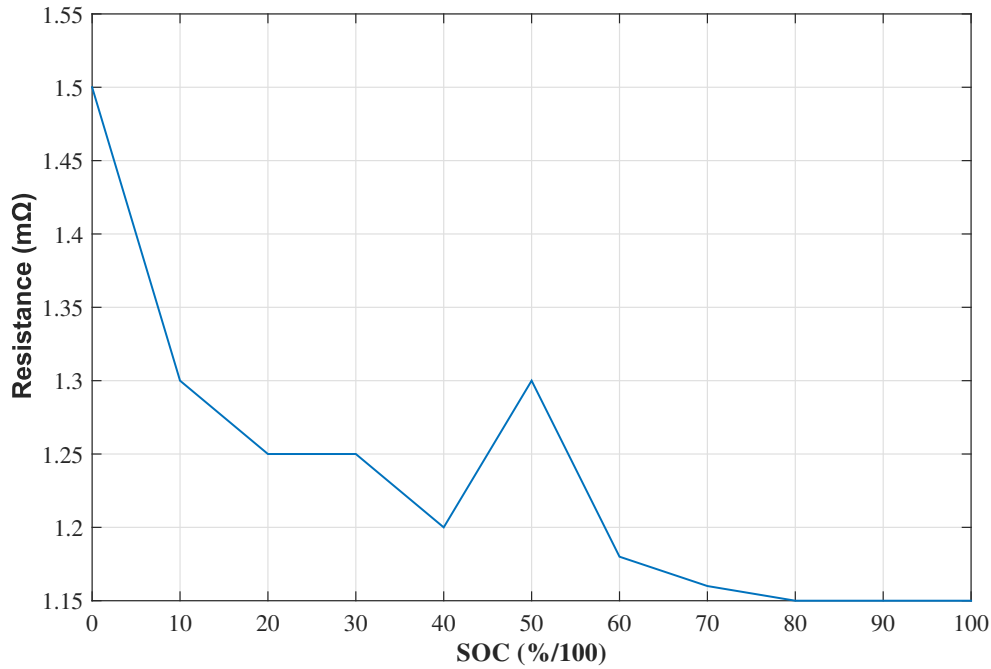


Figure 3.4: 1-D Look-up table for R_0

The most important factor which influences the R_0 estimation accuracy is the sampling time. Hence, tests with higher, optimal and lower sampling time will be conducted to understand the influence of sampling time on the estimation

3.1.3 Validation test for time constant τ estimation

Similar to the previous case, for the estimation tests of τ all the parameters are fixed. A 1-D look up table with τ as shown in the figure 3.5 is used to check if the estimation is in tact with the reference value. Also, both test inputs (i_{cell} and U_{cell}) are used to verify the function behaviour.

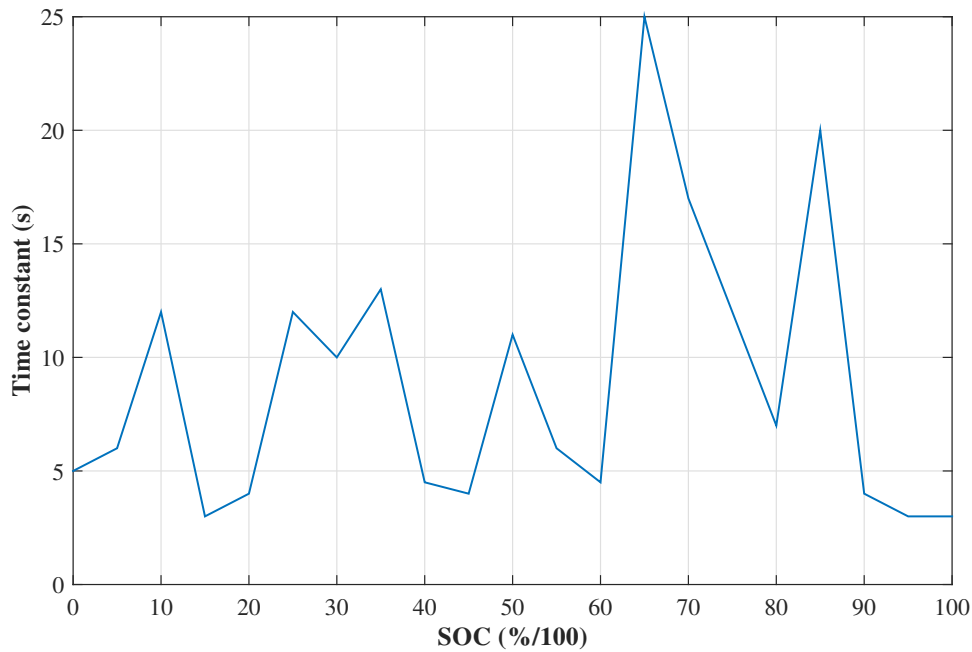


Figure 3.5: 1-D Look-up table for τ

3.1.4 Validation test for SOC estimation

In these segment, a series of tests with different initial guesses will be conducted for the Extended Kalman filter. All the parameters of the system will be provided to the Extended Kalman filter instead of using the estimated value. Similar to the previous test cases, both test inputs are used to check the function behaviour.

3.1.5 Combined test with complete algorithm

For these tests all the three estimation blocks will be connected to each other. Unlike the previous test cases, the test with all estimation functions will only be based on the cell current and voltage. The result of the complete algorithm test will shows the system performance.

4

Available data and cell specifications

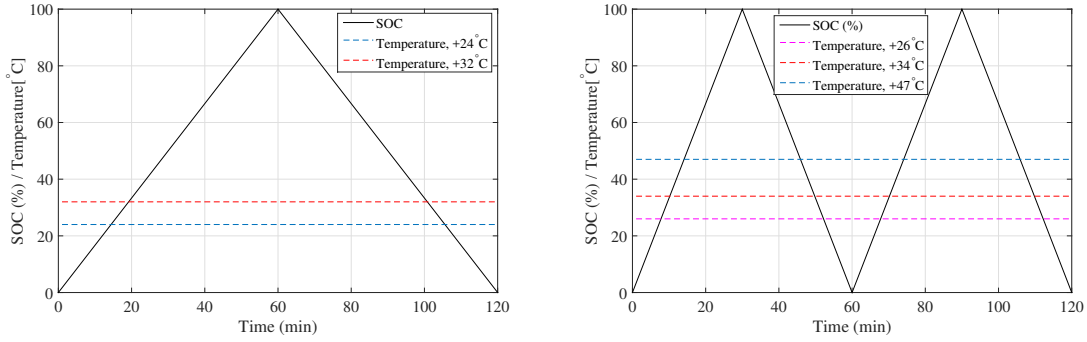
4.1 Available test data

Simple charge and discharge cycles with constant currents at different temperatures reveal the cell behaviour precisely rather than analyzing with dynamic load cycles like the Hyzem and NEDC drive cycles. The current levels tested in this thesis are 1, 2, 3 and 4C at temperatures ranging from 24°C to 50°C. To identify the effect of SOC window, cycles with 10% and 20% SOC windows are used at a constant temperature and current. To simplify the notation of these drive cycles, they are coded as CXDYTUSZ where, C, D, T and S stand for charge and discharge rates, temperature and SOC with X, Y, U and Z values respectively. The first 120 minutes of the test data and the model inputs are as shown in the figure 4.2.

Table 4.1: Test data available for LFP cells[19]

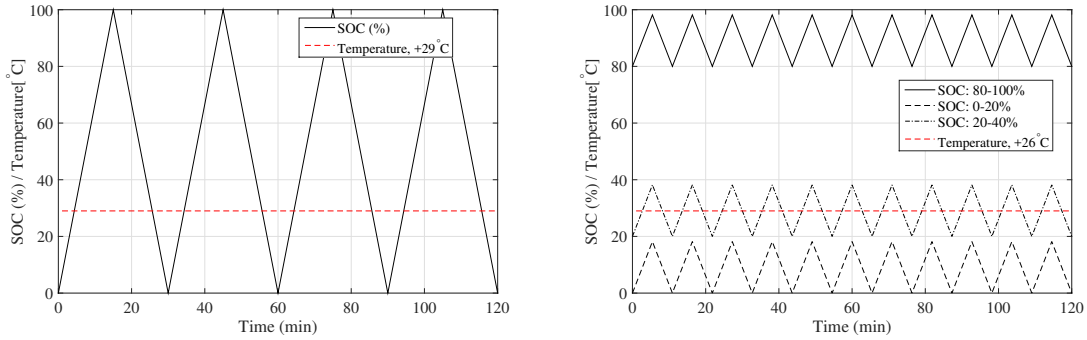
Data ID	Charge/Discharge rate	Temperature [°C]	SOC range [%]
C2D2T25S0-0.9	1/1, 2/2, 3/3	25	0-100
C2D2T35S0-0.9	1/1, 2/2, 3/3	35	0-90
C2D2T45S0-0.9	1/1, 2/2, 3/3	45	0-90
C2D2TXSY-Y	4/4	25,35,45	20% window from X to X range

4. Available data and cell specifications



(a) Black solid: SOC, red dash: $32^{\circ}C$, (b) Black solid: SOC, megenta: $26^{\circ}C$, blue dashed: $24^{\circ}C$, red: $34^{\circ}C$, blue: $47^{\circ}C$

Figure 4.1: Obtaining the OCV curve



(a) Black solid: SOC, red: $29^{\circ}C$

(b) Different SOC ranges at $29^{\circ}C$

Figure 4.2: Available data and model inputs

For NMC/LMO cells, most of the data available is with a C-rate of 2C, which was one of the setbacks during the model development. However, there was massive testing data at different temperatures and SOC ranges. The author in [21] has performed SOC dependent ageing experiments with a SOC window of 10% at $25^{\circ}C$, $35^{\circ}C$ and $45^{\circ}C$ which helped in extending the model operation zone. The built model is validated against a physics based ageing model developed by the author of [21]. Finally, the results established in this thesis is compared with the experimental data in [21].

Table 4.2: Test data available for NMC/LMO cells

Data ID	Charge/Discharge rate	Temperature [$^{\circ}C$]	SOC range [%]
C2D2T25S0-0.9	2/2	25	0-90
C2D2T35S0-0.9	2/2	35	0-90
C2D2T45S0-0.9	2/2	45	0-90
C2D2TXSY-Y	2/2	25,35,45	10% window spread over 0 - 100%
Validation test	2/2	25	0-90 (Comsol data)

4.2 Cell Specifications

Cell Specifications	Cell A	CellB
Cathode	LFP	NMC(70wt%) and LMO(30wt%)
Anode	Graphite	Graphite
Capacity	2.3 Ah	26 Ah
Nominal voltage	3.3 V	NA
Maximum discharge current	70 A continuous	NA
Charge current	10 A continuous	NA
Type	Cylindrical	Pouch

5

Method for SoC estimation

5.1 Battery parameters estimation

Based on the previous description, a single RC model will be used by the Extended Kalman filter for estimating the SOC. The equivalent circuit model [2] discretized with sampling time Δt and zero order hold is given as,

$$u_{RC}(k+1) = e^{-\frac{\Delta t}{RC}} u_{RC}(k) + R(1 - e^{-\frac{\Delta t}{RC}}) i_{cell}(k) \quad (5.1)$$

$$z_{soc}(k+1) = z_{soc}(k) + \frac{\eta \Delta t}{Q_{nom}} i_{cell}(k) \quad (5.2)$$

$$u_{cell}(k) = u_{ocv}(z_{soc}(k)) + u_{RC}(k) + R_0 i_{cell}(k) \quad (5.3)$$

the Coulombic efficiency η and nominal capacity Q_{nom} are constants. The ohmic resistance R_0 changes as the current changes, while u_{RC} correspond to a slower effect. To improve the accuracy, the estimation part has been divided into two parts as:

- Ohmic resistance estimation
- RC parameter estimation

5.1.1 Ohmic resistance estimation

For a short sampling time both u_{ocv} and u_{RC} are almost unchanged [2]. Therefore, R_0 is written as,

$$R_0 = \frac{u_{cell}(k) - u_{cell}(k-1)}{i_{cell}(k) - i_{cell}(k-1)} \quad (5.4)$$

by changing the input to $u_{cell}(k) - u_{cell}(k-1) = \Delta u_{cell}(k)$ and $i_{cell}(k) - i_{cell}(k-1) = \Delta i_{cell}(k)$, a recursive form equation can be written as,

$$\Delta u_{cell}(k) = R_0 \Delta i_{cell}(k) \quad (5.5)$$

this form is implemented in the RLS algorithm (2.8)-(2.11). Further improvements in Ohmic resistance estimation will be discussed in the following sections.

5.1.2 RC parameter estimation

The exponential term in (5.1) can be split into α and β as

$$\alpha = e^{-\frac{\Delta t}{RC}}$$

$$\beta = R(1 - e^{-\frac{\Delta t}{RC}})$$

also from the general structure, the estimated state of charge will be sent into the estimation steps to create a new measurement signal as,

$$y(k) \triangleq u_{cell}(k) - u_{ocv}(\hat{z}_{soc}(k)) - R_0 i_{cell}(k)$$

if the estimation of the state of charge is correct, then the measurement signal $y(k)$ is the same as u_{RC} . As a result, the time constant of the simplified single RC model can be estimated from the recursive form,

$$y(k+1) = \alpha y(k) + \beta i_{cell}(k) \quad (5.6)$$

by defining the parameters vector,

$$\theta = \begin{pmatrix} \alpha \\ \beta \end{pmatrix}$$

and the state vector,

$$\varphi = \begin{pmatrix} y(k) \\ i_{cell}(k) \end{pmatrix}$$

to improve the RLS algorithm behaviour, the sampling time should be a proper value according to the time constant. Otherwise, two parameters which are to be estimated will be either 1 or 0. Introducing an error term $e(k)$ in creating a measurement signal gives

$$y(k) \triangleq u_{cell}(k) - u_{ocv}(\hat{z}_{soc}(k)) - R_0 i_{cell}(k) + e(k)$$

then the recursive form of one RC model becomes,

$$y(k+1) = \alpha y(k) + \beta i_{cell}(k) + e(k) - \alpha e(k-1) \quad (5.7)$$

estimation of R and C will be based on the Kalman filter algorithm according to (2.14) - (2.16), where R_v and R_w are designed by testing several data cases.

5.2 Factors influencing the accuracy

As the system is built on two estimators interlinked, there will be several key factors lowering down the estimator accuracy and even causes self-oscillation of the system. In this section, such elements and methods to overcome them are discussed.

5.2.1 Model errors

Since one RC model is used to predict the plant model, the output errors cannot be avoided and these errors will cause a drift in estimation.[2] There are three main error factor:

- Undermined behaviour according to some long time constant.
- Gaussian noise in both current and voltage.

- OCV fitting errors.

Since the errors are composed of these three factors and most of them are not included in the model structure, a model for the error should be built. According to results from the model simulation with no error term included, the estimation error shows a steady bias with slow changing rate. Hence, a reasonable model for the error can be written as,

$$e(k) = ce(k-1) + \nu(k) \quad (5.8)$$

where c is a parameter defining the correlation between the error and the white noise which will be determined by the estimator. Another problem is that the noise term is unknown and it is required to represent the input of the estimator. One way to deal with this problem is to use the estimation error term in the RLS algorithm as,

$$\varepsilon(k) = y(k) - \varphi^T(k)\hat{\theta}(k). \quad (5.9)$$

5.2.2 Dead zone in RLS method

A normal ohmic resistance estimation method has been shown in (5.4)-(5.5). However, it can not handle noisy signals. A dead zone is added into the ohmic resistance estimation to prevent the noise covariance matrix which is winded up by the white noise. Using difference of two steps between input and output, a dead zone can filter most of small current and voltage changes caused by white noise and it lowers down the reaction speed to an acceptable level. The subsequent iteration for ohmic resistance estimation is,

$$\hat{R}_{ohm}(k) = \hat{R}_{ohm}(k-1) + K_R(k)(\Delta u_{cell}(k) - \hat{R}_{ohm}(k-1)\Delta i_{cell}(k))$$

and the RLS gain becomes,

$$K_R(k) = \left\{ \begin{array}{l} \frac{P_R(k-1)\Delta i_{cell}(k)}{\lambda + \Delta i_{cell}^2(k)P_R(k-1)}, \quad \text{if } |\Delta i_{cell}| > \text{deadzone} \\ 0 \end{array} \right\} \quad (5.10)$$

5.2.3 Time variant forgetting factor in RLS method

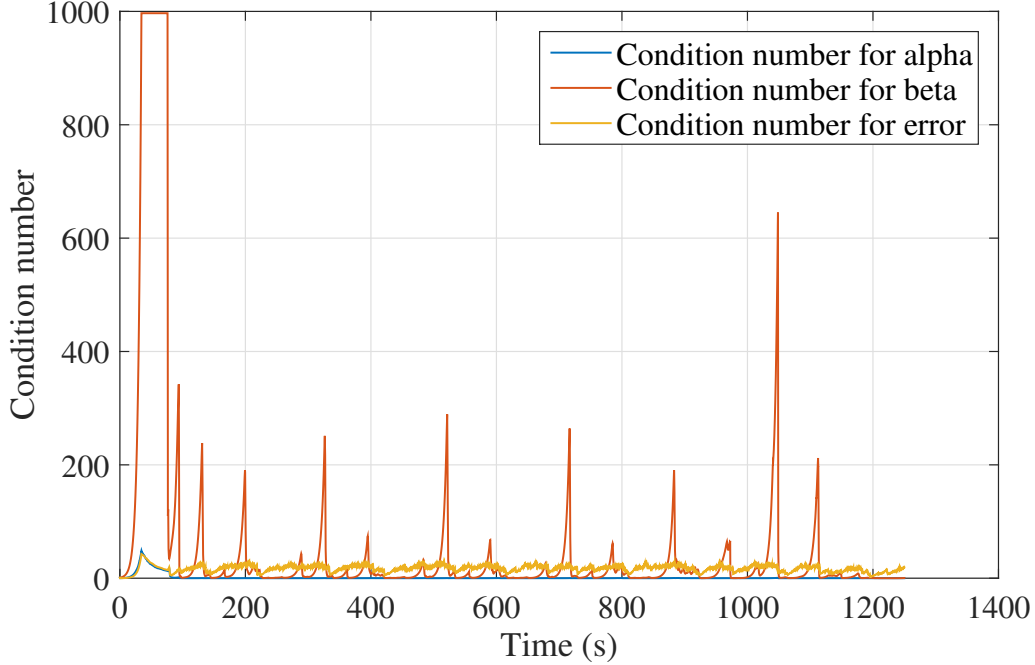


Figure 5.1: Noise covariance winded up problem

As figure 5.1 shows, a typical RLS directly implemented to the noisy signal will cause the noise covariance matrix to wind up, which makes the estimation oscillate around the actual value. To prevent the covariance matrix P to be winded up by the noise, a forgetting factor λ should be used, which is a time-varying factor that varies with the current estimation accuracy. At the same instant, the covariance matrix updating iteration is limited to prevent the wind-up problem. The RLS algorithm is as shown in (2.8)-(2.11), the difference in the iteration is,

$$\lambda(k) = 1 - \frac{\varepsilon^2(k)}{1 + \varphi^T(k)P(k-1)\varphi(k)}$$

$$W(k) = I - K(k)\varphi^T(k)P(k-1)$$

$$P(k) = \begin{cases} \frac{W(k)}{\lambda(k)}, & \frac{W(k)}{\lambda(k)} \leq C \\ W(k), & otherwise \end{cases}$$

where C is a predefined matrix to limit the covariance matrix. Figure 5.2 shows the condition number restricted by using the time-varying forgetting factor in the same test condition.

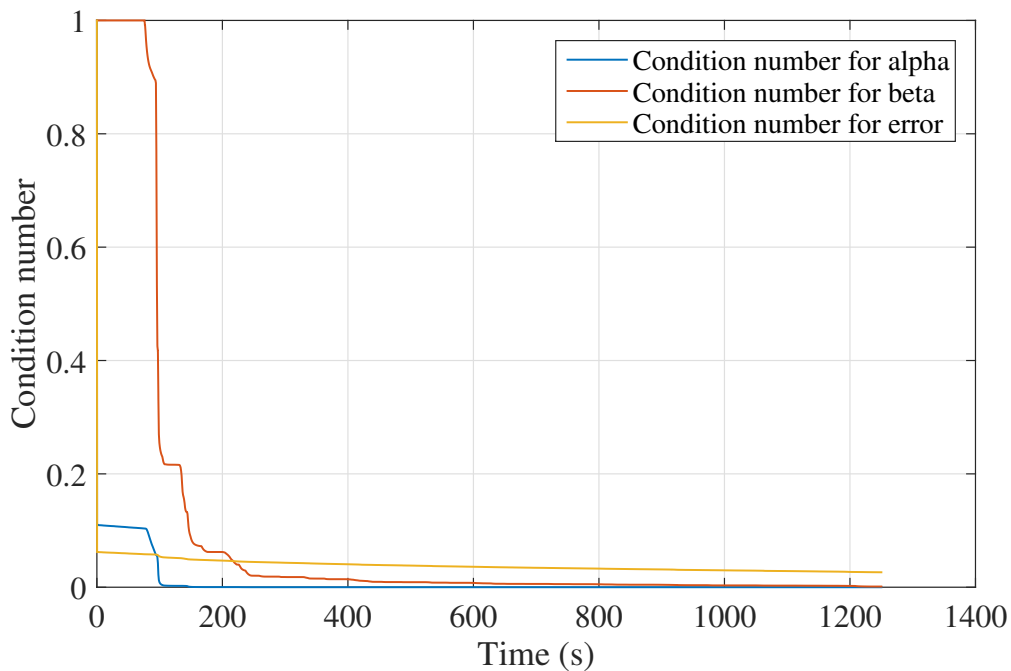


Figure 5.2: Noise covariance limited by time variant forgetting factor

5.2.4 Adaptive Kalman filter

An alternative method to bypass noise covariance winded-up is to change the RLS algorithm to an adaptive Kalman filter. In the original Kalman filter (2.14)-(2.16), the matrix R_w is a user defined value and it will affect the covariance matrix P calculation. In the adaptive Kalman filter, the covariance matrix P has a user-defined destination P_d which means that all the values in P have only one direction to go and there is no chance to wind up. Therefore, the matrix R_w need not be defined anymore, and it is now a function of P_d . The new equation for R_w is,

$$R_w(k) = \frac{P_d \varphi(k) \varphi^T(k) P_d}{R_v(k) + \varphi^T(k) P_d \varphi(k)} \quad (5.11)$$

With the implementation of updating algorithm to the Kalman filter iteration (2.14) to (2.16), the noise covariance matrix can be well limited. However, the reaction speed of the system is not as expected.

5.2.5 Data scaling

To get a better accuracy in the estimation, the input and output should be scaled to the same magnitude. That is because the correction gain in the estimation function uses the calculation errors. Otherwise, the estimation results will probably not converge to the reference value. Scaled measurements $\tilde{y}(k) = k_u y(k)$, $\tilde{i}_{cell}(k) = k_i i_{cell}$ are put into (5.7) which gives,

$$\tilde{y}(k+1) = \alpha \tilde{y} + \frac{k_u}{k_i} \beta \tilde{i}_{cell}(k) + k_u e(k) - k_u \alpha e(k-1). \quad (5.12)$$

5.3 State-of-charge estimation

This section will explain the method for state-of-charge estimation. Since there is a non-linear element which is the OCV curve in the state space equation, several steps are to be performed to make the non-linear function function reasonably in the estimator.

5.3.1 State space equation building

As discussed in the theory before, the Extended Kalman Filter (EKF) will majorly be involved in the estimation. A series of state space equations are required for the EKF based on (5.1)-(5.3), and they are,

$$x(k+1) = A_k x(k) + B_k u(k) + N_k \omega(k) \quad (5.13)$$

$$y(k) = C_k x(k) + D_k u(k) + \nu(k) \quad (5.14)$$

where A_k and B_k contains the battery parameters and the Coulomb counting equation for the SOC.

$$A_k = \begin{pmatrix} \alpha & 0 \\ 0 & 1 \end{pmatrix}$$

$$B_k = \begin{pmatrix} \beta \\ \frac{\eta \Delta t}{Q_{nom}} \end{pmatrix}$$

$$C_k = \begin{pmatrix} 1 \\ f_{u_{ocv}}(z_{soc}) \end{pmatrix}$$

$$D_k = R_0$$

Since, all the information in the matrix A_k , B_k and D_k are real time estimates, they can be considered as linear terms at that instant of time. It is clear that the function of OCV in matrix C_k is nonlinear. Therefore, linearization of the OCV function is required [3], and Matlab curve fitting tool is used.

5.3.2 Curve-fitting for OCV

Figure 5.3 shows the agreement between the fit curve and the experimental data for the OCV curve of NMC/LMO cell [10]. It is evident that there are only two data points for SOC ranges below 0.025 which leads to errors. Hence, the data points below 0.025 are neglected, and a linear fit is used to guide the Kalman filter to identify the changing trends in the OCV [3].

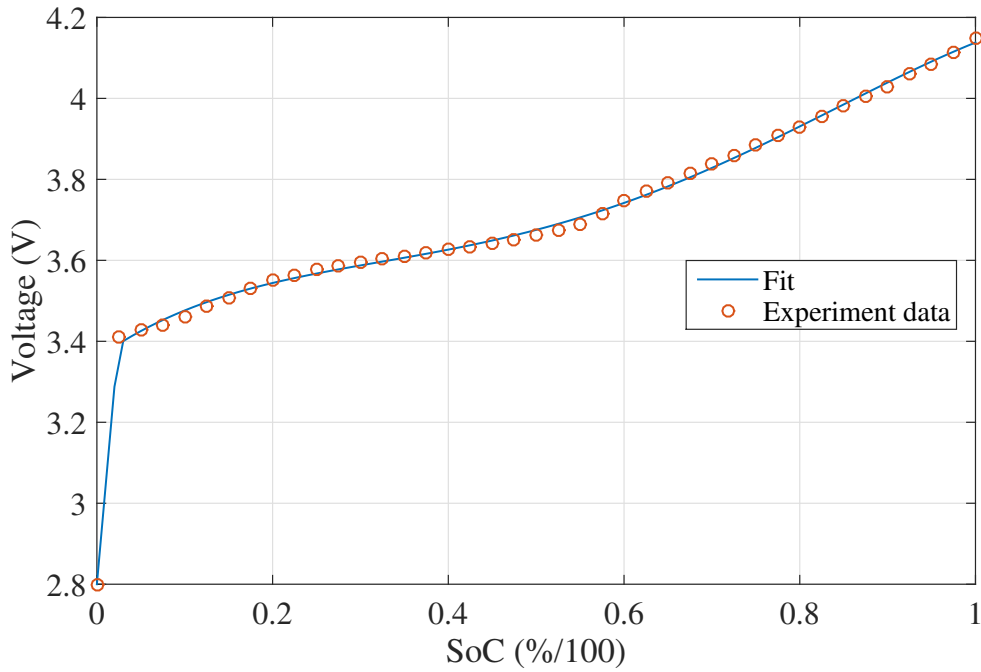


Figure 5.3: Fitted OCV curve

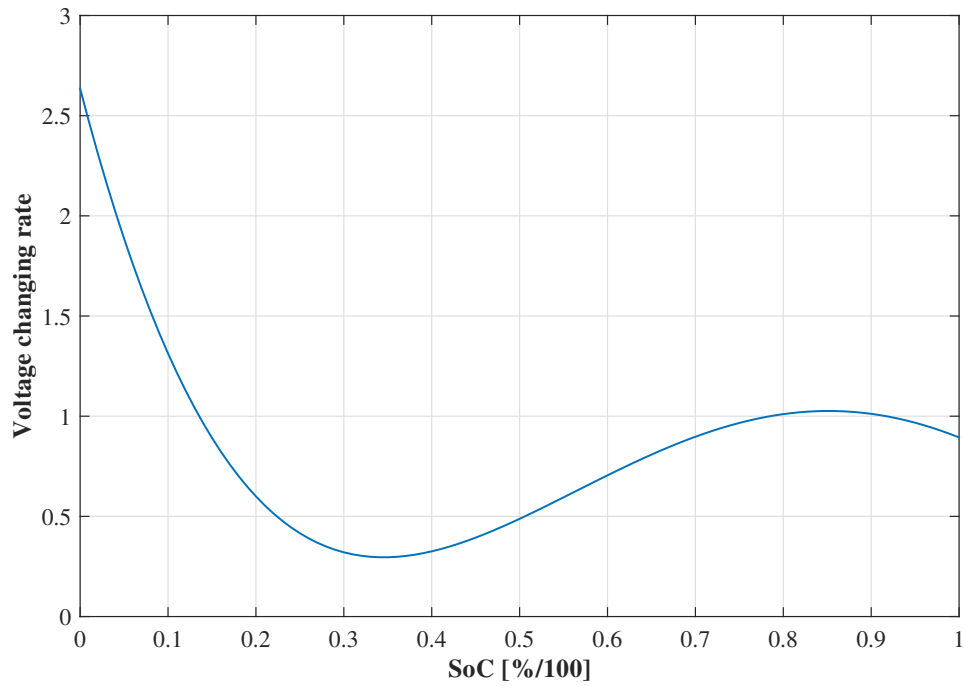


Figure 5.4: Relationship with OCV, OCV changing rate and SoC

A fourth order polynomial function is used to fit the curve. For convenience, the equation is written in a matrix form as,

$$u_{ocv} = \theta_{ocv}^T \varphi_{ocv} \quad (5.15)$$

where

$$\theta_{ocv} = \left(-2.498 \quad 5.843 \quad -4.102 \quad 1.537 \quad 3.358 \right)^T$$

$$\varphi_{ocv} = \left(z_{soc}^4 \quad z_{soc}^3 \quad z_{soc}^2 \quad z_{soc} \quad 1 \right)$$

this form makes the fitted curve usable in the EKF. The derivative of the curve and the intersection should be calculated online while estimating. As figure 5.4 shows the slope changes as SOC goes from 0 to 1. The EKF only works for the zero mean value. Thus the intersection is needed in the estimation process, and it can be calculated by,

$$b = u_{ocv} - \dot{u}_{ocv} z_{soc} \tag{5.16}$$

where b is the intersection of current linearization of the curve. While implementing the linearization result in the EKF, the intersection should be removed. In (5.14), the measurement of the new signal $y(k) = u_{cell} - \hat{R}_{ohm} i_{cell} - b$ is implemented in the EKF.

6

Calculations for Aging models for LFP cells

6.1 Model A

To start with, a verification model is built using the data presented by the author in [19] and is addressed as Model A.

6.1.1 Temperature and C-rate dependent loss factor

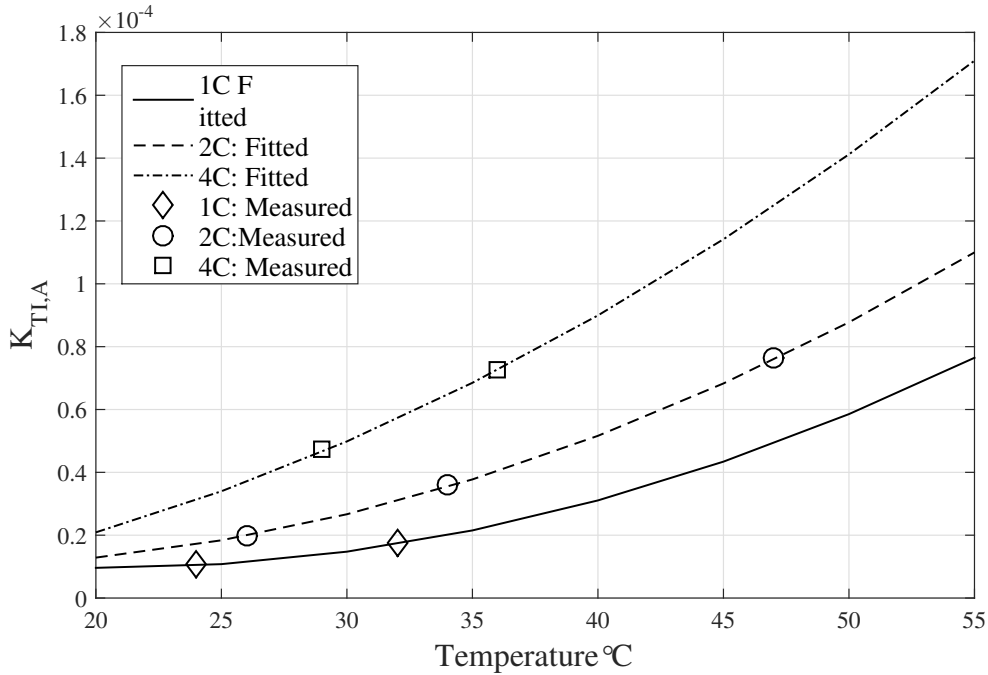


Figure 6.1: Ageing function $K_{TI,A}$ (LAAM - Loss of Active Anode Material) measured values and Fitted curves for C1D1T24-32S01, C2D2T26-34-47S01, C4D4T29-53S01 cycles. Where T24-32, T26-34-47 and T29-53 represent the loading conditions at different temperatures.

The author in [19] has measured LAAM (Loss of Active Anode Material) for the above mentioned cycles and fitted a second order polynomial equation as

$$K_{TI,A/L} = k_{1,A/L} + k_{2,A/L}T + k_{3,A/L}I + k_{4,A/L}T^2 + k_{5,A/L}TI + k_{6,A/L}I^2 \quad (6.1)$$

where, T is the temperature, and I is the C-rate, A is the anode, and L is the lithium, the coefficients $k_{1-6A/L}$ are based on a fitting algorithm. The same equation holds good for loss of cyclable lithium with different coefficients. Loss of cyclable lithium has a linear relation with temperature and on the other side LAAM has an exponential trend.

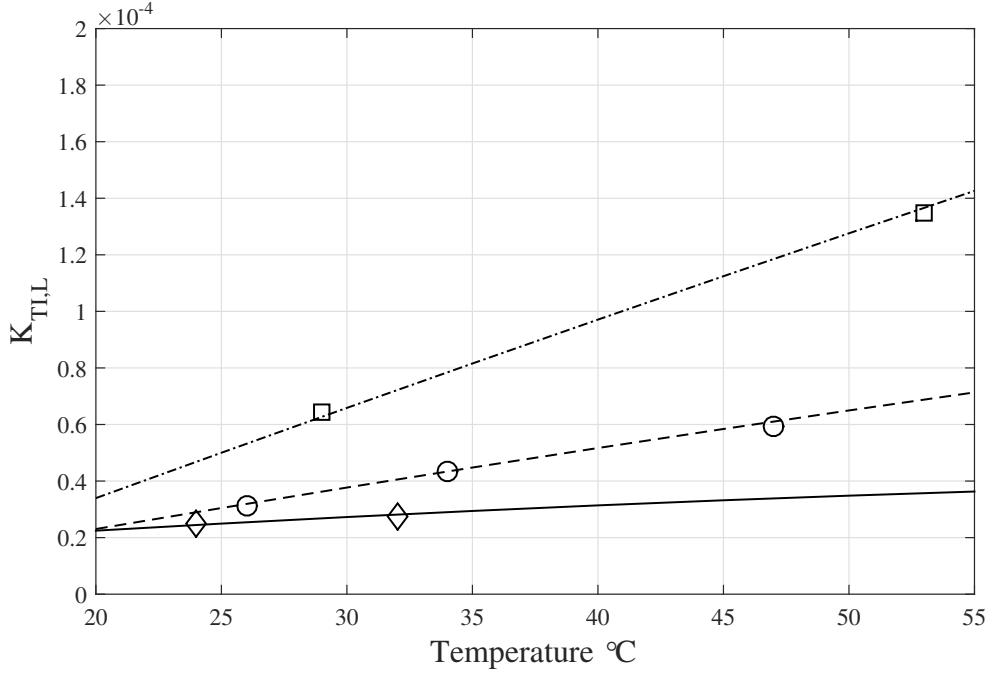


Figure 6.2: Ageing function $K_{TI,L}$ Fitted values for C1D1T24-32S01, C2D2T26-34-47S01, C4D4T29-53S01 cycles

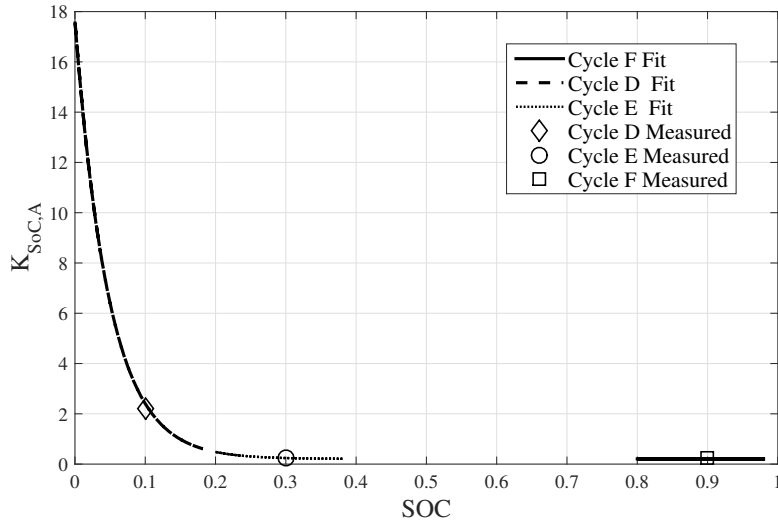
6.1.2 SOC window loss function

Similar to the loss factors in the previous section the author in [19] has measured the losses and modelled an exponential empirical equation for different SOC ranges with fixed SOC window of 20%. The equations are

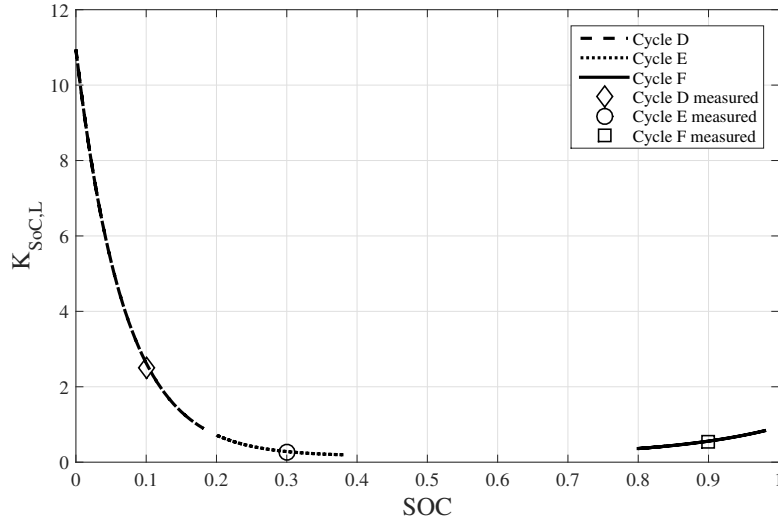
$$K_{SoC,A} = k_7 \exp(-k_8 SoC) + k_9 \quad (6.2)$$

$$K_{SoC,L} = k_{10} \exp(-k_{11} SoC) + k_{12} \exp(-k_{13} SoC) + k_{14} \quad (6.3)$$

where, subscripts A and L stand for anode and lithium. These two SOC related loss functions are shown in figure 6.3 (a) and (b) respectively.



(a) LAAM



(b) Loss of cyclable lithium

Figure 6.3: SOC window loss function for C4D4T29S0-20, 20-40 and 80-100 cycles.

A notable observation can be made from the above figures that, the loss of lithium is high for extreme low SOC region in case of LAAM, and in the event of loss of cyclable lithium it is high for both shallow and high SOC regions.

6.1.3 Loss function dependent on capacity throughput of segment on the Anode

According to [19] the current flowing in each segment of the anode depends on its distance from the separator. Usually, the current is highest in the segment closest to the separator, and hence the capacity throughput of this segment will be the

highest. This loss function is defined as

$$K_{CT} = CT_{segment}/CT_{cell} \quad (6.4)$$

where,

$$CT_{Cell} = 5 \int_0^{t_{end}} |I_{segment}| dt / 2Q_{ref,cell} \quad (6.5)$$

where, $Q_{ref,cell}$ is the total cell capacity in As. $I_{segment}$ is the segment current, for simplicity it is assumed to have a uniform throughput and hence, $I_{segment} = I_{cell}$, t_{end} is the total time of the current flow.

6.2 The loss function K_{SoH}

As the number of cycles increases the actual capacity of the cell reduces, and this causes an increase in the current rate which is higher than the actual C-rate. The effect of reduction in capacity of the cell according to [19] is represented using a simple empirical relation as

$$K_{SoH,A/Cell} = 1/(SoH_{A,cell})^2 \quad (6.6)$$

where,

$$SoH_{A,cell} = Q_{Anode,Cell}/Q_{Anode,Cell,BoL} \quad (6.7)$$

6.2.1 Summary of the loss functions

The loss of cyclable lithium and LAAM are initially not time dependent. To make them time dependent the following equations are used (obtained from [19]) as

$$K_{TI,A/L} = \int_0^{Q_{end}} k_{TI,A/L} dQ / Q_{electrode} \quad (6.8)$$

$$K_{SoC,A} = \int_0^{Q_{end}} k_{SoC,A} dQ / Q_{electrode} \quad (6.9)$$

$$K_{SoC,L} = \int_0^{Q_{end}} k_{SoC,L} dQ / Q_{end} \quad (6.10)$$

where, $Q_{electrode}$ is the actual capacity of the battery and

$$Q_{end} = \int_0^{t_{end}} I_{segment} dt. \quad (6.11)$$

After obtaining all the loss functions, the total loss function can be calculated as

$$K_{Loss,A/L} = K_{TI,A/L} \cdot K_{SoC,A/L} \cdot k_{CT} \cdot k_{SoH,A/Cell} \quad (6.12)$$

the total loss function is used to calculate capacity retention as

$$C = C_{BOL}(1 - k_{loss,A/L})^{CT} \quad (6.13)$$

where, C is the capacity at particular instant of time, C_{BOL} is the capacity at the beginning of life and CT is the capacity throughput.

6.3 Model B

In this segment, a new model is built for LFP cells; however, the integration of the loss functions is inspired by the Model A. The experimental data in [19] is used to develop the loss functions.

6.3.1 Calculation of Activation Energy

A simple cycle life model represented in (2.26) itself explains the effect of temperature on the capacity retention. An increase in the temperature will reduce the negativity of the exponential term and increases the magnitude of the right-hand side of (2.25). Further, the activation energy has to be extracted from the capacity retention curves. A simple calculation method is developed to calculate the activation energy as illustrated below

- The Matlab curve fitting tools is used with the following options

Table 6.1: Fit Options

Method	Nonlinear Least Squares
Robust	LAR
Algorithm	Levenberg-Marquardt

- Select the custom equation and enter the equation (2.23) at temperature T_1 with the value of the shaping factor b . The value of severity factor a_1 at temperature T_1 is given by the curve fitting tool. The same procedure is repeated at another temperature T_2 and the value of a_2 is noted down.
- The severity factor a is parameterised using the Arrhenius equation as

$$a_1 = A_1 \exp\left(-\frac{E_a}{RT_1}\right) Ah^b \quad (6.14)$$

$$a_2 = A_2 \exp\left(-\frac{E_a}{RT_2}\right) Ah^b \quad (6.15)$$

where, A_1 and A_2 are rate constants at temperatures T_1 and T_2

- From Lee et al.[14] it is seen that the activation energy has a minor dependence on the temperature. Also the over potential does not depend on the temperature [13]. Hence, the first assumption that activation energy E_a is independent of temperature. Further, it is assumed that the the rate constant A is identical at different temperatures.
- Natural log is applied to (6.14) and (6.15) and simplified as

$$\ln\left(\frac{a_1}{a_2}\right) = \frac{E_a}{R} \left[\frac{1}{T_1} - \frac{1}{T_2} \right] \quad (6.16)$$

rearranging the terms,

$$E_a = \frac{R \ln\left(\frac{a_1}{a_2}\right)}{\left[\frac{1}{T_2} - \frac{1}{T_1} \right]} \quad (6.17)$$

the rate constant A can be calculated from the above equation by substituting the value of calculated activation energy.

The above procedure is followed for all the C-rates. It can be seen from the figure 6.4 that the variation of the exponential term is almost linear with all C-rates. One main observation is the magnitude of this term,

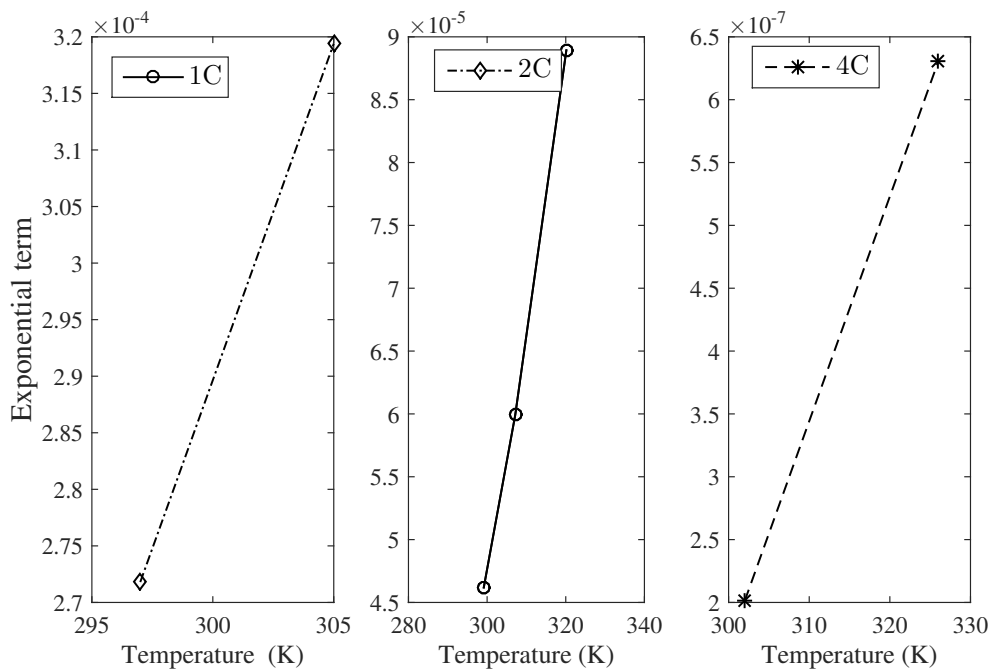


Figure 6.4: Exponential term with different C-rates.

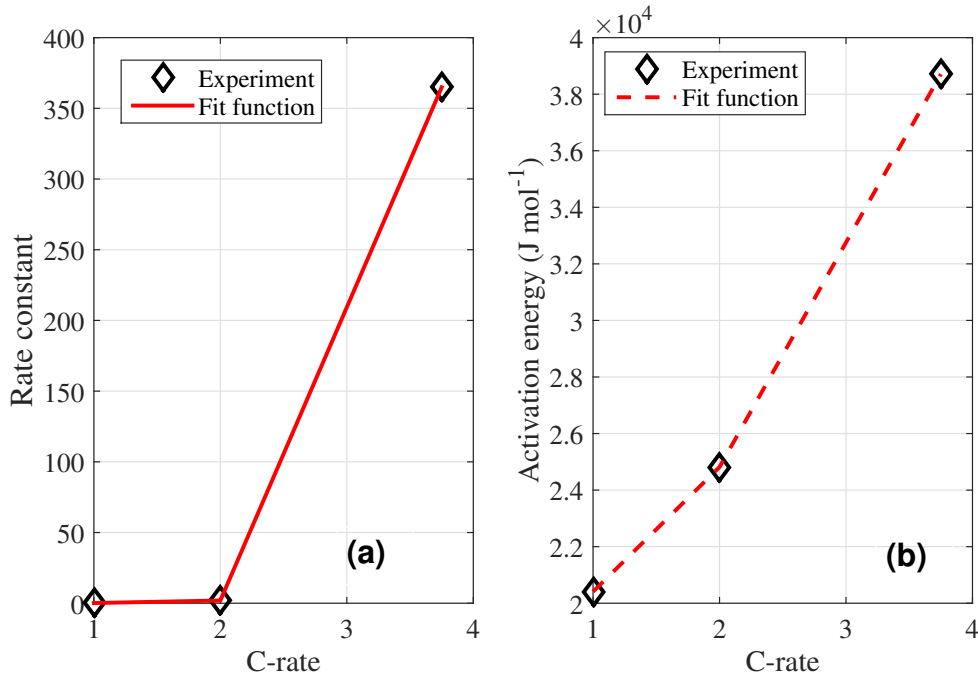
the value is maximum for 1 C-rate and is minimum for 4 C-rate. This relation tells that, at lower C-rates the main reason for the loss of capacity is temperature but this analysis might lead to lots of confusions as temperature and C-rates (current) are highly inseparable terms. In section 6.3.3 the effect of current and its combined effect with temperature is illustrated.

6.3.2 Parameterising rate constant and activation energy with C-rate

Using the procedure illustrated in section 6.3.1 the activation energy was found out at all the C-rates and temperatures and illustrated in the table below. The rate constant A in (2.26) increases with increasing C-rate. An increase in A can be attributed to the solid and liquid phase diffusion and lithium ion concentration across the electrodes. To preserve the simplicity of the model and make calculations easy, the rate constant is parameterized as a function of C-rate only. The variation of rate constant A and activation energy is shown in figure 6.5.

Table 6.2: Activation energy and rate constant for the different cycles

Cycle	Temperature [°C]	E_a [Jmol ⁻¹]	A
C1D1T24S01	24	20410	0.1131
C1D1T32S01	32	20410	0.1131
C2D2T26S01	26	24816	1.018
C2D2T34S01	34	24816	1.018
C2D2T47S01	47	24816	1.018
C4D4T29S01	29	38714	365
C4D4T53S01	53	38714	365

**Figure 6.5:** (a) represents variation of Rate constant and (b) represents variation of Activation energy with C-rate.

In [14] the rate constants and activation energy have been parameterised a function of C-rate with exponential terms. The same equations were adopted in this thesis also, and the equations are given as,

$$E_a(C_{rate}(t)) = k_1 e^{(k_2 C_{rate}(t))} + k_3 \quad (6.18)$$

$$A(C_{rate}) = exp(k_4 C_{rate}(t)^2 + k_5 C_{rate}(t) + k_6) \quad (6.19)$$

where k_1 to k_3 is the activation energy coefficients and k_4 to k_6 are the rate constant coefficients.

6.3.3 Combined C-rate and Temperature function

From the above two subsections, it has been described how the parameters in the exponential term and rate constant varies with respect to temperature and C_{rate} . Hence they must be combined after being parameterized individually, and a general equation for capacity loss as a function of temperature, C_{rate} and capacity throughput is given as

$$C_{loss}(T(t), C_{rate}(t), Ah) = k_{TC,LFP} Ah^{1.36}. \quad (6.20)$$

where $temp(t)$ is the temperature at that instant of time, and likewise all the other loading conditions are functions of time. The above expression was used in the model with some slight changes in the k values to make an acceptable fit for the measured values. From now on the combined temperature will be termed as k_{TC} , found as

$$k_{TC,LFP} = A(C_{rate}(t)) e^{\frac{-E_a(C_{rate}(t))}{RT(t)}} \quad (6.21)$$

Figure 6.6 gives an overall picture of the effect of temperature and current. This is

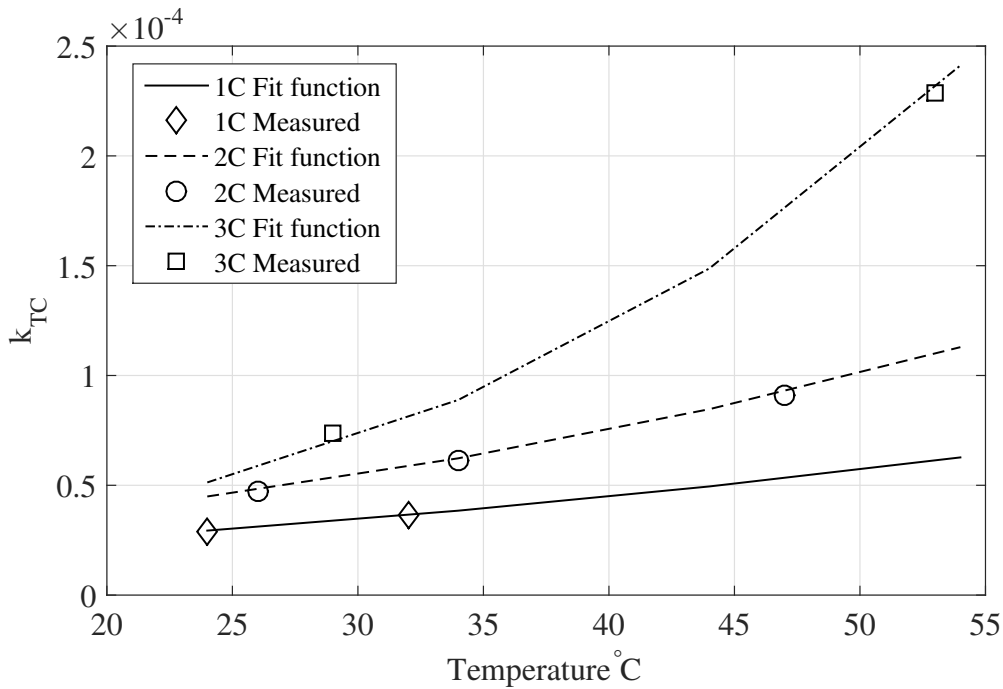


Figure 6.6: Combined loss function of temperature and C_{rate} .

similar to the loss function in [19], but the only difference is instead of a second order polynomial we have Arrhenius equation as a function of C-rate and temperature.

6.3.4 Parameterising severity factor with SOC window

To develop a life cycle model based on the SOC window, along with the experiment data an accurate OCV data is required. The OCV data was taken from [18], and a function for it was modified by replacing the hyperbolic function in [13] with

exponential function as

$$OCV(SOC) = a + b \frac{1}{1 + e^{-14(SOC-g)}} + c \frac{1}{1 + e^{-18(SOC-h)}} + d \frac{1}{1 + e^{-28(SOC-1)}} + e \frac{1}{1 + e^{40(SOC)}} + fSOC \quad (6.22)$$

where a to h are the fitting coefficients for the OCV curves. Figure 6.7 shows the

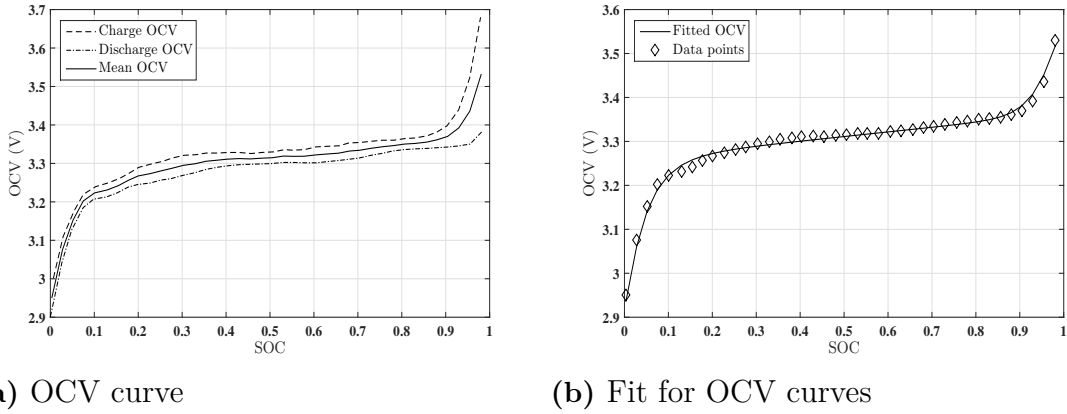


Figure 6.7: Obtaining the OCV curve

OCV data from [6] and fitted OCV equation. Further, a general equation similar to (6.20) was developed as

$$C_{loss}(SOC(t), T(t)) = k_{SOC,LFP} \times k_{TC,LFP} \times e^{-\frac{E_a(t)}{RT(t)}} Ah^{1.36} \quad (6.23)$$

where A is now a function of SOC. The activation energy is almost constant, but A varies as the SOC range changes. The value of A is high where $\frac{dOCV}{dSOC}$ is high, and it is minimum in the flat region of OCV. With this motivation, $\frac{dOCV}{dSOC}$ and A are compared, and it is seen that they seem to agree with each other as shown in Figure 6.8. Hence, a weighted function based on $\frac{dOCV}{dSOC}$ is developed as

$$k_{SOC,LFP} = P_{Bat} \left(k_7 s \frac{e^{k_8 s (SOC-1)}}{e^{(k_8 (SOC-1)+1)^2}} + k_9 s \frac{e^{-k_{10} s (SOC+k_{11} s)}}{e^{(-k_{10} s (SOC+k_{11} s)+1)^2}} + k_{12} s \right) \quad (6.24)$$

where, k_{6s} to k_{12s} are the SOC related fitting coefficients and P_{Bat} is a battery specific scaling value. P_{Bat} scales the values of A so that the cumulative value over one complete cycle is equal to 1 and based on the SOC range this value either scales up or scales down the capacity retention rate. From now on, $A(SOC)$ is represented as k_{SOC} and figure 6.8 shows the safe and danger zones of operation, where A_{max} and A_{mod} corresponds to the danger zone, and A_{min} corresponds to safe zones of operation.).

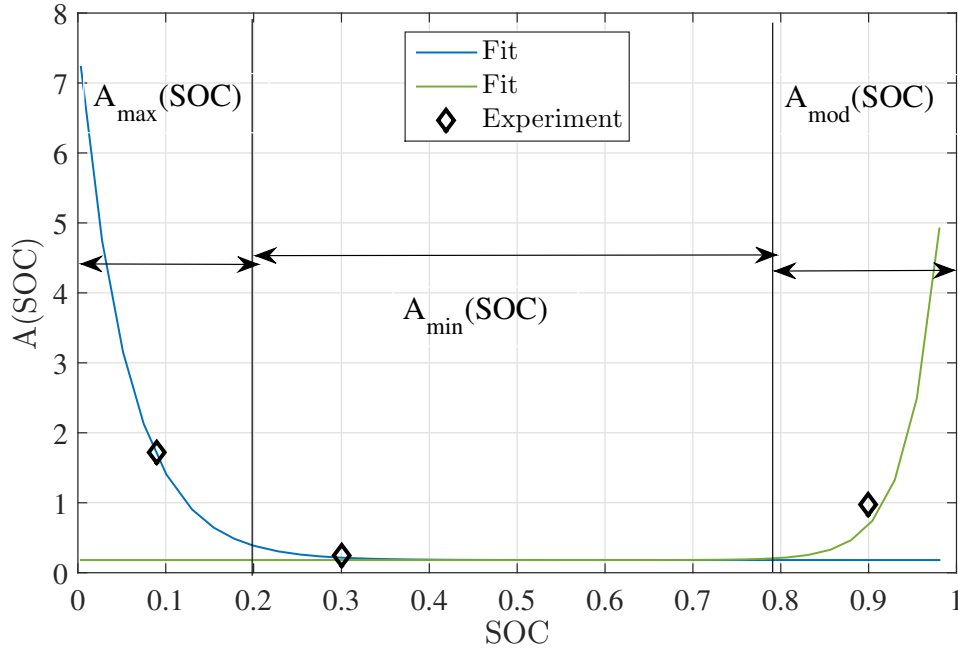


Figure 6.8: SOC dependent loss function.

According to [20] high average SOC and low average SOC leads to accelerated ageing, especially in the low SOC ranges due to high mechanical stress on graphite anode. The designed loss function is very much in line with this theory.

6.3.5 Combining all the loss functions

All the factors discussed above cause capacity retention, but their effects were examined individually in the above subsections. From the experience of Model A, all the loss functions are to be multiplied to obtain the capacity loss; the same principle holds good here also. It was seen that for cycles C2D2 and C4D4 the ageing rate was pretty high, this is the condition of accelerated ageing. To compensate the accelerated ageing, a number was found out empirically. Though the number varied between 0.8 – 1 for the majority of the cases, it was fixed to 0.9 to reduce the complexity of the model, and this figure is coined as error ageing k_e term (or factor). However, for unsymmetrical cycles this value varies significantly, for instance, a cycle with $+1C/-4C$ and $+4C/-1C$ has the same mean value of current, but the later has adverse effects on ageing. Hence the error ageing value will be high for the latter case. Therefore, when a real drive cycle like the NEDC is applied to this model, ideal ageing is obtained as it is not capable of differentiating the severity of charge and discharge rates.

The life cycle models discussed and presented in the above sections are constant for a particular loading condition. A life cycle model which is applicable for both steady and variable loading condition can be given as

$$C_{loss}(t) = 100 - \left[\frac{1}{T_{cycle}} \int_{t_0}^t A(t) e^{\left(\frac{-E_a(t)}{RT(t)}\right)} dt \right] \left[\left(\int_{t_0}^t I_{rms} dt \right)^{1.36} \right] k_e \quad (6.25)$$

where, $A(t) = k_{TC,LFP} \times k_{SOC,LFP}$, $E_a(t) = E_a(C - rate(t))$. Which means the capacity retention is a function of loading condition at that particular instant of time.

7

Developing model for NMC/LMO cells

7.1 Structure of the algorithm

Model A was based entirely on the research made by the author [19], and Model B was built wholly based on research made by [14][13][15][12] and [16]. However, all the models were built only for cylindrical LFP cells. Further, an attempt is made to create a model for NMC/LMO from the scratch which includes deciding the shape factor b , calculating the activation energy E_a , parameterising the pre-exponential term (A) in the Arrhenius expression. All these small bits form the necessary parts of the primary ageing model, a simple block diagram of these calculations is shown in figure 7.1. The black lines show the flow of the calculations and blue lines show the interdependence between the calculations.

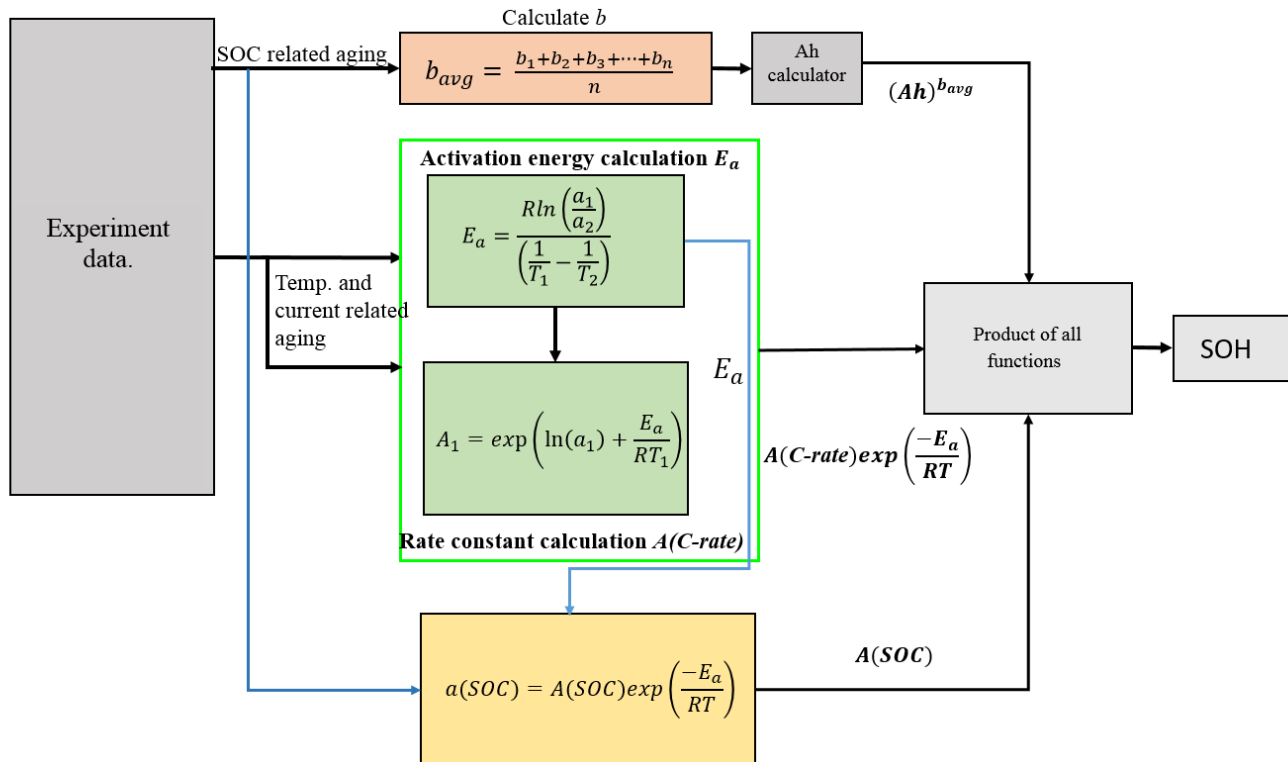


Figure 7.1: General block diagram of the ageing algorithm

7.2 Deciding the shaping factor b

The chemical composition of the battery is a primary factor influencing the shape of the capacity retention curve, and the type of ageing phenomena occurring is a secondary factor as it depends on the loading condition. The purpose of this section is to define a shaping factor for NMC/LMO cells using the available experimental data and to evaluate the goodness of the fit with a fixed value of b . The

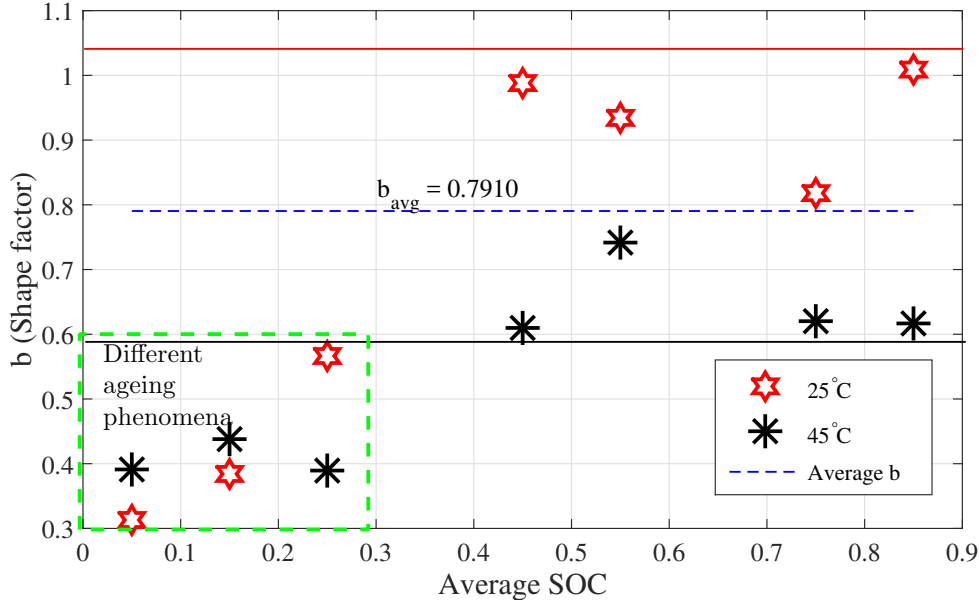


Figure 7.2: b values at different average SOC values

experimental results set with data ID C2D2TXSY-Y that is with 10% SOC window ranging from 0-90% SOC at 25°C and 45°C are used. Initially, the b value is calculated by the curve fitting algorithm in Matlab for every loading condition. After calculating b for all loading conditions, its average value is calculated as

$$b_{avg} = \frac{1}{n} \sum_{i=1}^n b_i \quad (7.1)$$

where n is the number of experiments, b_i is the value of shaping factor b at i^{th} loading condition. At a lower SOC region the capacity retention curves do not fit with the power law equation 2.23 and is illustrated in the figure 7.8a. For the SOC ranges above 40%, the capacity retention curves are in good agreement with the power law. Therefore, only the b values falling in the range specified between solid black and solid red lines in the figure 7.2 are considered to calculate its average value. The method mentioned above is purely statistical and is based on [12]. It is also stated in [?] that the value of b depends on the type of ageing phenomena and as far as this thesis is concerned only the loss of cyclable lithium is considered hence the value of b is a rough estimate. The Incremental Capacity Analysis (ICA) made by the author [21] show that for NMC/LMO cells there is a large loss of peaks in the ICA curves for SOC ranges starting from 60%. On the other hand, at lower SOC levels

the reactions at the negative electrode get blocked and do not participate in the side reactions. Therefore, at lower SOC levels other ageing phenomena is causing the loss of capacity and Arrhenius expression does not hold good. Hence, ignoring the b values for low SOC holds good in our case.

In this case, we have eight experimental data sets therefore $n = 8$, and the values of b is shown in figure 7.2. With all these data the value of b_{avg} is calculated using (7.1) and hence the value of $b_{avg} = 0.7910$. To check the goodness of fit with the new value of b the new power law expression was plotted with the experimental data as shown in figure 7.3. The capacity retention agrees with the experimental results for 25°C , but for 35°C and 45°C , there is a deviation from the experimental data at EOL.

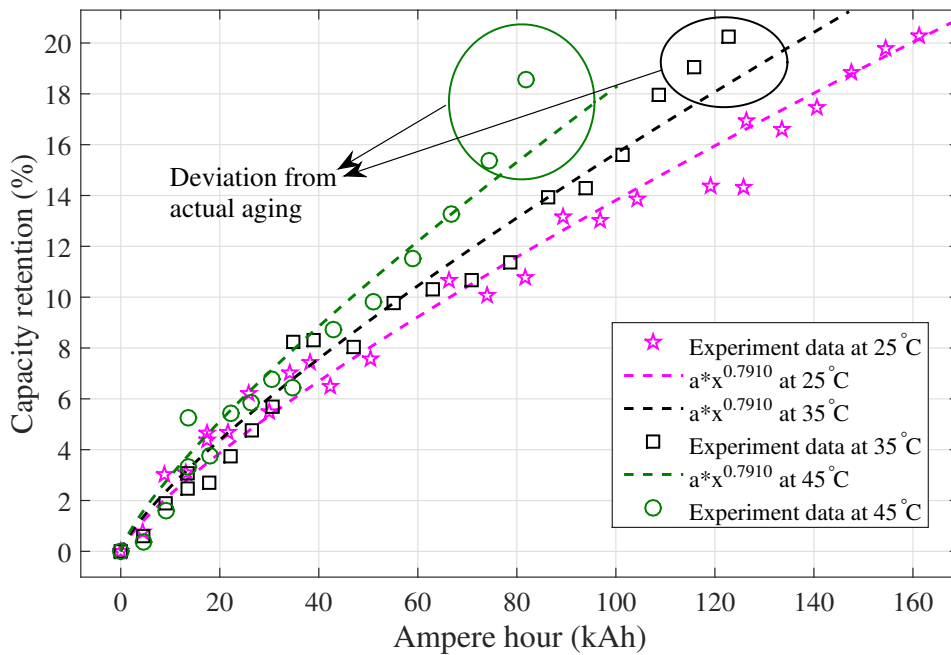


Figure 7.3: $a(Ah)^{0.7910}$ Vs Experimental data. Start, square and circle represent experimental data for C2D2 at 25°C , 35°C and 45°C respectively. Dashed magenta, black and green represent $a(Ah)^{0.7910}$ for C2D2 at 25°C , 35°C and 45°C respectively.

7.3 Extracting the activation energy at 2 C-rate

Calculating the activation energy is one of the crucial parts of the ageing model as shown in the figure 7.1 since it defines the value of the pre-exponential term (A) for the side reactions. The procedure illustrated in 6.3.1 is used for calculating the activation energy. As mentioned initially, only 2C cycling experiments were performed at three distinct temperatures which are 25°C , 35°C and 45°C . Hence, this model is not parameterized and only applicable for the 2C rate at different SOC ranges and temperatures. It was noticed that the value of activation energy for NMC/LMO cell is $9422.72 \text{ Jmol}^{-1}$ which is around two times lower than that of the LFP cells (analysed in this thesis) for the same C-rate. After the calculation of

the activation energy, the value of the pre-exponential term A is calculated which is equal to 0.11.

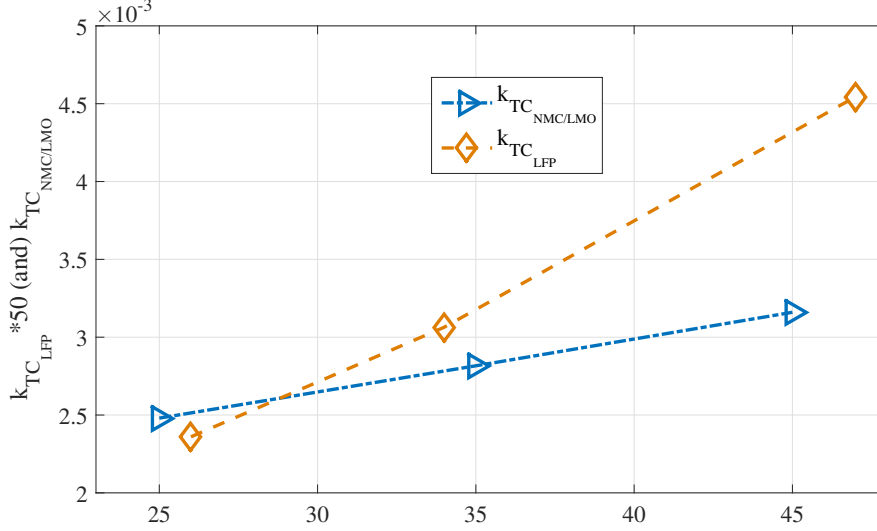
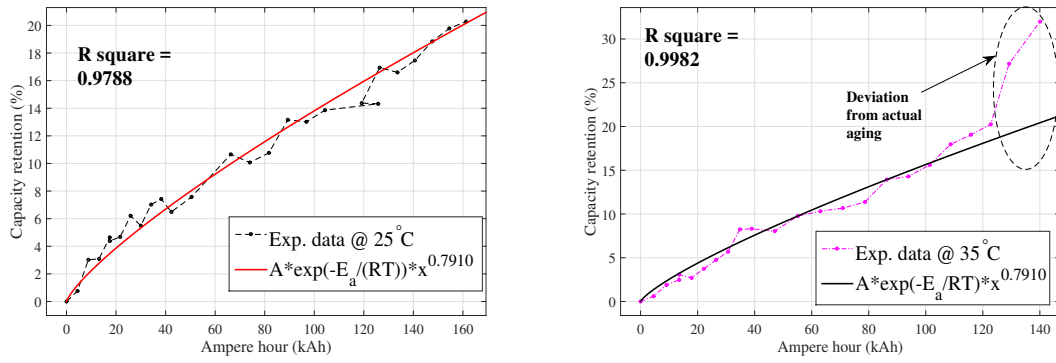


Figure 7.4: Ageing function dependent on temperature and current (K_{TC}) for LFP and NMC/LMO cells.

With the values of activation energy and pre-exponential term for the NMC/LMO cells, the loss function $k_{TC,NMC}$ is calculated and plotted as a function of temperature as shown in figure 7.4. The impact of temperature and current is high in case of NMC/LMO cells when compared to that of LFP cells as shown in figure 7.4. A higher value of pre-exponential term means that the effect of current is high and lower value of activation energy implies that the effect of temperature is high and the combined effect is the loss function $k_{TC,NMC}$. As mentioned in the previous chapters the effect of current and temperature is inseparable; however, the effect of each can be evaluated by keeping either of one parameter constant at an instant of time. To check the goodness of the fit, the pre-exponential term (A), activation energy (E_a) and shaping factor (b) is plugged into (2.26) and written as

$$Q_{loss}(C - rate, T(t)) = k_{TC,NMC}(Ah)^{0.7910} = 0.11 \exp\left(-\frac{9422}{RT(t)}\right)(Ah)^{0.7910} \quad (7.2)$$

where, R is the universal gas constant, and T is the temperature. The R square value is the measure of goodness of agreement between the experimental data and the life cycle model (7.2) and it is between 0.9778 and 0.998 for all the experimental results with ID C2D2TXS0-0.9. Hence, the life cycle model fits decently with the experimental data and also the model passes through majority of the data points as shown in figure 7.5. In summary, temperature and current have an upper hand in the ageing of NMC/LMO cells.



(a) Model performance for C2D2T25S0-0.9 (b) Model performance for C2D2T35S0-0.9

Figure 7.5: Model for NMC/LMO Vs experimental results. Red solid and black solid represent model output. Black dashed and magenta dashed represent experimental data.

7.4 Loss functions for SOC effects on ageing

During the development of loss function for LFP cells, a hypothesis that the region with higher $\frac{dOCV}{dSOC}$ has negative effects on battery ageing was made and a loss function was developed accordingly. The experimental results illustrated in [21] show that as the SOC range increases the number of full equivalent cycles (FCE) reduces. Hence, the concept of $\frac{dOCV}{dSOC}$ does not hold good for NMC/LMO cells. Further in this section, the process of developing a semi-empirical relation for SOC related ageing is discussed. The activation energy found out in the previous section is used and a life cycle model can be written as

$$Q(SOC(t), T(t)) = k_{ST,NMC} \times k_{TC,NMC} \exp\left(\frac{-E_a}{RT(t)}\right) (Ah)^{0.7910} \quad (7.3)$$

where $k_{ST,NMC}$ is the pre-exponential term as a function of SOC and temperature at a particular instant of time. The above equation is plugged into the Matlab curve fitting tool, and the value of the pre-exponential term A is extracted for every 10% SOC interval ranging from 0-90%. The so obtained pre-exponential term values at different temperatures are plotted as shown in the figure 7.6. The pre-exponential term values illustrate a nonlinear behaviour, but in general, they increase with an increase in the SOC range. It is apparent from the statistical analysis that, $25^\circ C$ and $45^\circ C$ are not optimal temperatures for NMC/LMO cells. Another notable observation from figure 7.6 is that the effect of temperature is significant only at high SOC ranges (60-90%) and at low SOC ranges the pre-exponential term is almost constant irrespective of the temperature.

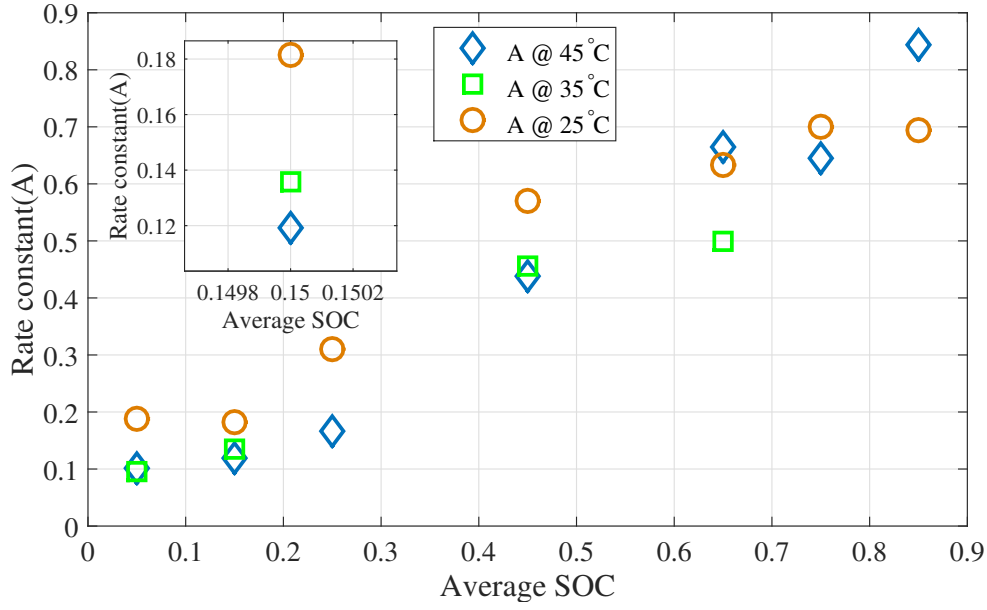


Figure 7.6: A values at different temperatures. Blue solid represents A at 45°C , brown at 25°C and green at 35°C . Inset image shows the A values at an average SOC of 0.15.

A two-dimensional polynomial equation with SOC and temperature as variables is used to represent the pre-exponential term(A) as

$$\begin{aligned}
 k_{ST,NMC} = A(SOC(t), T(t)) = P_{bat_{NMC}} & \left(k_{1N_{ST}} + k_{2N_{ST}} SOC(t) + k_{N3_{ST}} T(t) + k_{4N_{ST}} SOC^2(t) \right. \\
 & + k_{5N_{ST}} SOC(t)T(t) + k_{6N_{ST}} T^2(t) + k_{7N_{ST}} SOC^3(t) \\
 & \left. + k_{8N_{ST}} SOC^2(t)T(t) + k_{9N_{ST}} SOC(t)T^2(t) \right)
 \end{aligned}$$

where $k_{1N_{ST}}$ to $k_{9N_{ST}}$ are coefficients based on the least-square fitting made towards measured pre-exponential term A , $P_{bat_{NMC}}$ is a battery specific scaling factor. The subscripts S and T stand for SOC and temperature. Figure 7.7a and 7.7b show the surface and residue plot for the empirical equation. The empirical equations have an R square and RMSE equal to 0.96 and 0.0068 respectively which implies that the equation has a good agreement with the measured pre-exponential terms as shown in figure 7.6. Nevertheless, there are some SOC and temperature regions where the fitted equation generates an error which is represented by red lines in the illustration 7.7b.

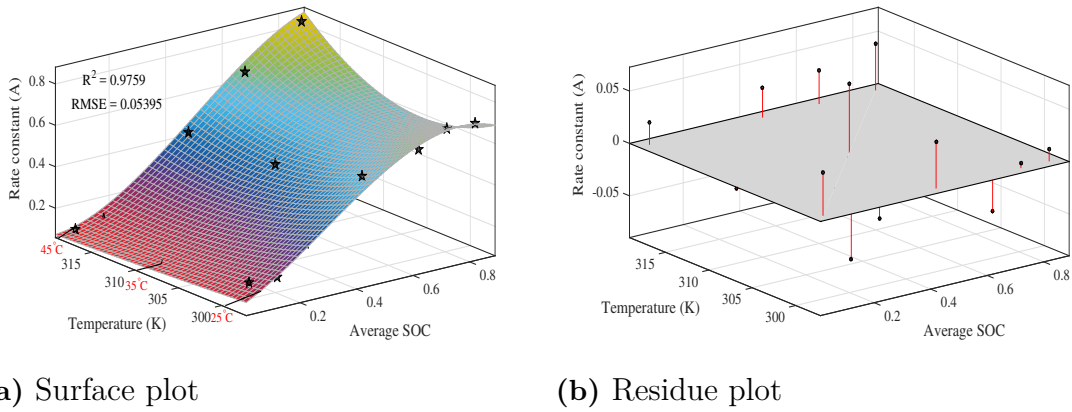


Figure 7.7: 2-D plot of the empirical relation. Figure(a): Black solid pentagon represents measured pre-exponential term A , figure(b): black dots with red lines depict the error.

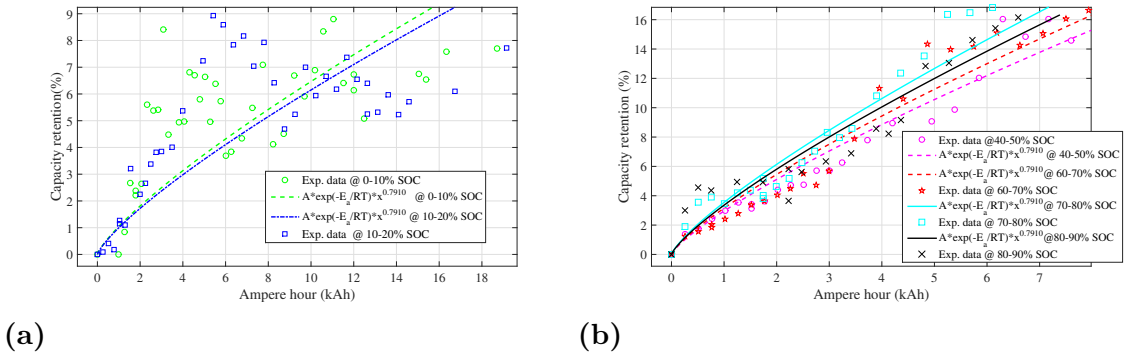


Figure 7.8: Symmetric +2C/-2C cycling test Vs Model for NMC/LMO at 25°C. Figure(a): SOC range of 0-10% and 10-20%, figure(b): SOC range from 40-90% with 10% window.

Similar to the previous chapter, the derived life cycle model for SOC related ageing is compared with the experimental capacity retention. It is apparent from figure 7.8a that the model developed completely disagrees with the experimental data for low SOC ranges. This behaviour was predicted since the reactions are blocked for SOC ranges below 30%. At high SOC ranges the built model has a good correlation with the experimental data as shown in figure 7.8b. Thus, a general ageing equation for NMC/LMO cells which is only applicable for 2C is written as

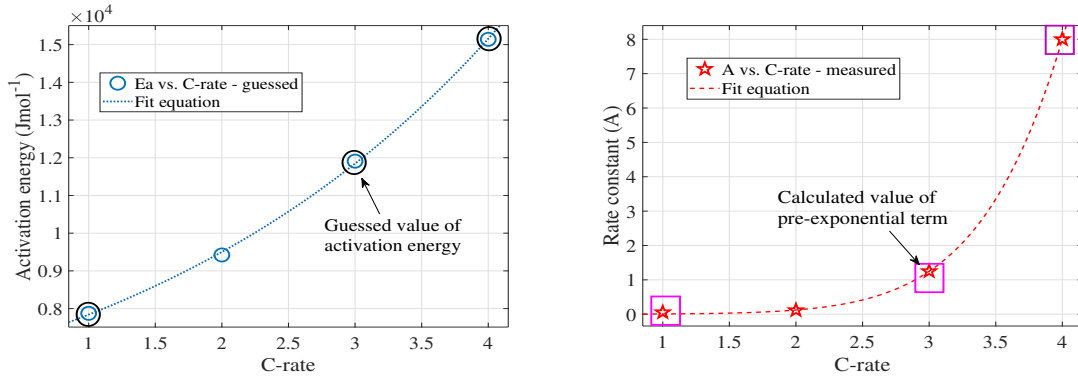
$$C_{loss}(t) = 100 - 0.11 \left[\frac{1}{T_{cycle}} \int_{t_0}^t A(t) e^{\left(\frac{-9422.11}{RT(t)}\right)} dt \right] \left[\left(\int_{t_0}^t I_{rms} dt \right)^{0.7910} \right] k_e \quad (7.4)$$

where, $A(t) = k_{ST,NMC}$, the number 0.071 is the value of $k_{TC,NMC}$ at 2C and k_e is the error ageing term. The process of building an ageing model for NMC/LMO cells is quite similar to that of LFP cells. However, there are two major differences and one setback, which are

- The concept of $\frac{dOCV}{dSOC}$ is not used for NMC/LMO cells.
- The pre-exponential term in the case of NMC/LMO is parameterized as a function of temperature and SOC while it is only a function of SOC for LFP cells.
- The setback is that the model is applicable only for 2 C-rate.

7.4.1 Guessing the loss function at different C-rates and temperature

From the previous sections is seen that to extract the value of the activation energy for a particular C-rate it is necessary to have ageing data at two different temperatures. Due to lack of available data, it is not possible to calculate the value of activation energy E_a . Thus the pre-exponential factor cannot be parameterised as a function of temperature and C-rate. However, in this section, an attempt is made to guess the activation energy, and the corresponding pre-exponential factor is calculated. The data available for this guessing process are 1/1C, 3/3C and 4/4C for a SOC window between 20 - 80% at a temperature of 40°C.



(a) Activation energy (E_a) Vs C-rate (b) pre-exponential term (A) Vs C-rate

Figure 7.9: Variation of activation energy and pre-exponential term with C-rate. Red pentagon and blue circle represents the guessed values, red and blue dotted line represent fit equations. The solid black circles represent the guessed value of activation energy and solid magenta squares represent the calculated pre-exponential factor A .

Based on the analysis in the previous sections, it is evident that the effect of temperature is predominant for ageing in NMC/LMO cells. With this as a starting point, the activation energy E_a was guessed such that the value of the exponent term in (7.3) is high meaning that the effect of temperature is distinguished. The so guessed E_a was used to calculate the pre-exponential term A in the Matlab curve fitting tool using the available data mentioned above. The resulting E_a and A were fit to the following equations

$$E_{a_{NMC}}(C_{rate}(t)) = k_{10_{NCT}} e^{(k_{11_{NCT}} C_{rate}(t))} + k_{12_{CT}} \quad (7.5)$$

$$A_{NMC}(C_{rate}) = \exp(k_{13_{CT}} C_{rate}(t)^2 + k_{14_{CT}} C_{rate}(t) + k_{15_{CT}}) \quad (7.6)$$

where, C and T stand for C-rate and temperature respectively, N for NMC/LMO cells. Further, the above two equations are combined to obtain the completely parameterised $k_{TC_{NMC/LMO}}$ as shown in the figure 7.10.

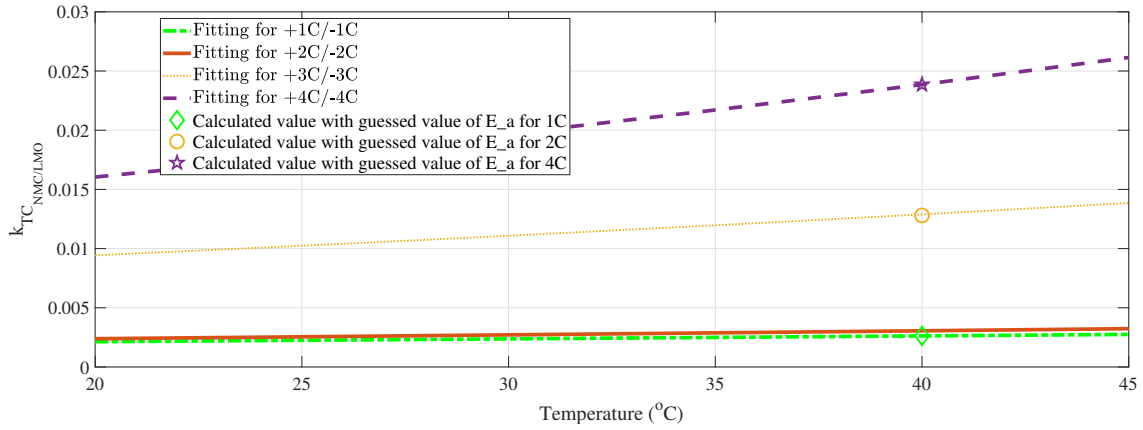


Figure 7.10: The combined current and temperature dependent loss function $k_{TC_{NMC/LMO}}$ at different temperatures and C-rates.

The possible drawback of guessing the loss function is that the model loses its accuracy and the error ageing factor has to be tuned to a value such that the hypothesised loss functions fit the experimental data.

8

Results and discussion: SOC

8.1 R_0 estimation result

Several cases have been used for R_0 estimation testing. For the sine-wave input, it has been tuned from high frequency to low frequency and different noise level have been added. For the NEDC test data, it is the logged data and it already includes noise, so there is no adjustment on this input signal. The effect of implementing the dead zone into the estimator has been shown in this section.

8.1.1 High sampling rate result

The sampling time is set to 0.001s, and the corresponding results are shown in figure 8.1 and 8.2. It can be seen that estimation results follow the reference value generated by the simulation model 3.1-3.3. Small spikes found in both figures are mainly caused due to the approximation error. Since the NEDC cycle contains high-frequency signals, its test result look much noisier than the estimation result with the sine wave as an input.

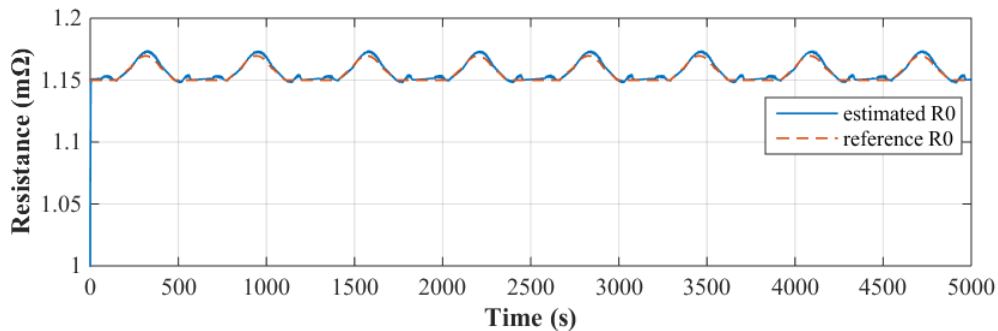


Figure 8.1: R_0 estimation result with sin-wave inputs

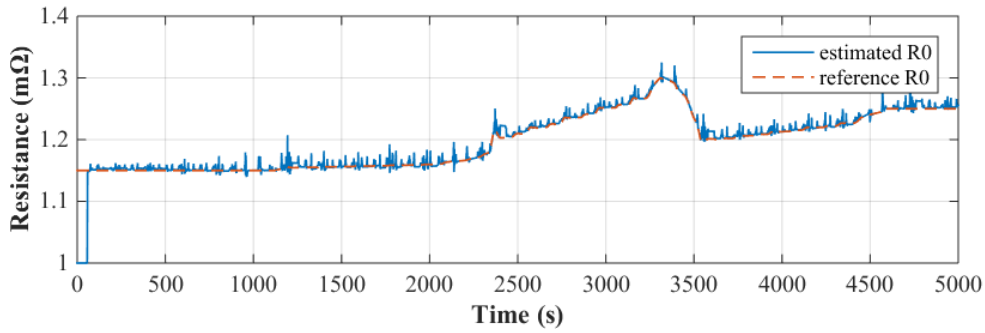
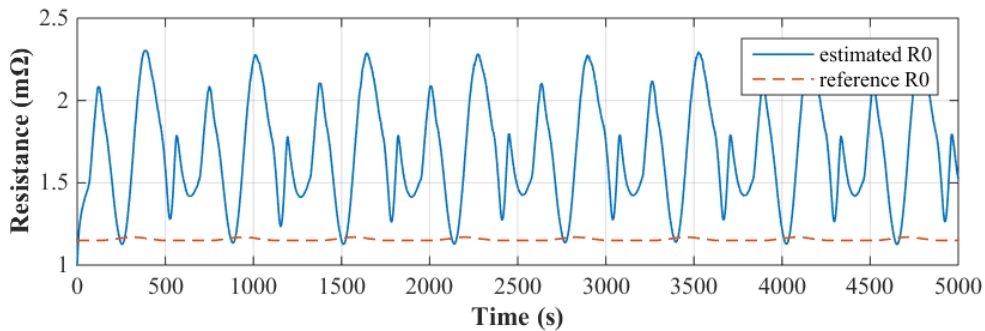


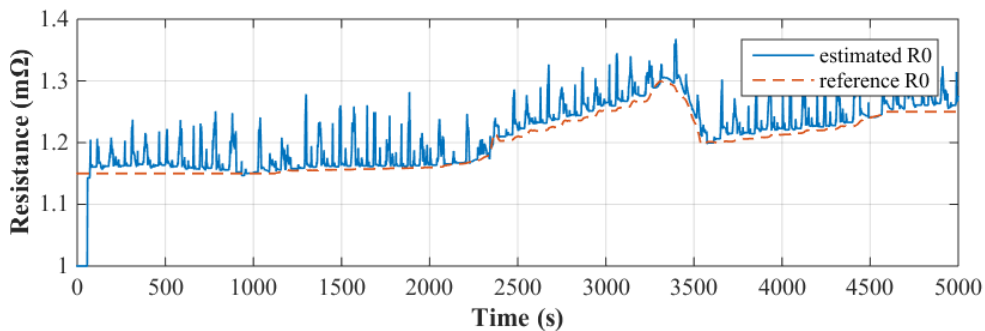
Figure 8.2: R_0 estimation result with NEDC cycle inputs

8.1.2 Low sampling rate result

By lowering the sampling time to 0.05s, it is quite obvious that the estimation accuracy drops down rapidly in both the cases. Surprisingly, error in the event of a sine wave is higher compared to NEDC test cycle as shown in the figures 8.3a and 8.3b. This indicates that for an input signal with fixed frequency is prone to have a higher error than a variable frequency signal in case of a lower sampling rate.



(a) R_0 estimation result with sin-wave inputs



(b) R_0 estimation result with NEDC cycle inputs

Figure 8.3: Low sampling rate R_0 estimation result.

In figure 8.4, the relationship between R_0 estimation accuracy and sampling time have been shown. It is clear that a proper sampling time should be chosen before the error winds up.

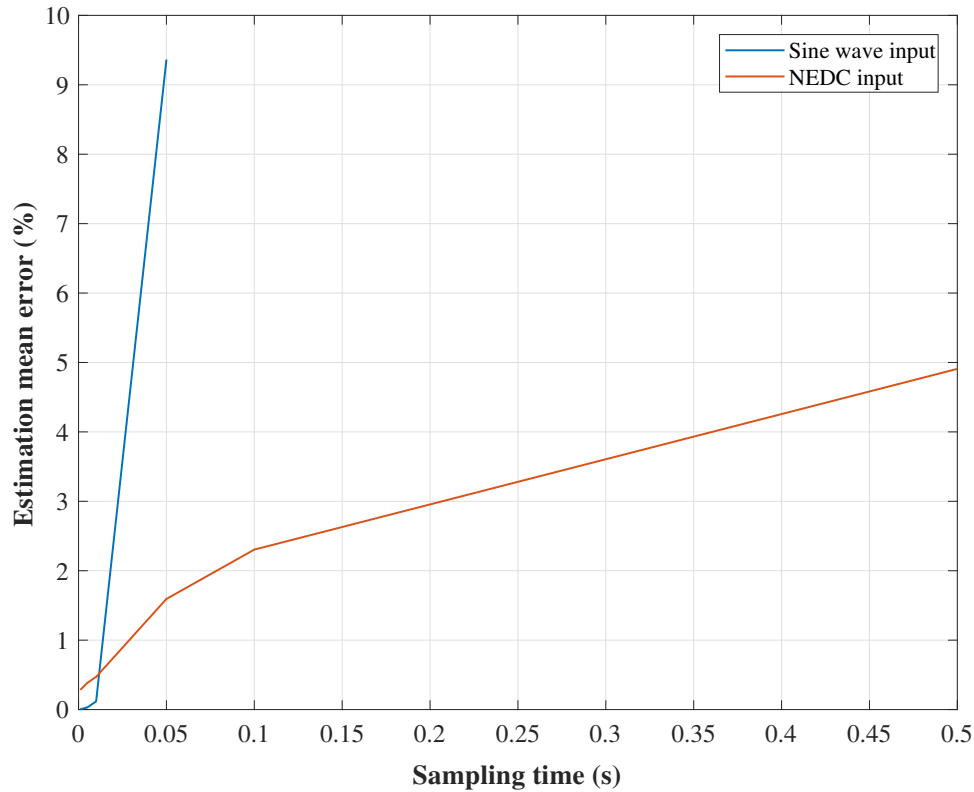
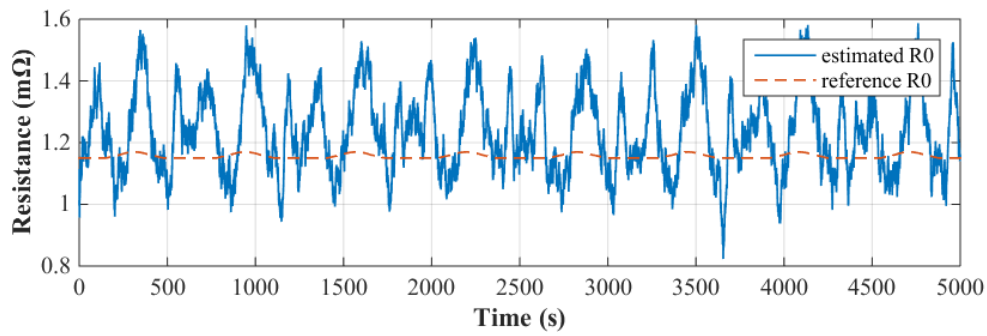


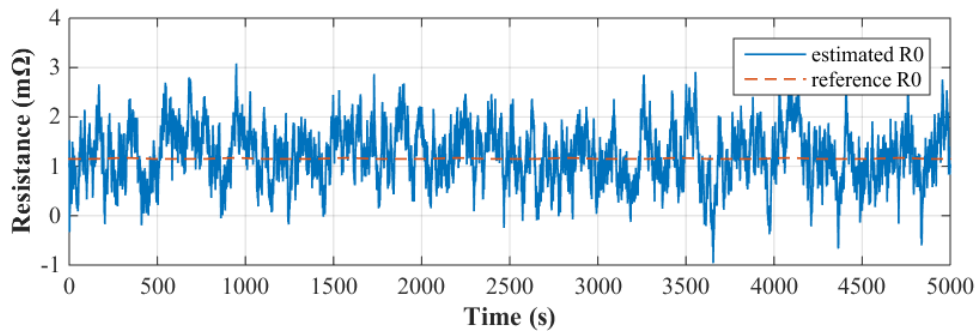
Figure 8.4: Relationship between R_0 estimation accuracy and sampling time

8.1.3 Noise effects

Hereby, a concept of SNR (Signal-to-noise ratio) should be introduced. It is a measure used in science and engineering that compares the level of a desired signal to the level of background noise. SNR ratio is defined as the ratio of signal power to the noise power, often expressed in decibels. A ratio higher than 1:1 (greater than 0 dB) indicates more signal than noise. Both figures above show significant effects anticipated by the addition of noise in the input signal. The target value is small, and the approximation in the calculation makes the function more sensitive to the noise effects. Therefore there is a need to implement dead zone method to curb the noise effects. In figure 8.6, the trends is clear that the estimation error grows with the drop of the SNR value. The data set for the noise signal remains the same to get the three results in the different sampling time. As a result, a lower sampling rate can somehow improve the SNR value while the noise level is the same, but the estimation error is still lager than higher sampling rates.



(a) R_0 estimation result with measurements SNR 90dB



(b) R_0 estimation result with measurements SNR 60dB

Figure 8.5: Noise effects on R_0 estimation result

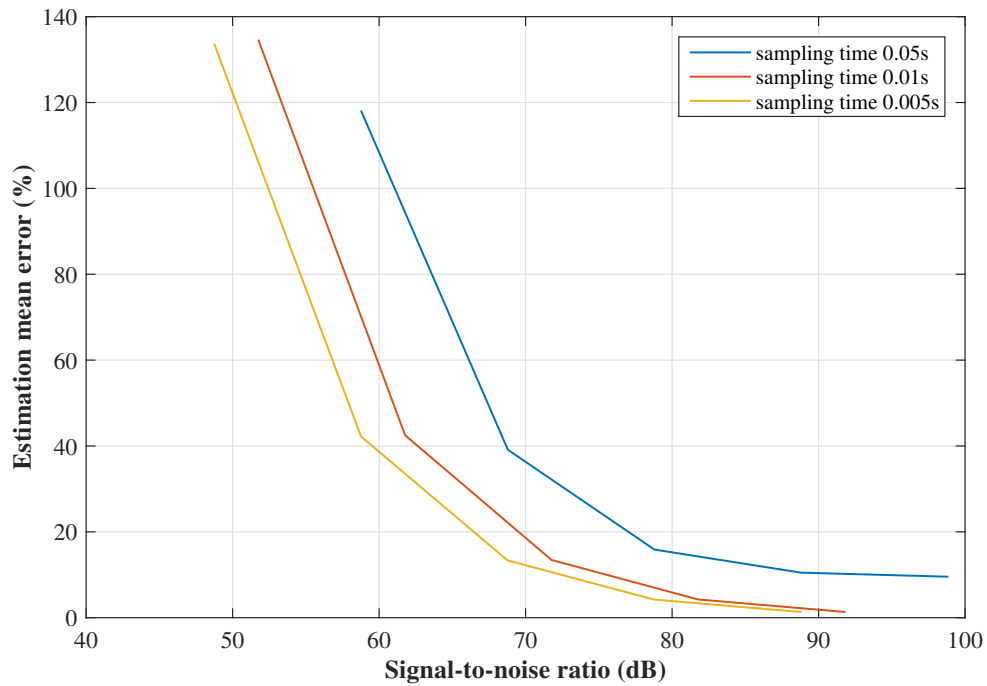
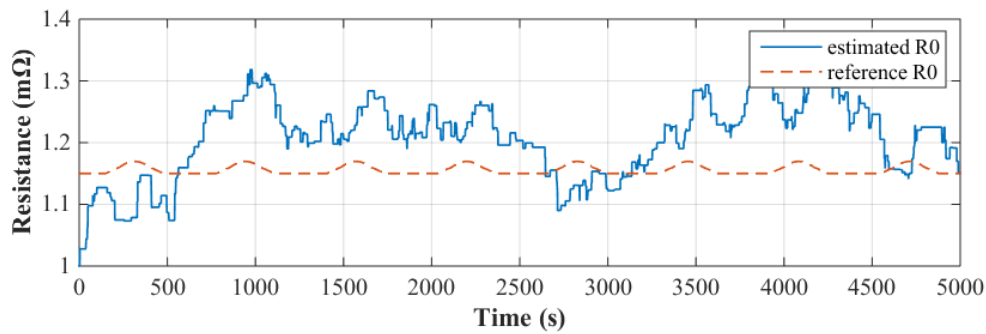


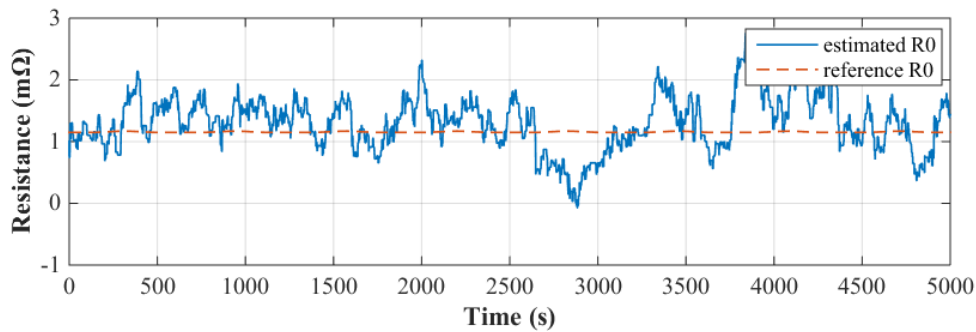
Figure 8.6: Relationship among R_0 estimation accuracy, sampling time and noise effects

8.1.4 Dead zone implementation

The below two figures show the benefits of using dead zone. From the figure 8.5 and 8.7 is clear that the oscillations in the estimations are mainly caused by the addition of noise signal in the input. However, implementing dead zone does not ensure accurate estimation results. Since the reference value is minimal, the accuracy of R_0 estimation is good enough for the other two estimation functions. From figure 8.8, obvious effects of the dead zone can be seen especially when the SNR value is low. However, the effects of dead reducing the system sensitivity can be conclude from figure 8.8b. When the SNR is high, lower dead zone setting or no dead zone implementation will be a better choice. So a proper dead zone setting need to be found according to the input signal strength levels.

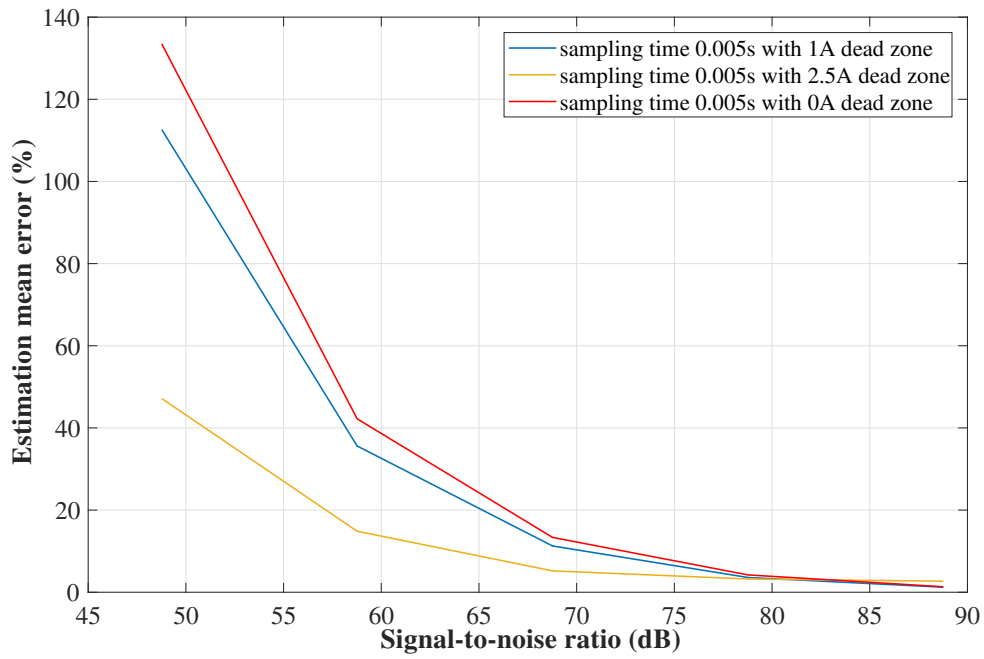


(a) R_0 estimation result with measurements SNR 90dB

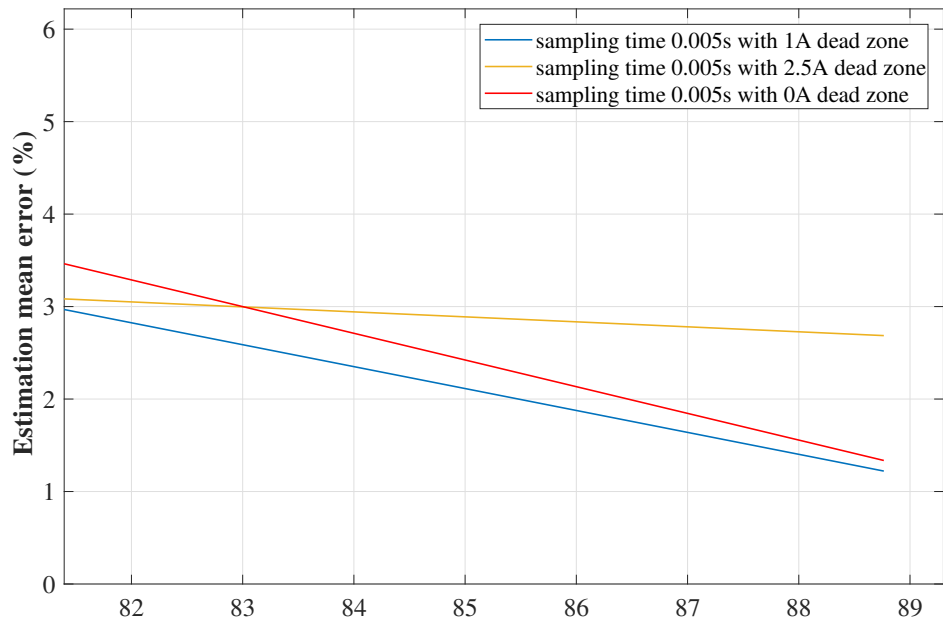


(b) R_0 estimation result with measurements SNR 60dB

Figure 8.7: Effects of dead zone implementation in R_0 estimation



(a) Relationship among R_0 estimation accuracy, dead zone and noise effects



(b) Relationship among R_0 estimation accuracy, sampling time and noise effects (enlarged)

Figure 8.8: Relationship among R_0 estimation accuracy, sampling time and noise effects

8.2 Time constant τ estimation

For the time constant τ estimation, the Adaptive Kalman filter (2.14)-(2.16) and (5.11) is used for estimation. Inputs and outputs are scaled to the same magnitude (5.12) to reduce the estimation error. At the same time, scaling factor will increase the system sensitivity to the noise. Hence, more effort is made to find out the value of the scaling factor with and without noise in the input signal.

8.2.1 Scaling factor test

The effect of scaling factor is evaluated with low, proper and higher scaling factors. As can be seen from figure 8.9d, that the reference and estimated value agree with each other and converge. However, the reaction speed (or time response) depends on the type of input.

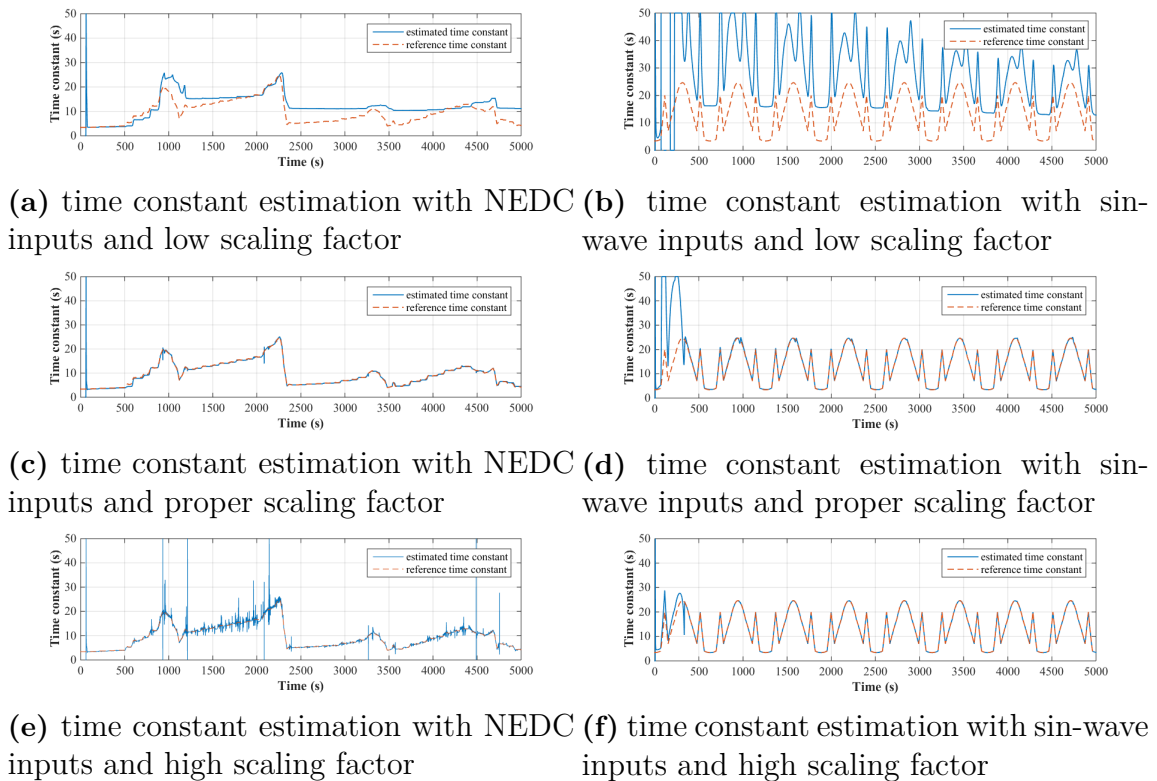


Figure 8.9: Test results for scaling factor in time constant estimation

The lower value of scaling factor will increase the error, and the result does not converge with the reference data as shown in Figure 8.9a. The increase in the scaling factor generates noise in the estimation in case of the NEDC test cycle, on the other hand, the estimation is smooth in the event of sine wave input.

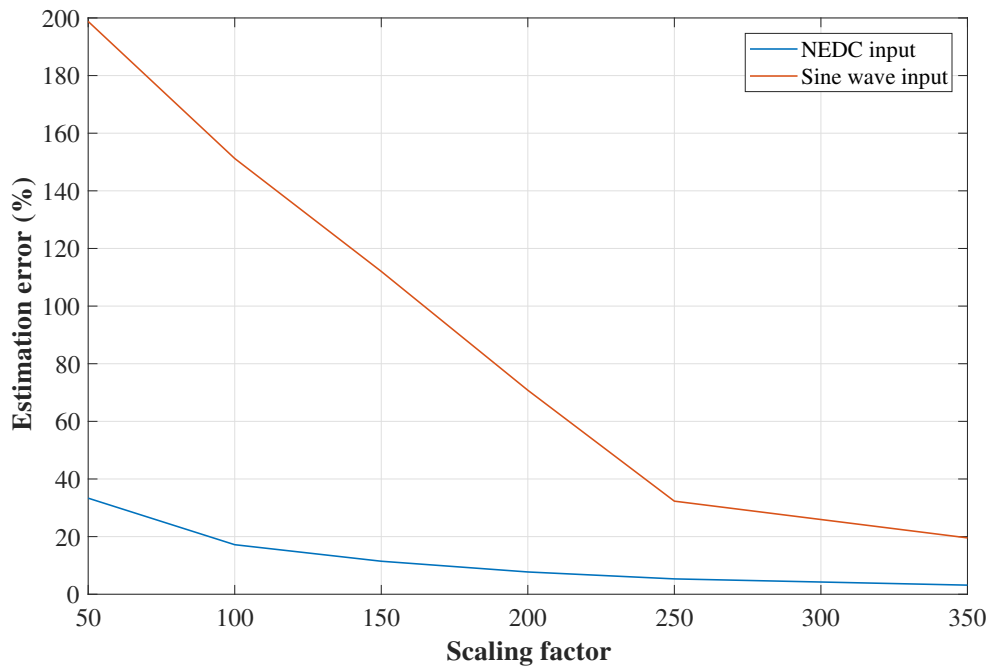


Figure 8.10: Relationship between time constant estimation accuracy and scaling factors

In figure 8.10, the relationship between time constant estimation accuracy and scaling factors have been shown. Similar to the results in figure (8.9), the estimation results based on sine wave inputs needs larger scaling factors to have better estimation results. In conclusion, a large scaling factor is needed to maintain the promising estimation result for time constant.

8.2.2 Relationship with SOC estimation

To begin with, the numerical issues in the time constant estimation should be mentioned. In (5.6), α and β are the true estimation value in the AKF estimation process. According to the sampling time, α is a number which approximately around 1 and β is a number which approximately equals to 0. The estimated time constant is calculated from the estimated α and β . As a result, small differences in α and β will cause huge gaps in the time constant estimation which affects the SOC estimation but it has a higher effect on the time constant estimation. On the other side, the error in R_0 estimation will not be tested. Since R_0 is not a big value and it does not changes a lot, so it will not heavily influence the time constant estimation accuracy. The figure below shows the relationship between the time constant and the α β calculation parameters.

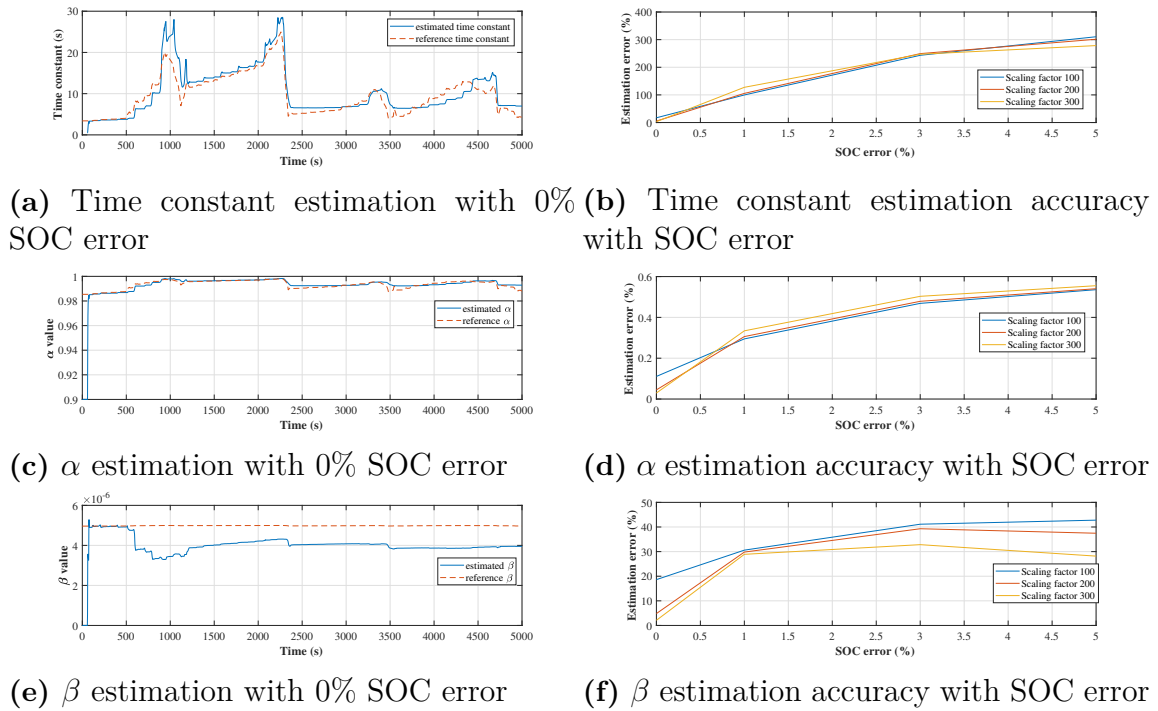
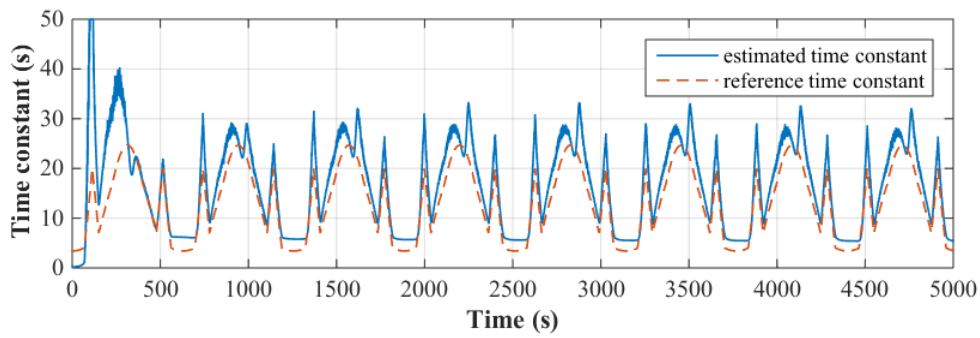


Figure 8.11: Time constant related estimation with SOC error

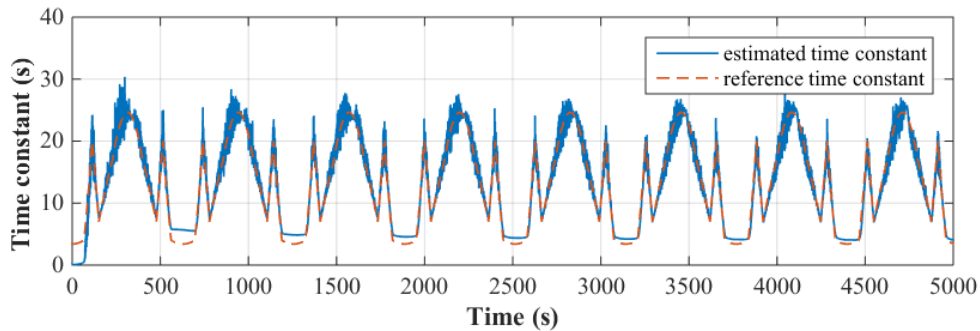
The figures above also show the relationship of the time constant estimation and SOC estimation with SOC error manually set in the input signals. As a result, the time constant estimation deviates a lot while the difference in α and β is not much. Meanwhile, the scaling factor does not affect the estimation accuracy decrease much. The estimation error in the time constant estimation will have adverse effects on SOC estimation accuracy. However, this kind of oscillations appears when the SOC value is repeatedly wrong, this will push the SOC estimation towards self-correction. Further, the time constant estimation will slowly converge to the correct value.

8.2.3 Noise effects

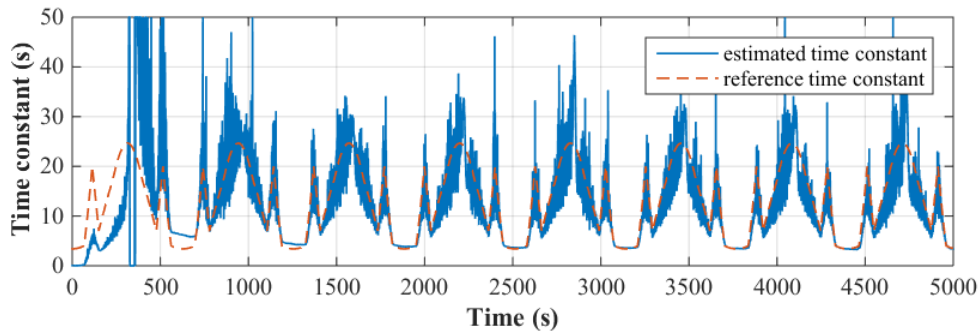
The estimator for the time constant estimation is the Adaptive Kalman filter. As a result, the noise in the signal can be filtered to a certain amount. All the test signals are the same as the tests in R_0 estimation tests.



(a) Time constant estimation with measurements SNR 100dB



(b) Time constant estimation with measurements SNR 90dB



(c) Time constant estimation with measurements SNR 80dB

Figure 8.12: Time constant estimation with measurements noise

Unlike the test results in R_0 estimation, the noise effects in the time constant estimation show completely different behaviour. Figure 8.12b which is the test result with SNR 90dB shows the best accuracy. To ensure that the estimation function can be connected to the SOC estimation function, a certain amount of the error will be expected. As a result, the scaling factor which also defining the noise level will be set to deal with the potential input error. However, this setting will reduce the accuracy. That is why the estimation result with least noise input does not show the best accuracy. Another study between the scaling factor and noise level will show the results.

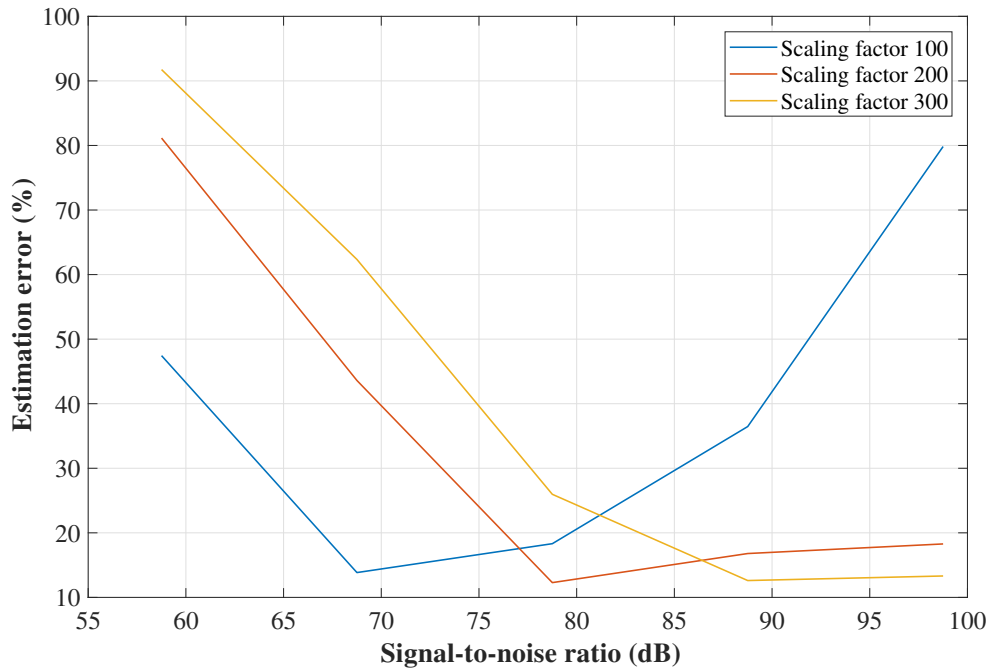


Figure 8.13: Relationship among time constant estimation accuracy, noise level and scaling factors

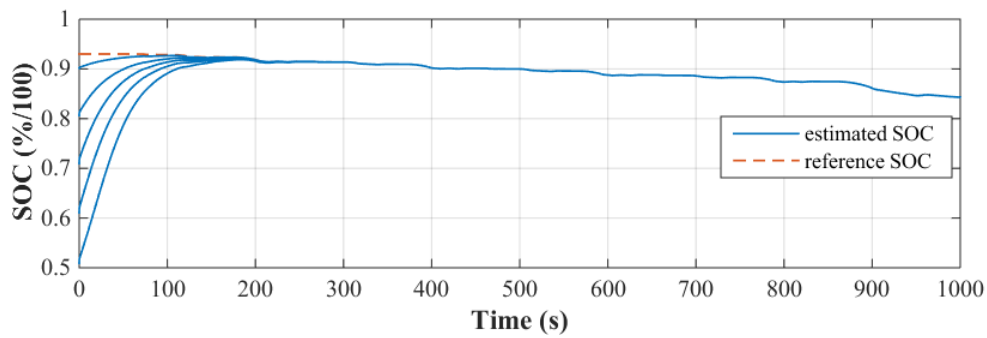
In the figure 8.13, it clearly shows the optimal working situation for different scaling factor values while dealing with the noisy signals. A rule can be found is the larger value for scaling factor can have a better estimation accuracy when the signal is less noisy and vice versa. As a result, the value selection for scaling factor is related to noise level which the system will be facing.

8.3 SOC estimation

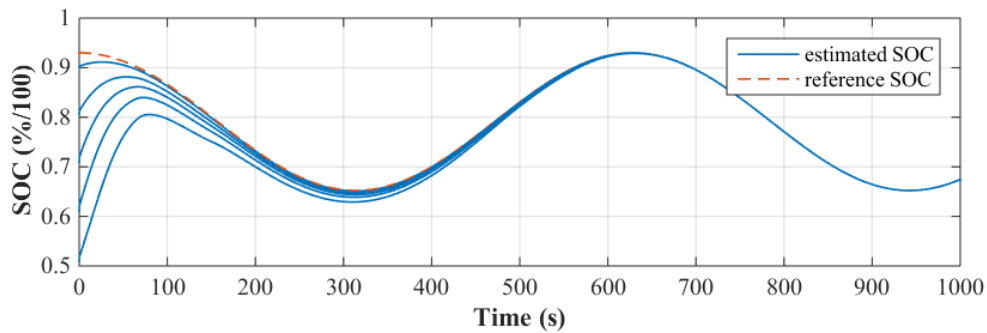
In this section, SOC estimation results will be shown by the influence of different initial guesses, relationship with time constant estimation and noise effects.

8.3.1 Test with different initial guess

It is necessary to test the Extended Kalman filter with its error correction ability which is a major performance criterion for the whole system. Hence, a series of different initial guess will be examined.



(a) SOC estimation with NEDC cycle inputs



(b) SOC estimation with Sin-wave inputs

Figure 8.14: SOC estimation with different initial guesses

The Figure 8.14a and 8.14b shows how the extended Kalman filter works with the different initial guess of SOC values. In both the cases, the estimated SOC value can converge to the reference value in a short time and keep track with the reference value.

8.3.1.1 Relationship with time constant estimation

The error in the time constant estimation will have some effects on SOC estimation. To make it more clear, the initial SOC estimation guess is set with a significant bias with respect to the reference value.

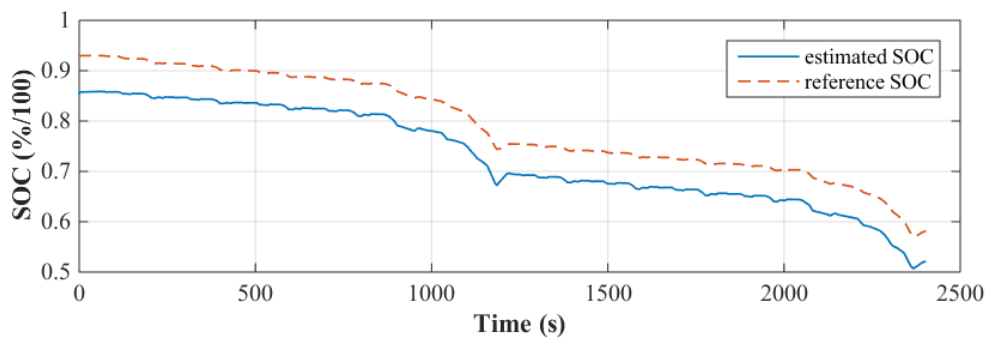


Figure 8.15: SOC estimation with 1000% error in time constant estimation

Since the time constant is not directly calculated in the EKF, it is not quite

sensitive to the error in the time constant. The error in the SOC estimation is due to constant bias and slower adapting speed. The effects of time constant error to the soc estimation is to create a constant bias. From figure 8.16, the increase of the SOC estimation error drops down with some certain amount of time constant estimation error which means the EKF does consider the states are not trustful and only correct the states with the measurements inputs.

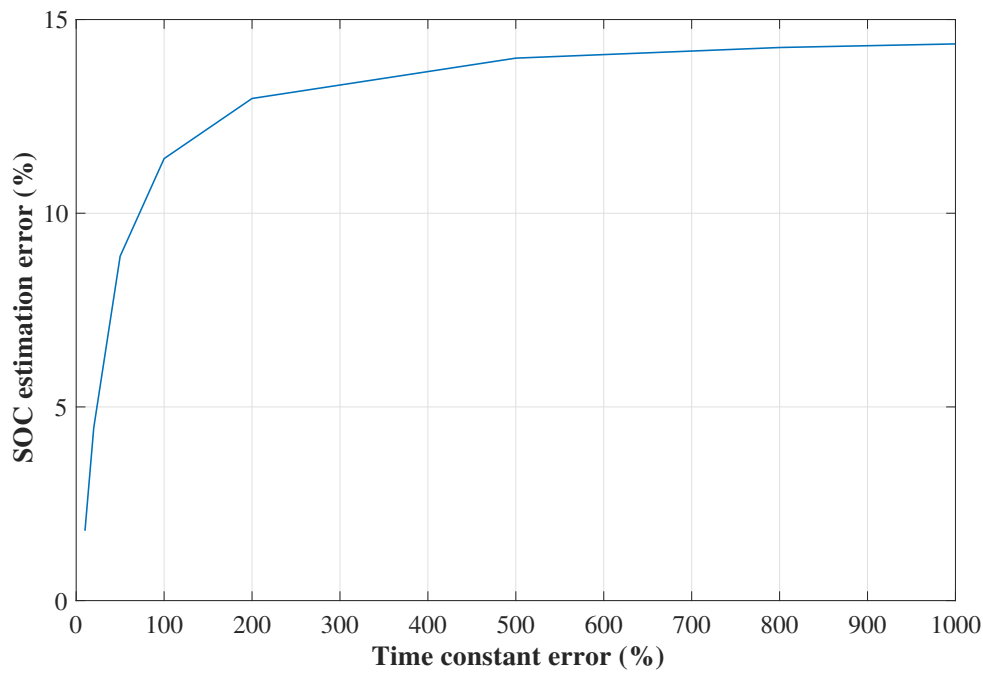
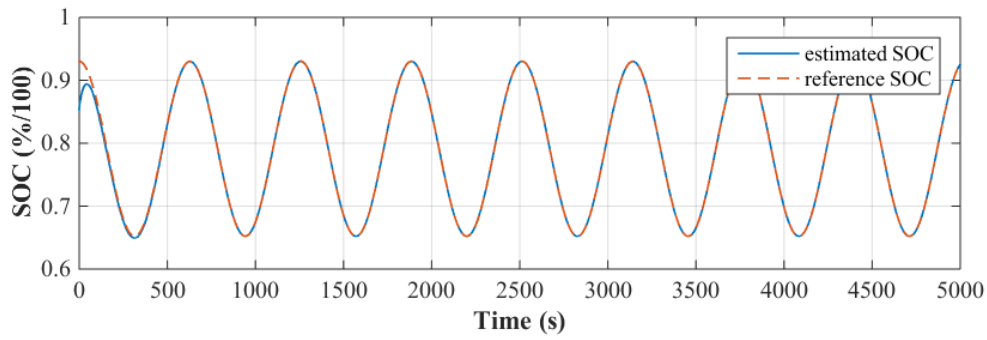


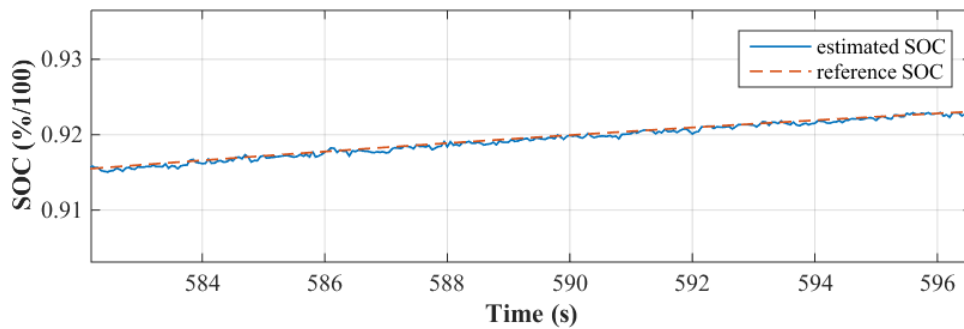
Figure 8.16: Relationship between SOC estimation and time constant estimation error

8.3.2 Noise effects

The results show that Kalman filter is capable of working smoothly under the noisy condition and hence fulfilling its purpose. The noisy signal is strong enough to cause huge oscillations in the estimation function blocks. However, the Kalman takes care of it. Hence, the Extended Kalman filter is not the bottle neck to the whole system.



(a) SOC estimation with SNR 60dB



(b) SOC estimation with SNR 60dB (enlarged)

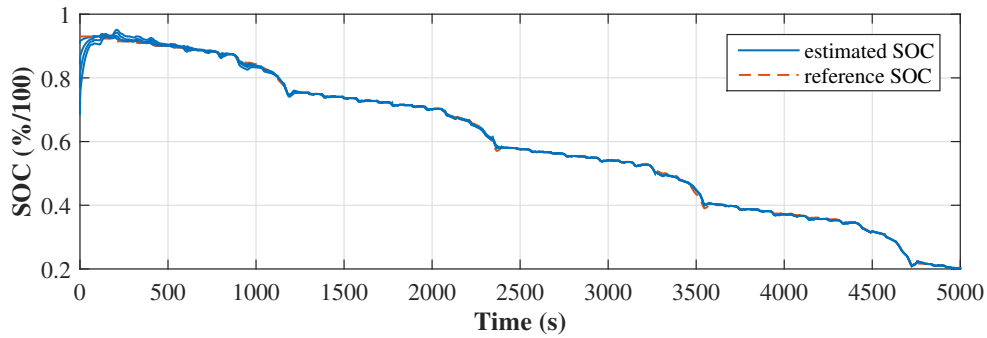
Figure 8.17: SOC estimation with noise effects

8.4 Combined test

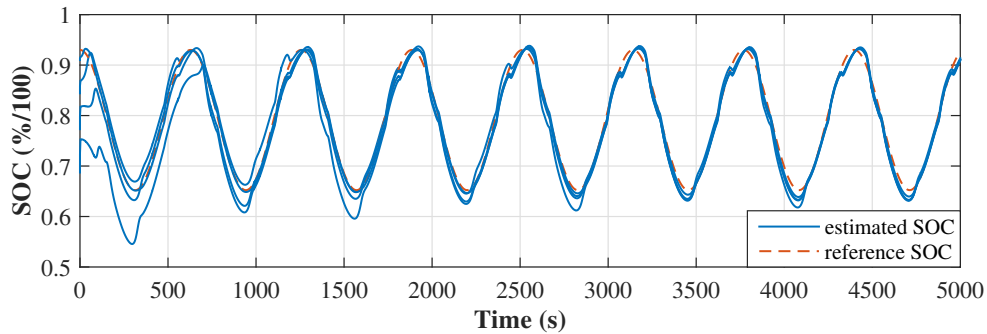
In this section, there will be the estimation results with the whole system with different initial errors. The influence of the signal noise will be shown as well.

8.4.1 Test results with optimal setting

As mentioned in previous sections, the three major important estimation functions (time constant, SOC and R_o) have different preferences in the sampling time. To simplify the whole system, the optimal sampling time has been used. Besides that, all other parameters use the optimal value for the testing. As figure 8.18a and 8.18b show, the SOC estimation can still follow the reference value with the system parameters given by the other two estimation function. However, the reaction speed and the accuracy are worse than the open loop test.



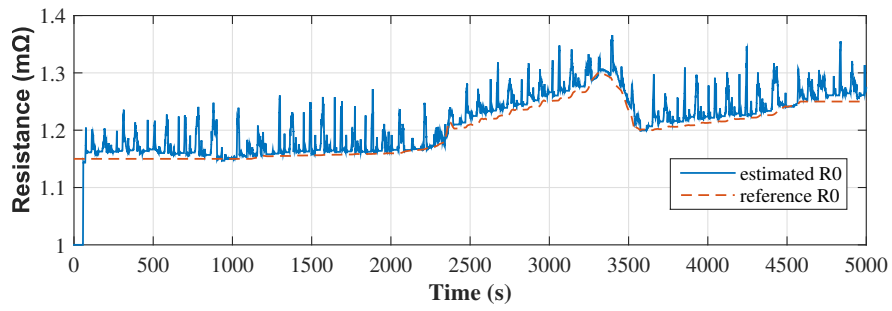
(a) SOC estimation with NEDC inputs



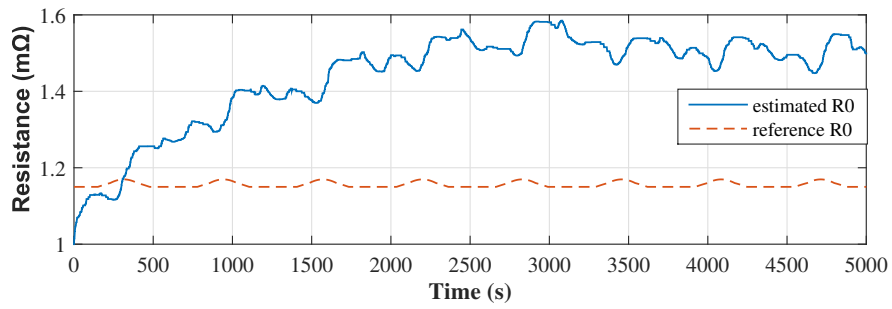
(b) SOC estimation with sin wave inputs

Figure 8.18: SOC estimation with the whole system

Besides the SOC estimation result, there are two prominent problems in the combined test of all estimators. One is the drop in the R_0 estimation accuracy due to the lower sampling rate. Another is the large oscillation caused by the inaccurate SOC estimation. In figure 8.19b, significant estimation error can be found compared to the result in figure 8.19a. The reasons why this bias occurs is mainly due the low sampling rate and the input frequency which has been addressed in the previous sections. At the same time figure 8.19a shows the result in which the input frequency is still high enough for the accuracy. However, the spikes can not be avoided which is similar to the result in figure 8.3b. The results for time constant estimation is shown in figure 8.20a and 8.20b. The time constant estimation accuracy is based on the estimation of SOC and R_0 . Summing-up, the system can work on the test signals which have been given.

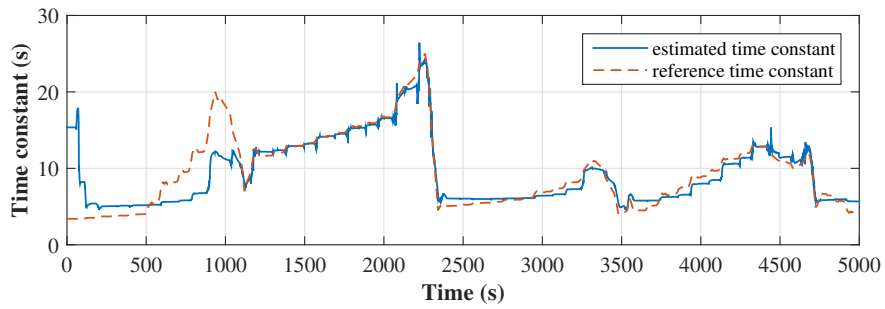


(a) R_0 estimation with NEDC inputs

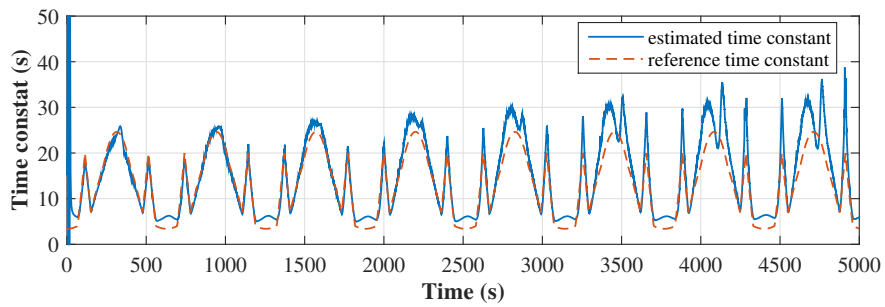


(b) R_0 estimation with sin wave inputs

Figure 8.19: R_0 estimation with the whole system



(a) Time constant estimation with NEDC inputs

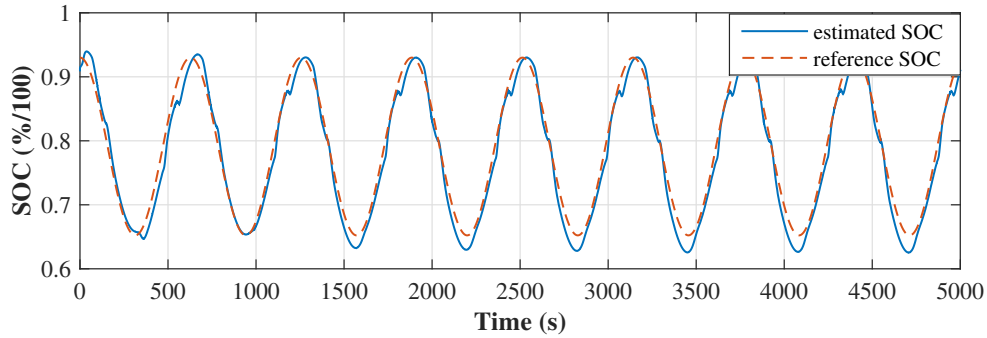


(b) Time constant estimation with sin wave inputs

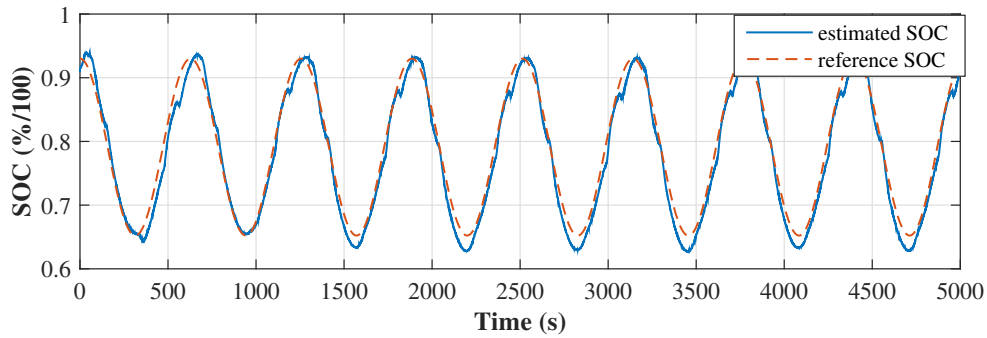
Figure 8.20: Time constant estimation with the whole system

8.4.2 Noise effects

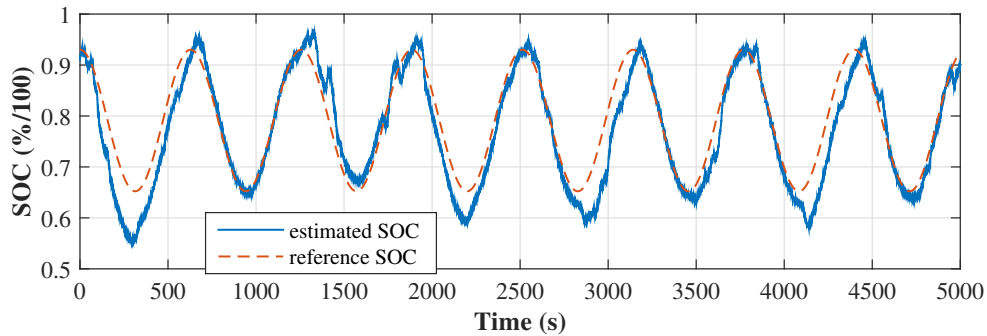
Similar as previous sections, noisy signal will be used to test the system stability. It is clear that the noise in the measurement signals affects the battery parameters estimation a lot expect the fact that the SOC estimation function is not quite sensitive with the noise. The noise affects the parameter estimation as previous sections mentioned and that leads to the results showed in figure 8.21b and 8.21c.



(a) SOC estimation with 0% mean error in noise



(b) SOC estimation with 5% mean error in noise



(c) SOC estimation with 10% mean error in noise

Figure 8.21: SOC estimation in complete system with noise

9

Results and Discussions: SOH

9.1 Model Performances

In this section, the performance of models for different loading conditions and assumptions which lead to these results will be discussed briefly. Model A gives capacity retention of both anode and cell, and on the other hand Model B provides capacity retention of only the cell.

9.1.1 Performance of model at Low Current rates

In this section, the ageing of the cell at 1 C-rate for two different temperatures will be discussed. Model A underestimates ageing during the initial cycles and corre-

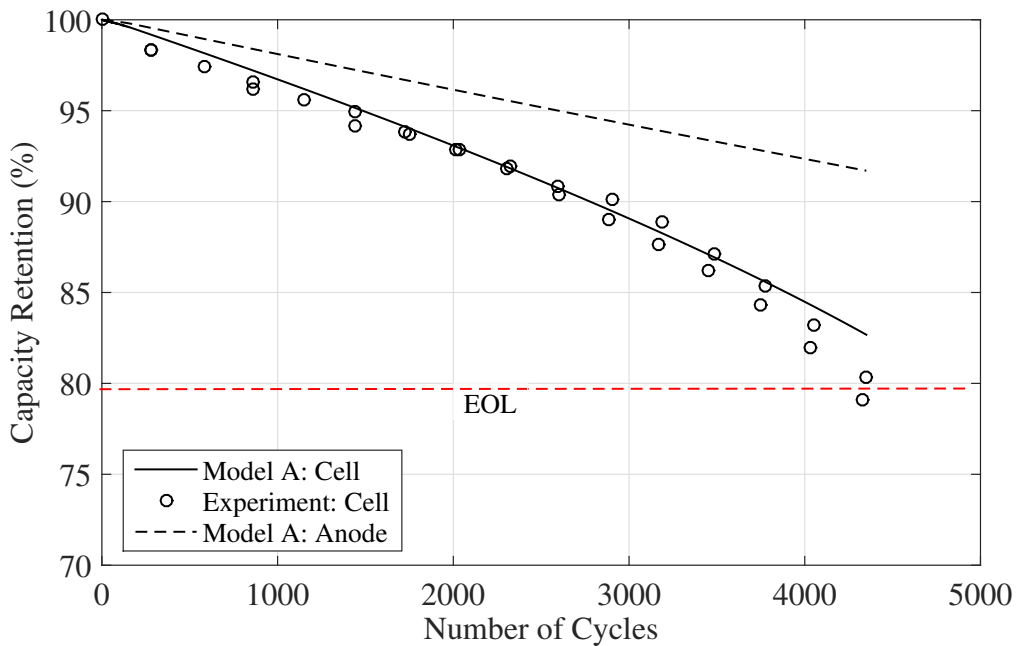


Figure 9.1: Model A: Capacity retention curves for C1D1T24S01

lates very well in the middle periods and again underestimates the ageing towards the EOL at $24^{\circ}C$ as shown in figure 9.1. This might be because of the assumption that $I_{segment} = I_{cell}$. However, the severity of this hypothesis is less in this case as the temperature, and the current rate is moderate. For the same temperature and C-rate Model B underestimates the experiment data until 1500 cycles and correlates

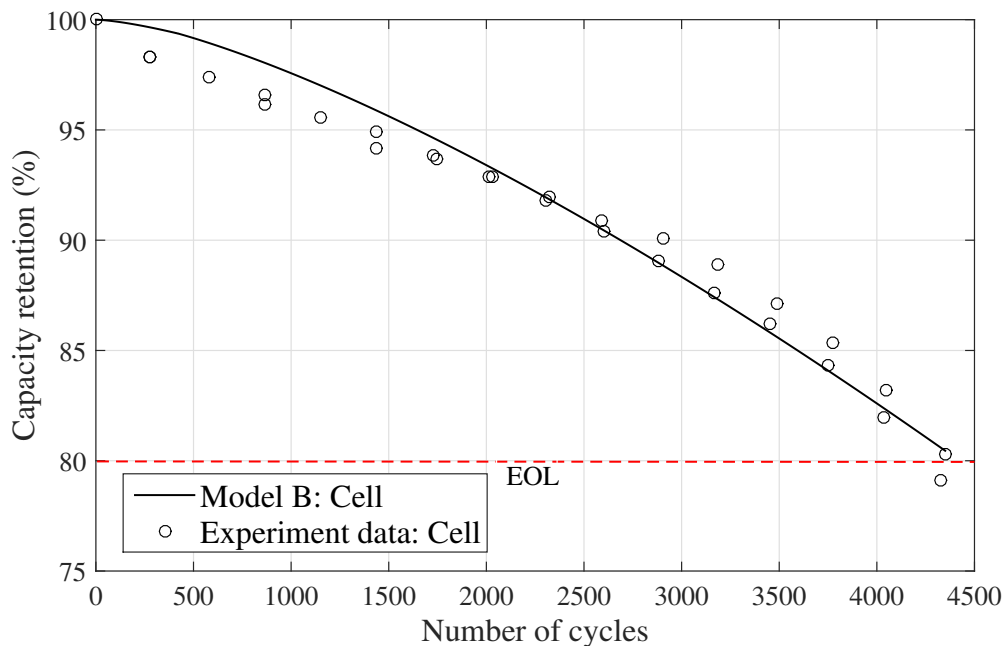


Figure 9.2: Model B: Capacity retention curves for C1D1T24S01

with experiment data to some extent and has almost the same EOL criteria as the experiment data as shown in figure 9.2. Nevertheless, all the calculations for model A and model B were based on the assumption that loss of cyclable lithium is the main reason for capacity retention.

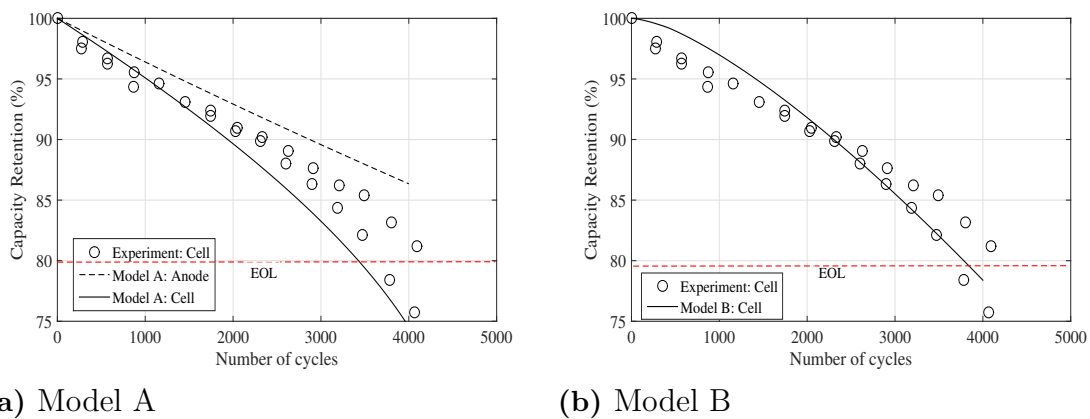


Figure 9.3: Capacity retention for cycle C1D1T32S01

Model A underestimates ageing during the initial cycles and correlates very well in the middle periods and again underestimates the ageing towards the EOL at $24^{\circ}C$ as shown in figure 9.1. This might be because of the assumption that $I_{segment} = I_{cell}$. However, the severity of this hypothesis is less in this case as the temperature, and the current rate is moderate. For the same temperature and C-rate model B underestimates the experiment data until 1500 cycles and correlates with experimental

data to some extent and has almost the same EOL criteria as the experimental results as shown in figure 9.2. Nevertheless, all the calculations for model A and model B were based on the assumption that loss of cyclable lithium is the main reason for capacity retention. The behaviour of model A and model B at 32°C is as shown in the figures 9.3a and 9.3b. At higher temperatures model A overestimates the ageing from cycle number 2000 and continues with minimum correlation until EOL. At higher temperatures, the charge transfer impedance is reduced [1] which leads to an increase in segment currents (slightly more than the cell current) and causes a faster rate of capacity reduction. Hence, the assumption $I_{segment} = I_{cell}$ affects the performance of model A. On the other hand model B has a similar performance as in the previous case. The exponential term in (2.26) increases with an increase in temperature and hence causes a reduction in some cycles. One should also keep in mind that the effect of SOC is also taken into consideration as the value of k_{SOC} is 1 (for $\Delta SOC = 1$). To summarise, the ageing in cycle C1D1T32S1, the aging rate is influenced more by temperature and lowers the overall cycle life.

9.1.2 Model performances at High current rates

In this section, the ageing of LFP cell at 2 C-rate and three temperatures (26° , 34° and 47°) will be discussed. From the calculations chapter, it was seen that an increase in current leads to an increase in activation energy, this lifts the energy barrier that the reactions should overcome [5] causing loss of cyclable lithium.

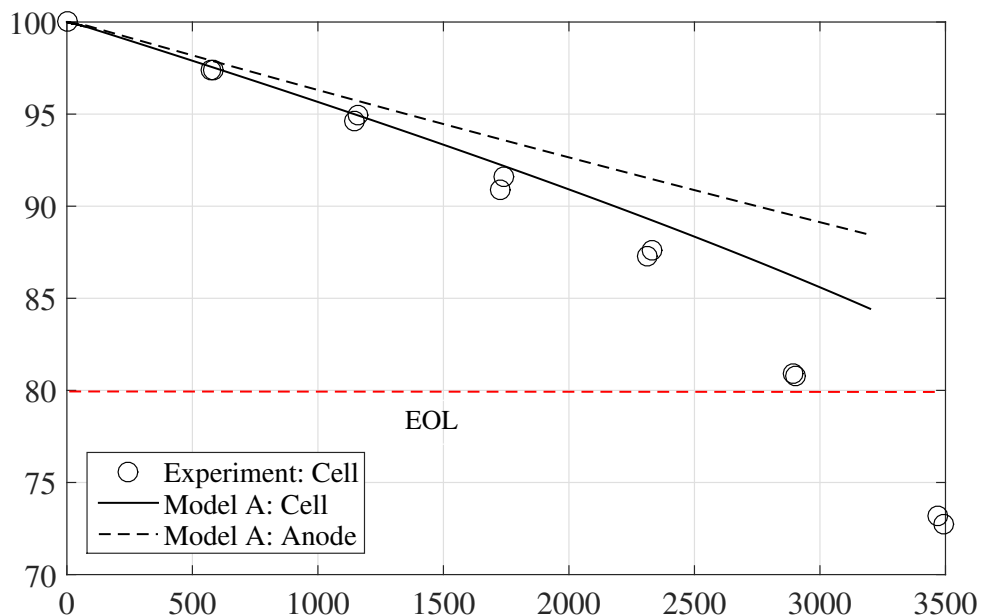


Figure 9.4: Model A: Capacity retention curves for C2D2T26S01

Figure 9.4 shows the behaviour of model A and the experiment data for cycle C2D2T26S1. The results are as expected, increase in current will reduce the overall cycle life of the cell by at least 20 percent when compared to reference cycle

C1D1T24S1. The model underestimates the ageing after 1000 cycles and has no correlation with the experimental data after that. Hence, the K_{CT} value was varied manually in the model, and the results are plotted, and they are shown in figure 9.5

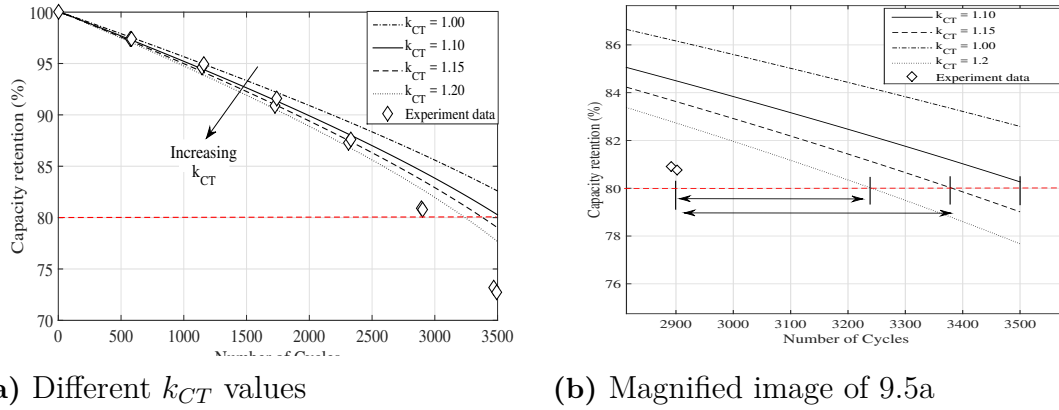


Figure 9.5: Effect of k_{CT}

It is seen that as the value of K_{CT} increased, the capacity retention curves started to approach the experimental data. This shows that the assumption $I_{segment} = I_{cell}$ leads to under estimation of the ageing. On the other hand, Model B had a better correlation with the experimental data and has the same EOL criteria as shown in figure 9.6.

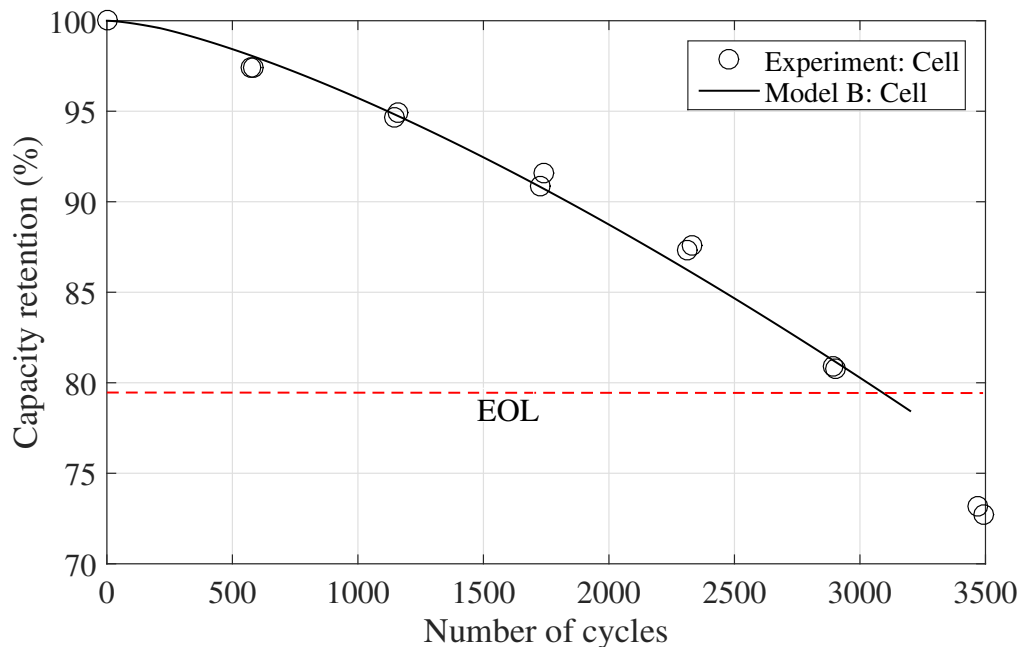


Figure 9.6: Model A: Capacity retention curves for C2D2T26S01

As discussed in the previous case, the increase in temperature affects the ageing, in this case, the effect of the increase in temperature is high since the current rate is

also high. High C-rates combined with high temperatures cause increased parasitic reactions (side reactions) which cause loss of cyclable lithium. To show the severity of high current and temperature cycles C2D2T26S1 and C2D2T34S1 are plotted together as shown in figure 9.7.

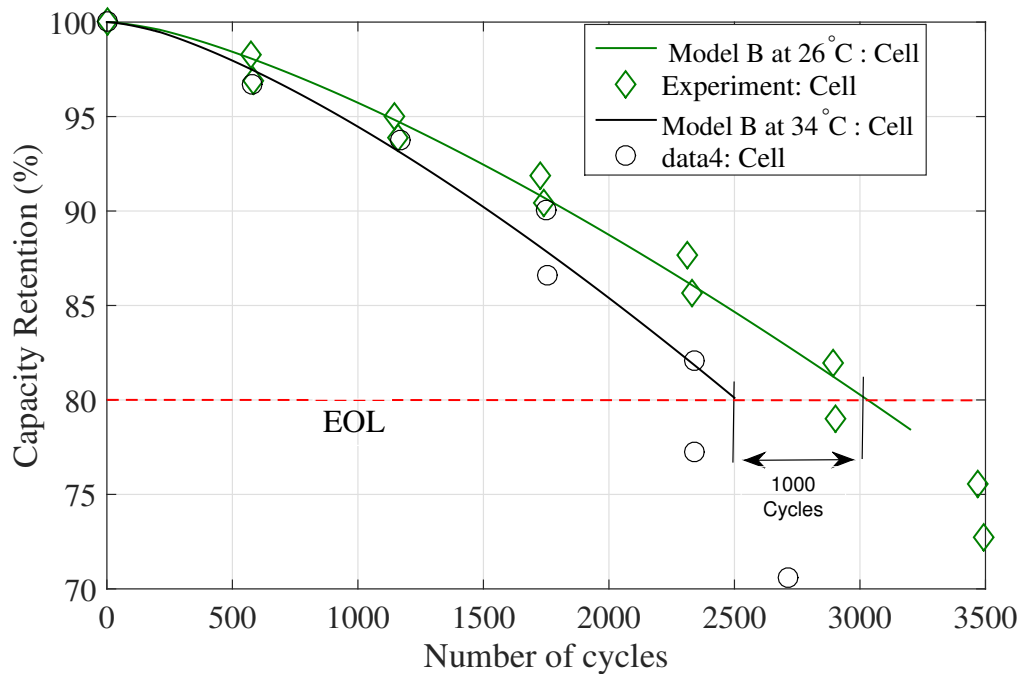


Figure 9.7: Comparison of capacity retention between cycles C2D2T26S01 and T34S01

Further, working under extreme temperatures such as 47°C will cause loss of active anode material (LAAM) as the intensity of parasitic reactions at the anode increase under these conditions. This phenomena is illustrated in figure 9.8. Though the experiment data and model A do not correlate very well after 1400 cycles due to the assumptions made, yet the model is capable of explaining the effect of temperature on the loss of lithium and LAAM. On the other hand, Model B performs decently even though the model loses a bit of correlation at the extremes. The relationship can be adjusted by varying the error ageing factor (k_e). Figure 9.9 shows the behaviour of model B

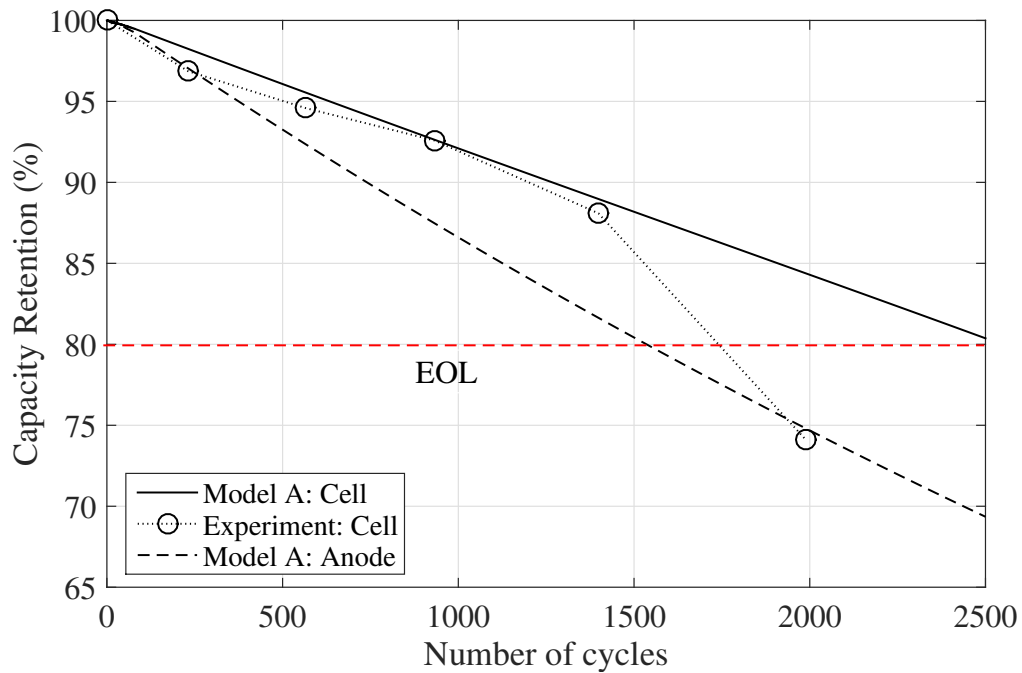


Figure 9.8: Model A: Capacity retention curves for cycle C4D4T47S01

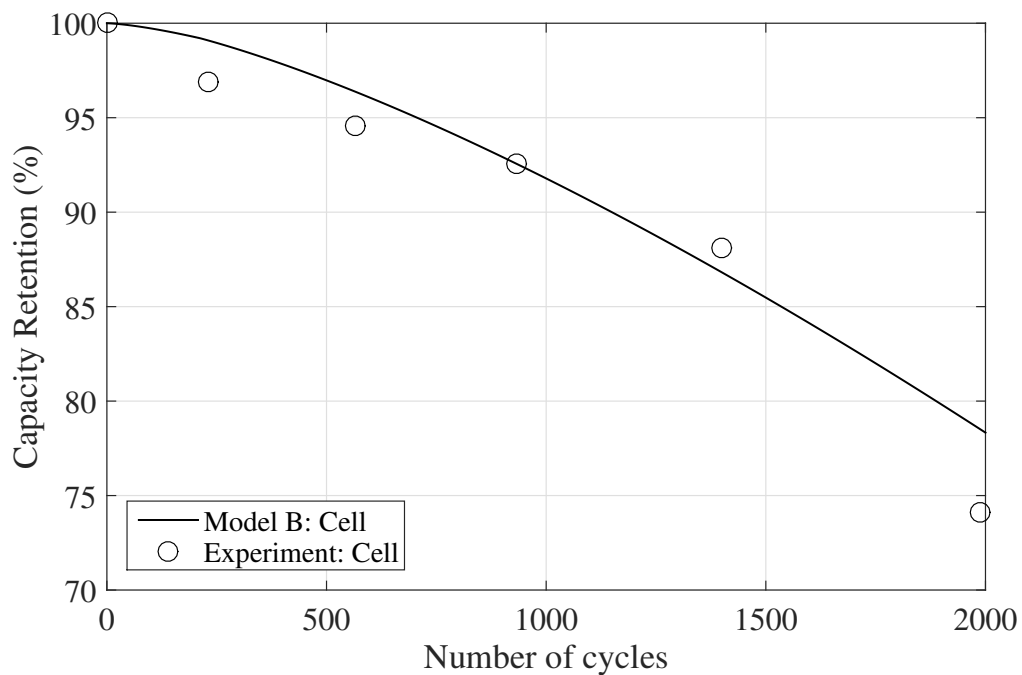


Figure 9.9: Model A: Capacity retention curves for cycle C4D4T47S01

To sum up, the ageing in cycles C2D2T26S01, C2D2T34S01 and C2D2T47S01 indicates that both temperature and current have severe effects on ageing. To inspect the effect of extreme current rate, cycle C4D4T29S01 was used. There was a loss of nearly 50 percent of overall cycle life when compared to reference cycle C1D1T26S01.

When it comes to model behaviour, model A overestimates the life time compared to experimental data towards the EOL but still in line with the experimental data. Model B has a decent performance in this case though it underestimates the life time in the beginning. Figures 9.10 and 9.11 show model A and model B performance for C4D4T29S01 cycle. Aging corresponding to C4D4T29S01 is generally due to the current under moderate temperatures.

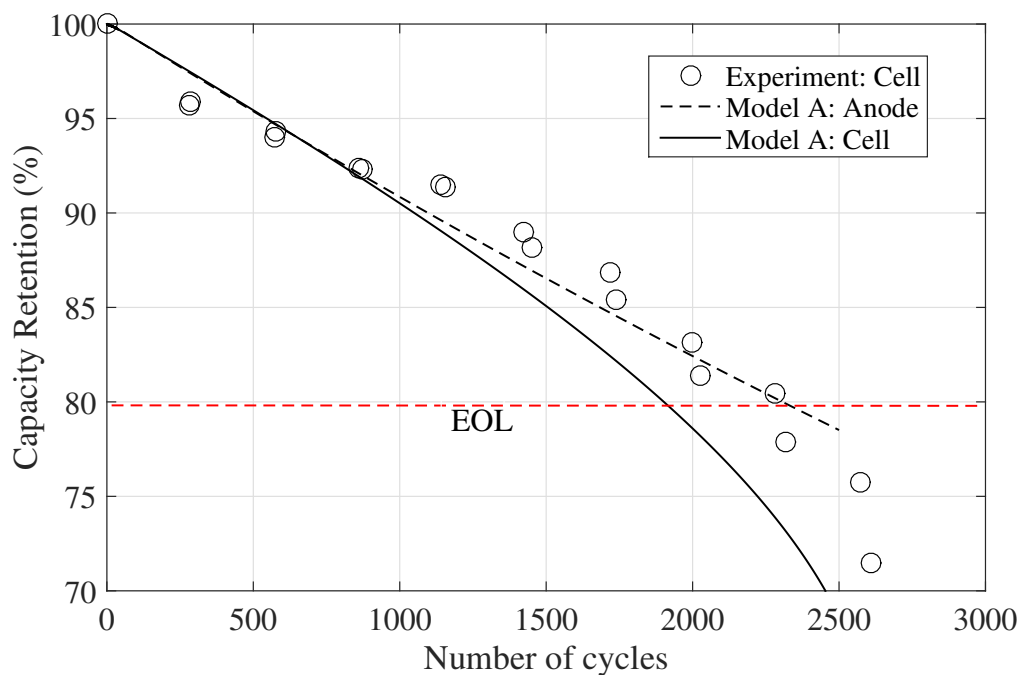


Figure 9.10: Model A: Capacity retention curves for cycle C4D4T29S01

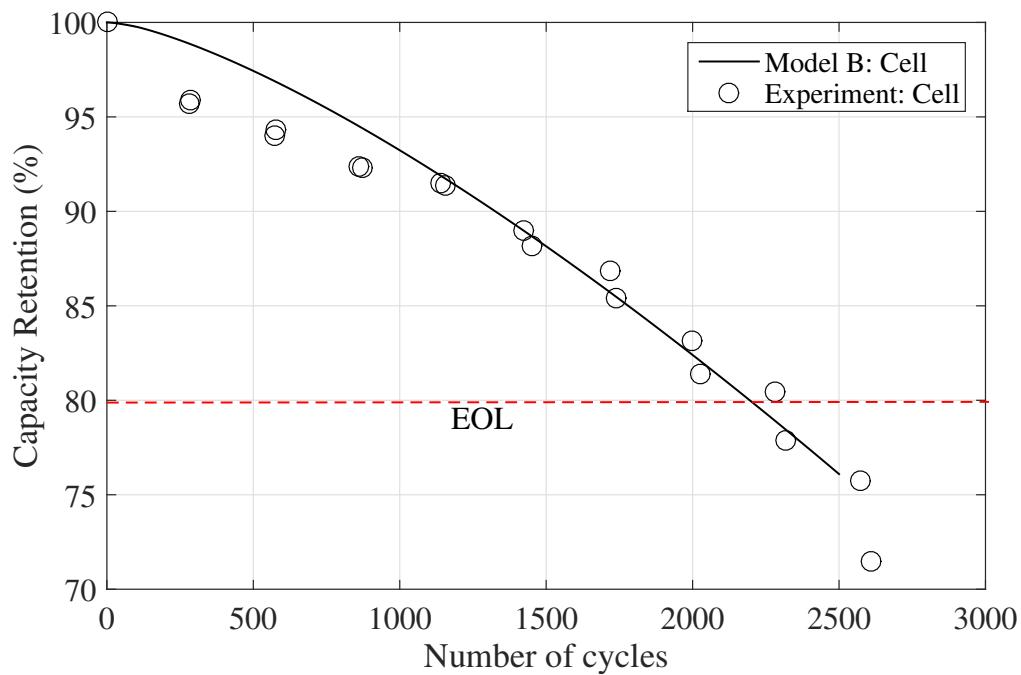


Figure 9.11: Model B: Capacity retention curves for cycle C4D4T29S01

9.1.3 SOC related aging

The behaviour of a cell for cycles C4D4T29S0-0.2, 0.2-0.4, 0.8-1 is unique, even though the current is high. With moderate temperatures, the cell has high capacity throughput for a SOC range between 0.2 – 0.4 and 0.8 – 1, but the battery reaches EOL quickly for SOC range 0 – 0.2 as shown in figure 9.12. Cycle C4D4T29S0.2-0.4 has different shapes at different instants of time. Therefore, an approximate fit was made to obtain the value of A and was parameterized as a function of SOC according to (6.24).

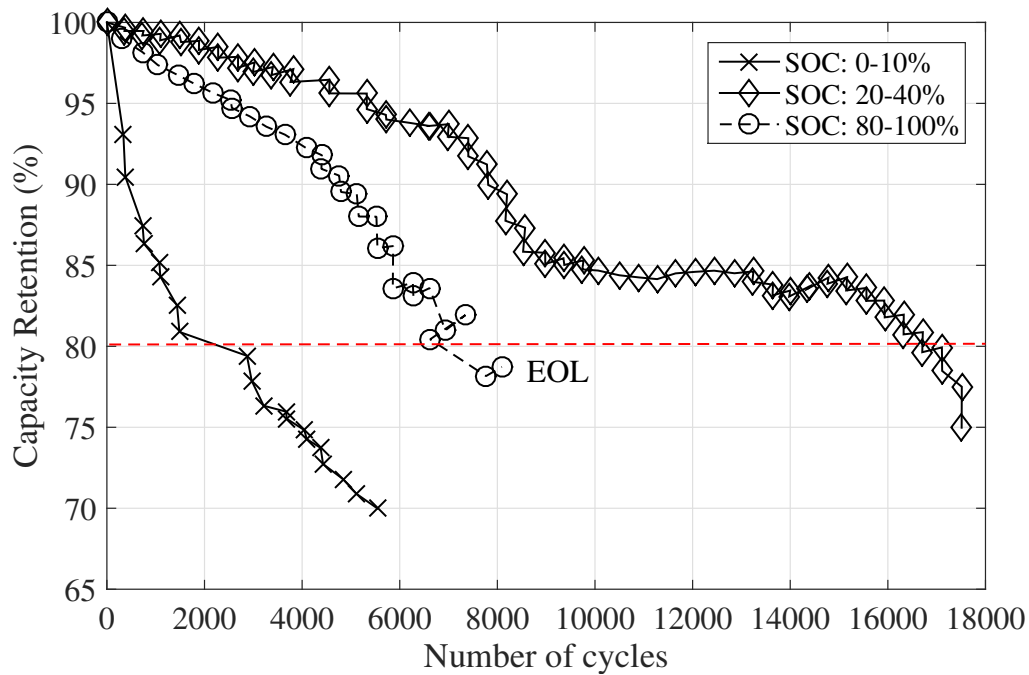


Figure 9.12: Experimental data for cycles C4D4T29S0-20, 20-40, 80-100

The Figure 9.13 shows the model A performance. The curves do not correlate exactly with the experiment data, but they have a good agreement with the calculations and theory, Model B also has similar performance. However, both the models fail to capture all the incidents (or stages) of the curve shown in figure 9.12. This might be because of the assumption that $K_{CT} = 1$ or bad curve fitting.

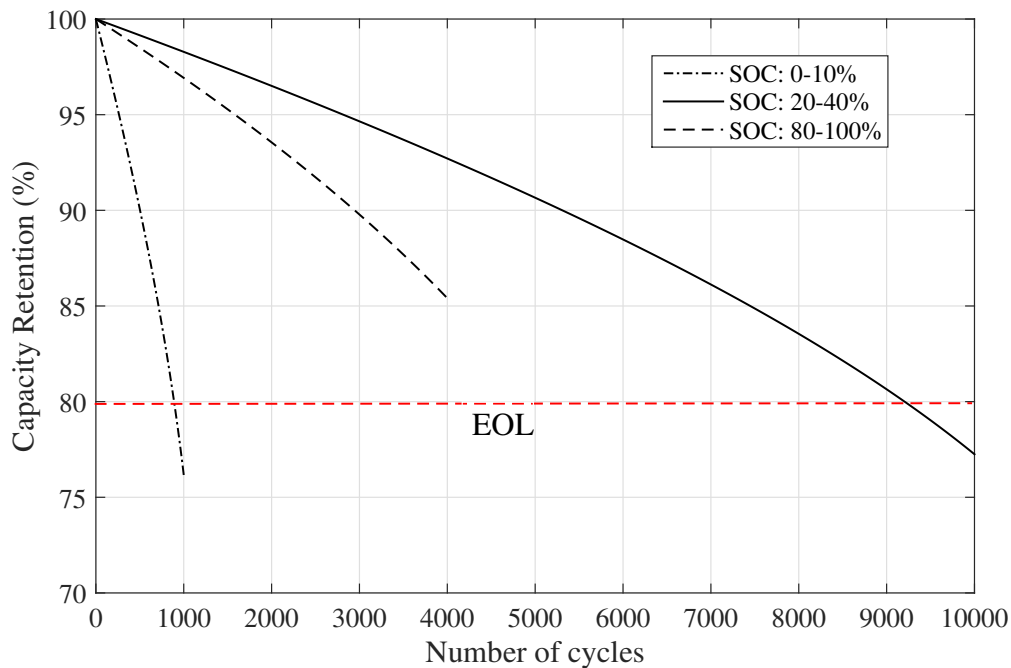


Figure 9.13: Model A results for cycles C4D4T29S0-20, 20-40, 80-100

9.2 Results: NMC/LMO cells

In the section 9.1 discussions were majorly based on the statistical performance of Model A and Model B which were for LFP cells only. In this segment, the results obtained from the model for NMC/LMO cells are analysed, and reasons for such results are briefly discussed. Also, the findings from the model are referred to research papers and hence strengthening the credibility of the model for NMC/LMO cells. The life cycle models were put to the test independently during the analysis phase concerning every loading condition. The results of cycle life model with all the functions as given in (7.4) is discussed in this segment.

9.2.1 Effect of SOC and temperature

To test the influence of temperature only, the experimental results at 2C current rate and 0-90% SOC is used, and the model inputs are set accordingly as shown in fig 4.1b. It is apparent from the figure 9.14 that the capacity retention curves stringently follow $(Ah)^b$ rule. The number of cycles gradually decline as the temperature is raised as shown in the figures 9.14(a) and 9.14(c). According to A. Cordoba-Arenas et al.[17] if the capacity fade follows the Arrhenius like kinetics the ageing is essentially related to the thermally stimulated process.

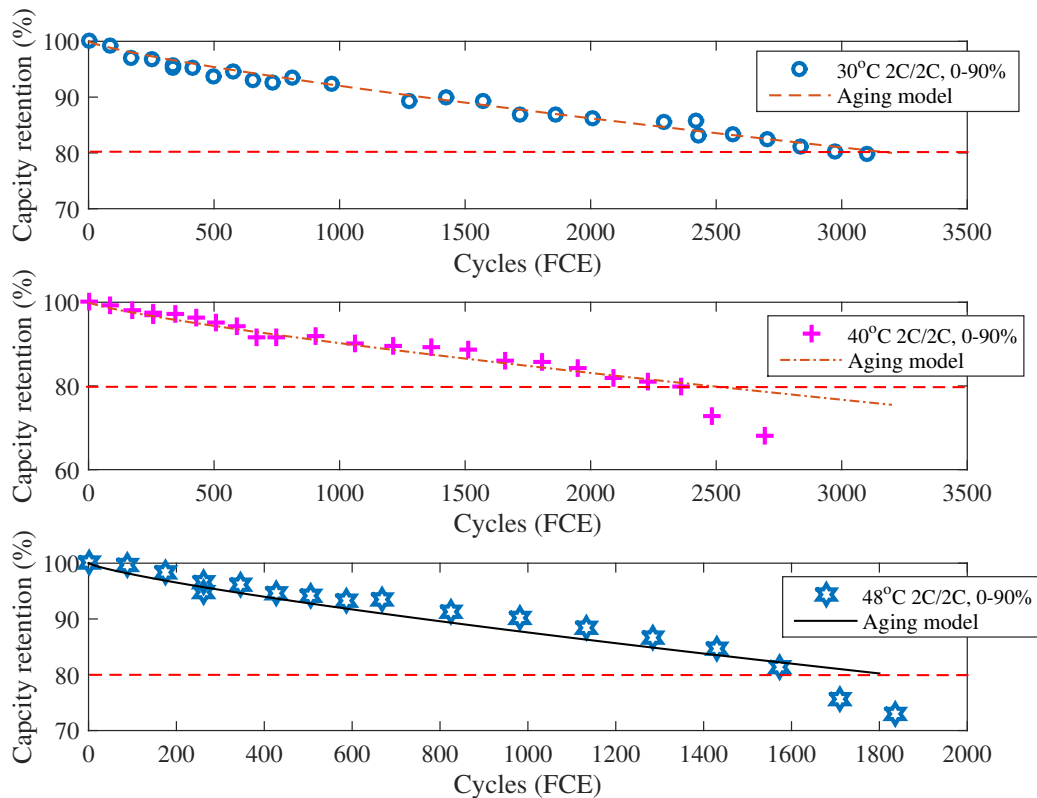


Figure 9.14: Symmetric +2C/-2C tests performed at 30, 40 and 48°C at 0-90% SOC range.

Many articles have reported that the growth of SEI layer is one of the major outcomes or negative effect due to increase in temperature [22, 17, 23]. Also, the loss of cyclable lithium ions is mostly because of side reactions producing SEI layer. Adding to the above statements the ICA analysis presented in [21] show a fall of peaks in the ICA curves with an increase in temperature meaning which the major ageing phenomena are the loss of cyclable lithium and SEI layer buildup. The value of error ageing factor K_e is very close to unity, which indicates that the (7.4) is capable of representing the temperature dependent ageing. However, there are many ageing events that the model is not capable of capturing and one such event is the increase in cell resistance. To sum up, the results illustrated in figure 9.14 agree with the experimental data with an R-square value close 0.989 and capable of capturing the major ageing events at high temperatures. Nevertheless, 90% SOC window and 2C current rate have their effects also.

9.2.2 Mid SOC range and temperature effects

Cycles with 2C current rate and 10% SOC window with a range of 40-50% at different temperatures are used to evaluate the cell ageing in this segment. Under these conditions, the experimental data illustrate abrupt capacity regain and retention event as shown in figure 9.15 which indicates that the ageing for these cells is eccentric. The multiplication of the pre-exponential terms which were derived for different conditions (7.4) leads to a very accelerated ageing in this case. To bypass the un-ideal ageing, the value of error ageing factor k_e is varied such that it fits the experimental data; this method holds good for all the SOC related ageing with 10% window. The value of k_e , in this case, betokens that the Arrhenius kinetics is partially successful in representing the ageing phenomena. Amidst the probable failure of the concept of multiplying the pre-exponential terms, the model has a decent performance at 28°C as it passes through the majority of the experimental data points as shown in the figure 9.15(a). On the other hand at higher temperatures, the model loses its coherence with the experimental data and rigidly follows $(Ah)^b$ rule as illustrated in figure 9.15(b) and (c). According, to the analysis made by [21] temperature has a moderate effect on ageing at mid-SOC ranges which is well represented by the model as the number of cycles reduce by approximately 500 cycles for 10-15°C increase in temperature. To sum-up, SEI layer accumulation is not the major reason for ageing in this case, and the number of FCE achieved by the cell is high as the SOC window is only 10%.

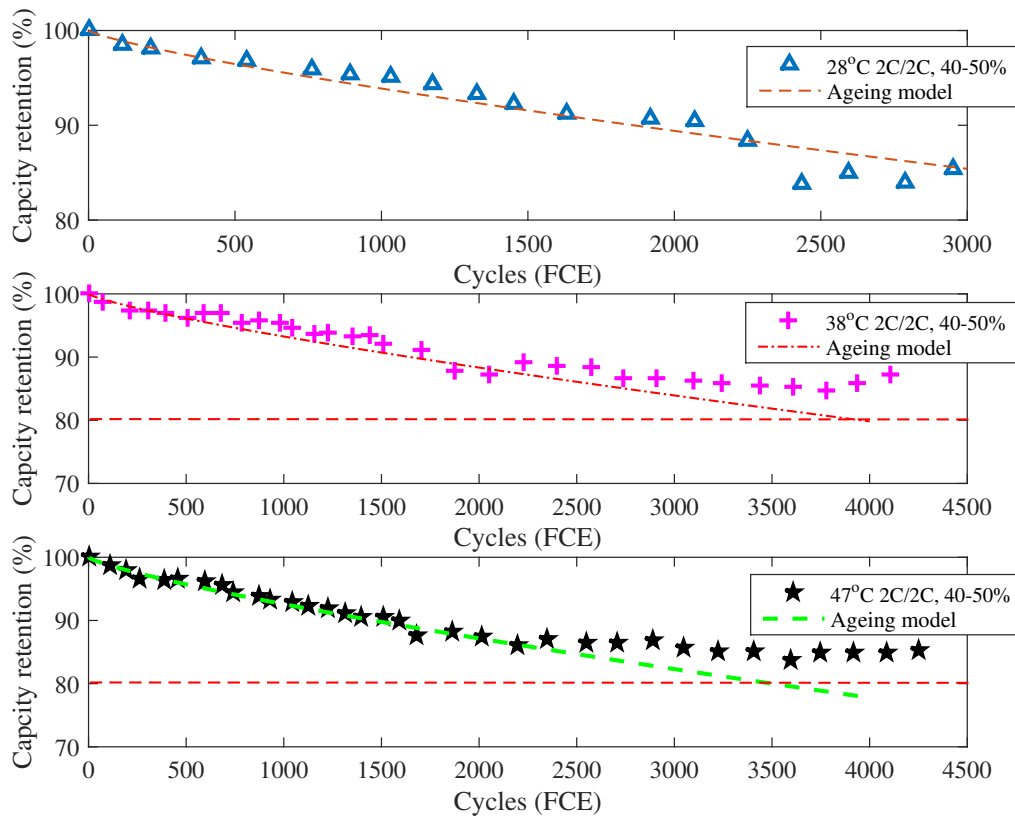


Figure 9.15: Symmetric +2C/-2C tests performed at 28, 38 and 47°C at 40-50% SOC range.

Further, the SOC range was stepped up by another 10% to 60-70%. The experimental data at this SOC range was much abrupt than the previous case as shown in figure 9.16. At all the temperatures the model maintains good consistency with the experimental data for only the first 1000 FCE. After which, the model starts to over estimate the experimental results which might be because of the error created by the equation for the pre-exponential term as shown in 7.7b. The impact of temperature is slightly higher in this condition as the number of cycles to EOL is considerably low. The presence of temperature effect symbolises that the Arrhenius kinetics comes into the picture from this SOC range. To sum up, for the ageing at 60-70%, the model performance is slightly influenced by the residues (errors) caused between the experimental and the empirical equation for the SOC dependent pre-exponential term. Finally, temperature makes its way to damper the battery life under these conditions.

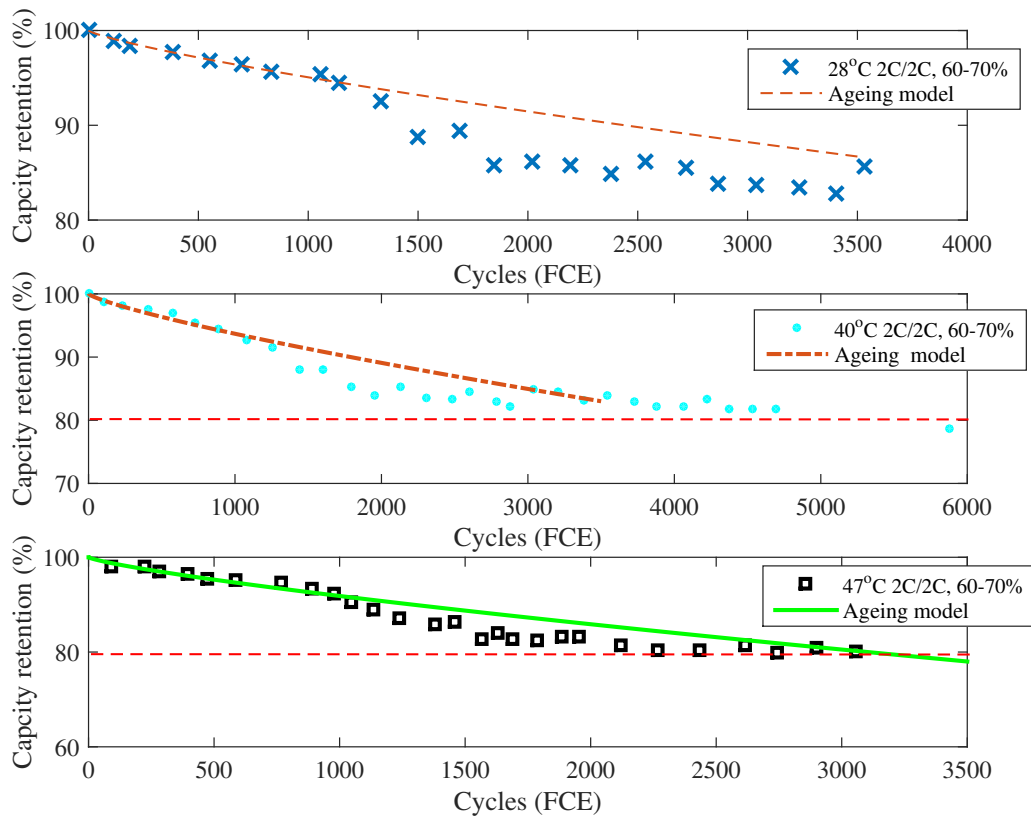


Figure 9.16: Symmetric +2C/-2C tests performed at 28, 38 and 47°C at 60-70% SOC range.

9.2.3 High SOC range and temperature effects

It is apparent from the figure 9.19 that high SOC ranges are deleterious to the battery life. In the previous cases, the increase in temperature did not alter the capacity retention exceedingly. However, in the case of higher SOC ranges temperature plays an important role which is well illustrated in the figure 7.6. According to J. Vetter et al. [22] the major reasons for the anode ageing at high temperature and SOC are continuous SEI growth (Power fade), loss of active material (Capacity fade). An accelerated ageing can be observed at an extreme temperature of 47°C at which the FCE is dramatically reduced indicating that ageing due thermally stimulated phenomena have a major role in this case.

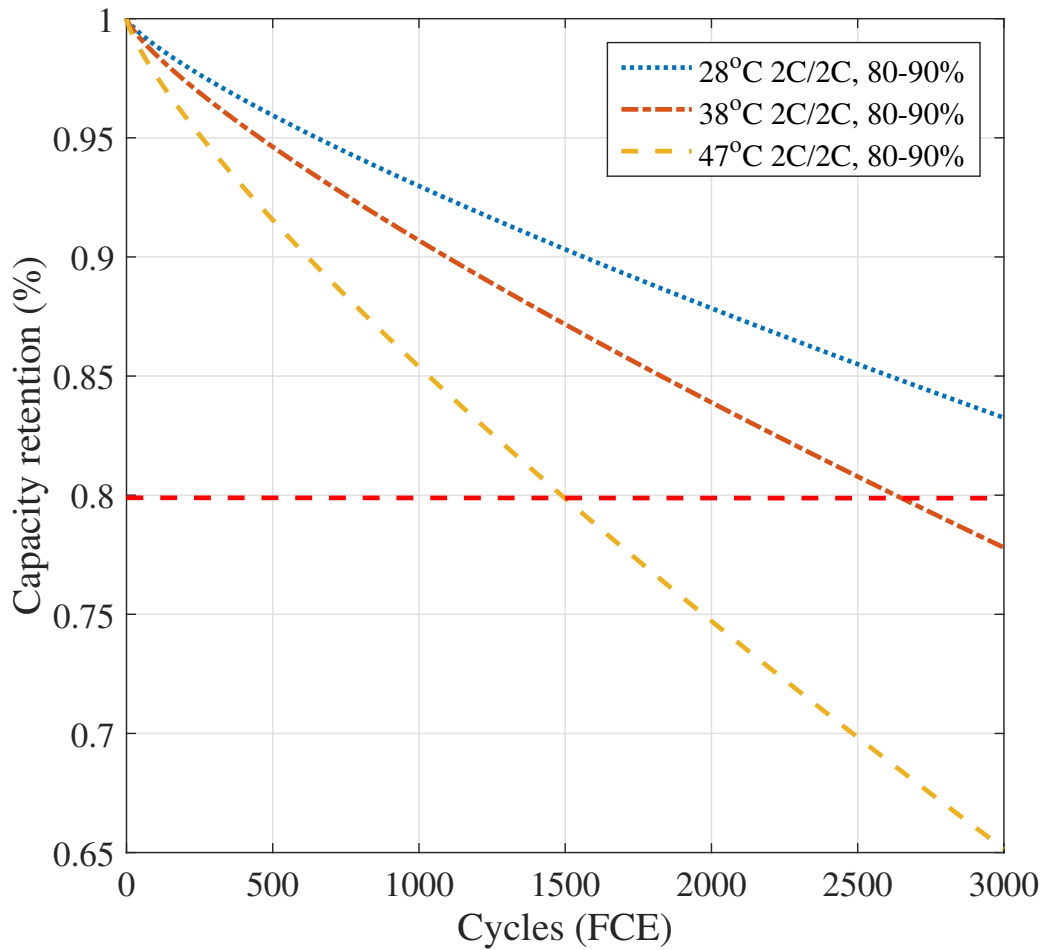


Figure 9.17: Simulation results for high SOC effects at different temperatures

9.2.4 Different C-rates at 60-70% SOC range

The guessed loss functions have been used in the model to simulate the ageing for various C-rates, and the error ageing factor for 1C and 4C current rate is 3 and 0.65 respectively. It is apparent from the figure 9.18 that 4C cycles have a faster rate of degradation compared to the 1C cycles. A notable observation is that the cell regains the capacity at cycle number close to 2000 and finally reach EOL after 4000 cycles, these capacity gain events are not captured by the semi-empirical ageing model as the cell reached EOL after 1800 cycles in the simulation results. On the other hand, the simulation results are in line with the experimental data for a 1C rate as shown in figure 9.18. To sum up, irrespective of the SOC range, increase in temperature and C-rates affects the ageing of the battery. However, the value of error ageing factor in this case also depicts that there might be other ageing events while operating at lower SOC windows.

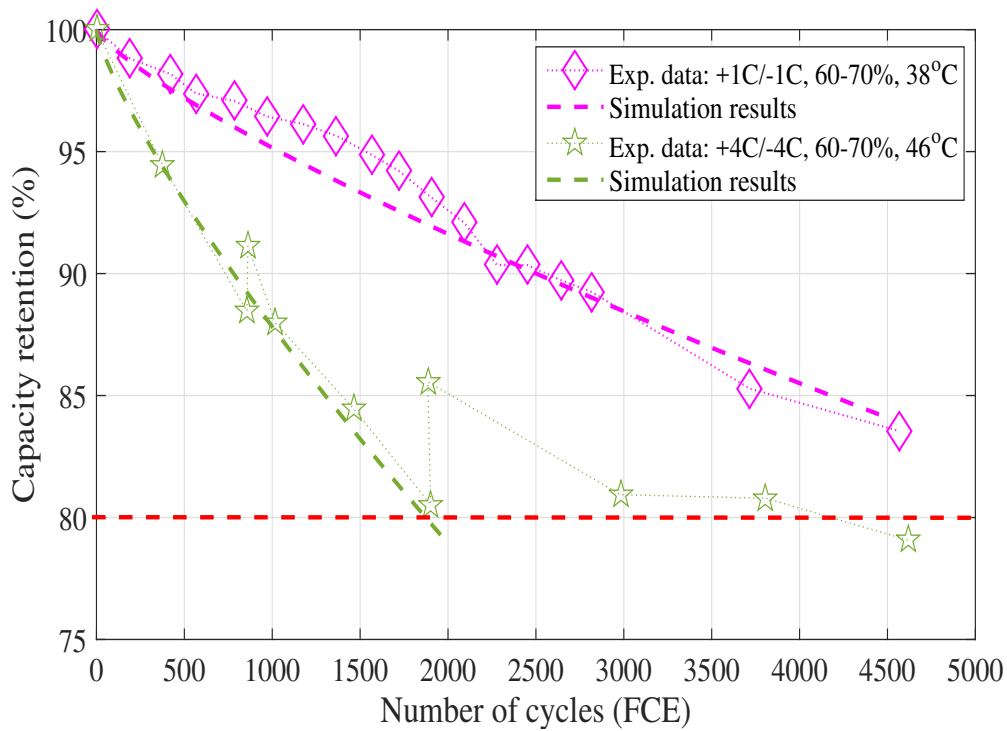


Figure 9.18: Symmetric +1C/-1C and +4C/-4C, SOC range of 60-70% at 38 and 47°C

9.2.5 COMSOL validation

The physics based ageing model built in COMSOL by [7], follows the Butler-Volmer reaction kinetics (2.1) and in our case, the Arrhenius equation is used to represent the reaction kinetics. In this segment, the COMSOL model is used to validate the semi-empirical ageing model for NMC/LMO cells. The simulations are conducted at 30°C with a 2 C-rate and 90% SOC window. Under these conditions, both the models have the same capacity retention with a slight deviation towards the EOL. The semi-empirical model has the same capacity retention shape as that of the physics model which confirms the calculations made for the shaping factor b as shown in figure 9.19. Further, the normalising factor $P_{Bat_{NMC/LMO}}$ holds good in these conditions as it normalises the SOC related ageing function to unity. The components of the semi-empirical ageing model are fitted to the experimental data, and these fitted functions can be linked to the Butler-Volmer. However, the fitting functions developed in this work is based on the Tafel equation (2.25) and the Arrhenius expression (2.26). To sum up, the semi-empirical model replicates the physics model under the conditions mentioned above and hence the validation increases the reliability of the model.

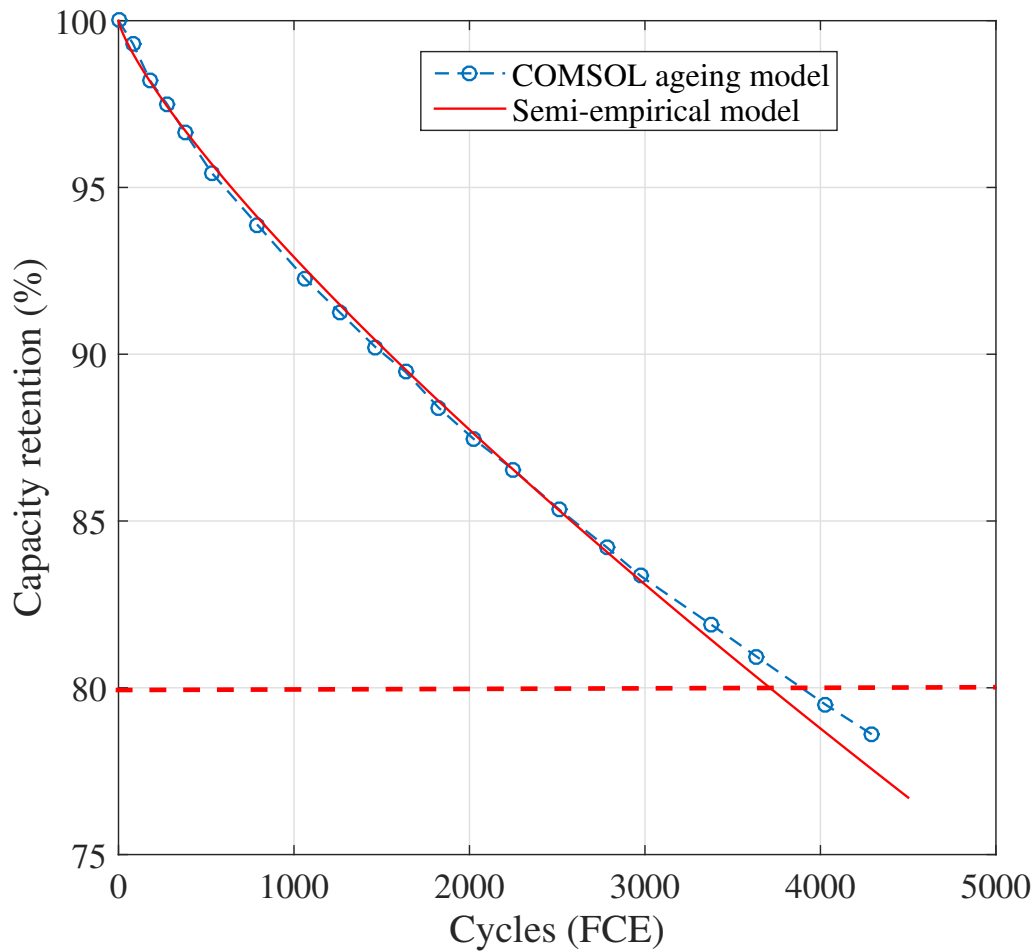


Figure 9.19: COMSOL physics model Vs Semi-empirical model. +2C/-2C, 0-90% at 30°C

9.2.6 Error Ageing value at different condition

One of the main hindrances of the model is that the variation of the error ageing factor. It is apparent from the figure that the model follows the assumptions for a SOC window of 80% and varies for other cases and the physical explanations were explained in the previous sections. There is a need for more data to inspect the behaviour of this value and build a function for it. Hence, the model is applicable only to SOC window of 80%. Another main observation from the figure 9.20 is the slight increase in the value for the case number two where it is slightly higher than one because of the function to SOC and Temperature related ageing as it has a significant error at 35 degrees as shown in the figure 7.7a

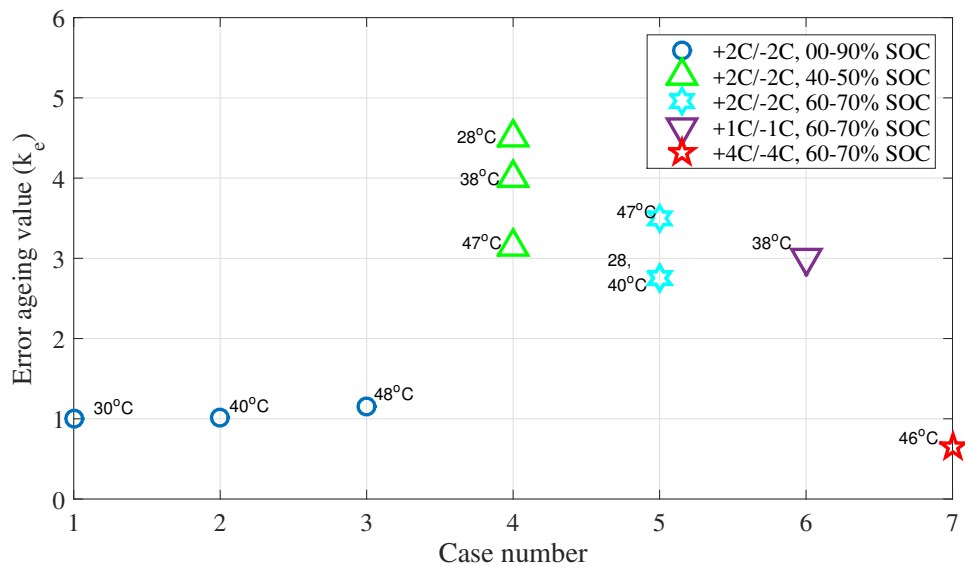


Figure 9.20: Variation of error ageing factor for different consitions.

10

Conclusion

10.1 Conclusion

In this thesis single RC model is used to represent the physical battery, this enables Linear regressive estimators like RLS and Kalman filters to be used for SOC estimation algorithms. The ohmic resistance R_0 is estimated separately by excluding the RC element estimation assuming that the RC elements change slowly compared to R_0 . This approximation helps in reducing the multiple order non-linear model to a first-order linear model. During the verification of the model, the SOC and parameter estimation produced promising results only until the noise was introduced in the inputs signals. Under noisy conditions, the performance of the estimation drastically reduced due to the simplification of the model. However, the model is capable of performing decently under real conditions with an acceptable error in the SOC estimation.

The models for LFP and NMC cells enumerate expected behaviours at 100% and 80% SOC windows with an operating temperature in the range of 20 - 55 degrees and for C-rates from 1 - 4C. Both the cells have a unique dependence on the SOC based ageing. For the LFP cells stresses are high at SOC less than 20% and greater than 80% while for NMC cells the stress is proportional to the SOC. It is observed that (figure 7.4) NMC cells experience more stress than the LFP cells at a given temperature and C-rate. However, this analysis does not have a firm basis as the analysed cells have a significant difference in capacity, hence the same procedure has to be applied to different cell chemistries for verification of the algorithm. The model developed in this thesis uses the RMS value of current and does not differentiate between severity of charging and discharging currents. Therefore, the Models developed are suitable and have valid results only for symmetric drive cycles. Also, there is a huge requirement of data to prove the validity of the Model C (NMC cells) at higher C-rates and temperatures since the loss functions are guessed. The non-linear behaviour of the error ageing value (k_{error}) should be parameterised for which more experimental data and tuning is required. Due to these setbacks, the model can only be used to analyse the effects of the operating conditions and not for prediction of the end of life or prognosis in electric vehicles.

10.2 Future work

The overall future of this thesis is to combine the SOC estimation algorithm and the ageing model and ultimately develop a reliable battery monitoring system. This can be achieved if the following tasks are performed in the future

1. Implement multiple non-linear estimators to predict the battery parameters accurately and hence SOC.
2. The Arrhenius equation implemented in this thesis is a good representation of the parasitic reactions in the battery and fails to explain other phenomena that are responsible for ageing. Hence, there is a need for a detailed study with which the severity factor can be modelled such that it can represent more ageing phenomena.
3. As mentioned before the model developed in this work is suitable only for symmetrical cycles. Hence, efforts must be made such that the model calculates reasonable SOH for real cases/driving cycles like NEDC and HYZEM.
4. Analysis of the capacity retention curves does not provide more information about the battery parameters such as the RC parameters. Analysis of EIS results (Electrochemical Impedance Spectroscopy) at different stages (EOL, MOL and BOL) reveal the behaviour of the battery parameter and help in parameterising the battery model as function of age. This parameterisation reduces the error in the SOC estimation algorithm eventually.
5. Collect more data related to the ageing of NMC/LMO and LFP cells under different loading conditions and parameterise the error ageing term k_{error} .

Bibliography

- [1] VME. (2014) *Electric vehicles in Europe: gearing up for a new phase?*, Amsterdam Roundtable Foundation and McKinsey & Company The Netherlands.
- [2] Fridholm, Björn. (2015) *On State-of-charge Estimation for Automotive Batteries*. Department of Signals and Systems, Chalmers University of Technology.
- [3] Fei Feng, Rengui Lu and Chunbo Zhu. (2014) *A Combined State of Charge Estimation Method for Lithium-Ion Batteries Used in a Wide Ambient Temperature Range*, energies. ISSN 1996-1073.
- [4] R. E. Kalman. (1960) *A New Approach to Linear Filtering and Prediction Problems*, Journal of basic engineering, vol. 82, no. Series D.
- [5] CBS. (2016) *Plug-in hybrid most popular type of electric car*, Amsterdam Roundtable Foundation and McKinsey & Company The Netherlands.
- [6] Wen-Yeau Chang. (2013) *The State of Charge Estimating Methods for Battery: A Review*, Applied Mathematics Volume 2013, Article ID 953792.
- [7] N. Watrin, B. Blunier, and A. Miraoui. (2012) *Review of adaptive systems for lithium batteries state-of-charge and state-of-health estimation*. Transportation Electrification Conference and Expo, pp. 1–6. Dearborn, Mich,USA.
- [8] Steve Knoth. (2012) *Know a Battery's State-of-Charge By Counting Coulombs*, Linear Technology Corporation.
- [9] F. Gustafsson. (2000) *Adaptive filtering and change detection*, John Wiley Sons,Ltd.
- [10] Sandeep. Nital. David, (2016) *Pulse power characterisation for lithiumion cells in automotive applications*, Department of Energy and Environment , Chalmers University of Technology.
- [11] Björn Fridholm, Torsten Wik, Magnus Nilsson. *Robust adaptive Kalman filter for online impedance estimation in automotive batteries*, 2016. Section 4.5.
- [12] Serrao, Lorenzo and Onori, Simona and Rizzoni, Giorgio and Guezennec, Yann. (2009) *A novel model-based algorithm for battery prognosis*, IFAC Proceedings Volumes, vol. 42, pp. 923–928.
- [13] Prada, Eric and Di Domenico, D and Creff, Yann and Bernard, J and Sauvant-Moynot, Valérie and Huet, François. (2012) *Simplified electrochemical and thermal model of LiFePO₄-graphite Li-ion batteries for fast charge applications*, Journal of The Electrochemical Society, vol. 159, PP. A1508–A1519.
- [14] Cui, Yingzhi and Du, Chunyu and Yin, Geping and Gao, Yunzhi and Zhang, Lingling and Guan, Ting and Yang, Lijie and Wang, Fuping. (2015) *Multi-stress factor model for cycle lifetime prediction of lithium ion batteries with shallow-depth discharge*, Journal of Power Sources, vol. 279, PP. 123–132.

- [15] Ramadass, P and Haran, Bala and White, Ralph and Popov, Branko N. (2003) *Mathematical modeling of the capacity fade of Li-ion cells*, Journal of Power Sources, vol. 123, PP. 230–240.
- [16] Todeschini, Fabio and Onori, Simona and Rizzoni, Giorgio. (2012) *An experimentally validated capacity degradation model for li-ion batteries in phev applications*, IFAC Proceedings Volumes, vol. 45, PP. 456–461.
- [17] Cordoba-Arenas, Andrea and Onori, Simona and Guezennec, Yann and Rizzoni, Giorgio. (2015) *Capacity and power fade cycle-life model for plug-in hybrid electric vehicle lithium-ion battery cells containing blended spinel and layered-oxide positive electrodes*, Journal of Power Sources, vol. 278, PP. 473–483.
- [18] Safari, M and Delacourt, C. (2011) *Modeling of a commercial graphite/LiFePO₄ cell*, Journal of the Electrochemical Society, vol. 158, PP. A562–A571.
- [19] Groot, Jens. (2014) *State-of-health estimation of Li-ion batteries: Ageing models*, Department of Energy and Environment , Chalmers University of Technology.
- [20] Groot, Jens. (2012) *State-of-health estimation of li-ion batteries: Cycle life test methods*, Department of Energy and Environment , Chalmers University of Technology.
- [21] Wikner, Evelina. (2017) *Lithium ion Battery Aging: Battery Lifetime Testing and Physics-based Modeling for Electric Vehicle Applications*, Department of Energy and Environment , Chalmers University of Technology.
- [22] Vetter, J and Novák, P and Wagner, MR and Veit, C and Möller, K-C and Besenhard, JO and Winter, M and Wohlfahrt-Mehrens, M and Vogler, C and Hammouche, A. (2005) *Ageing mechanisms in lithium-ion batteries*, Journal of the Electrochemical Society, vol. 147, PP. 269–281.
- [23] Bloom, I and Cole, BW and Sohn, JJ and Jones, SA and Polzin, EG and Battaglia, VS and Henriksen, GL and Motloch, C and Richardson, R and Unkelhaeuser, T and others. (2001) *An accelerated calendar and cycle life study of Li-ion cells*, Journal of the Electrochemical Society, vol. 101, PP. 238–247.
- [24] Agubra, Victor and Fergus, Jeffrey. (2013) *Lithium ion battery anode aging mechanisms*, Journal of the Electrochemical Society, vol. 6, PP. 1310–1325.
- [25] <https://www.weforum.org/agenda/2017/11/battery-batteries-electric-cars-carbon-sustainable-power-energy/>
- [26] <https://www.cbsnews.com/news/the-toll-of-the-cobalt-mining-industry-congo/>
- [27] Tsurukawa, N., Prakash, S., and Manhart, A. (2011). Social impacts of artisanal cobalt mining in Katanga, Democratic Republic of Congo. Freiburg: Öko-Institut eV, novembre